Development and~표지(A4) 2011.10.5 6:26 PM 페이지1 HP-LaserA4-2 2400DPI 210LPI

DEVELOPMENT AND APPLICATION OF REGIONAL CLIMATE MODELS

Mayfield Hotel, Seoul, Korea; October 11-12, 2011

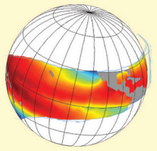

DEVELOPMENT AND APPLICATION OF REGIONAL CLIMATE MODELS

OCTOBER 11-12, 2011

RESEARCH INSTITUTE OF OCEANORGRAPHY SEOUL NATIONAL UNIVERSITY

DEVELOPMENT AND APPLICATION OF REGIONAL CLIMATE MODELS

Mayfield Hotel, Seoul, Korea; October 11-12, 2011

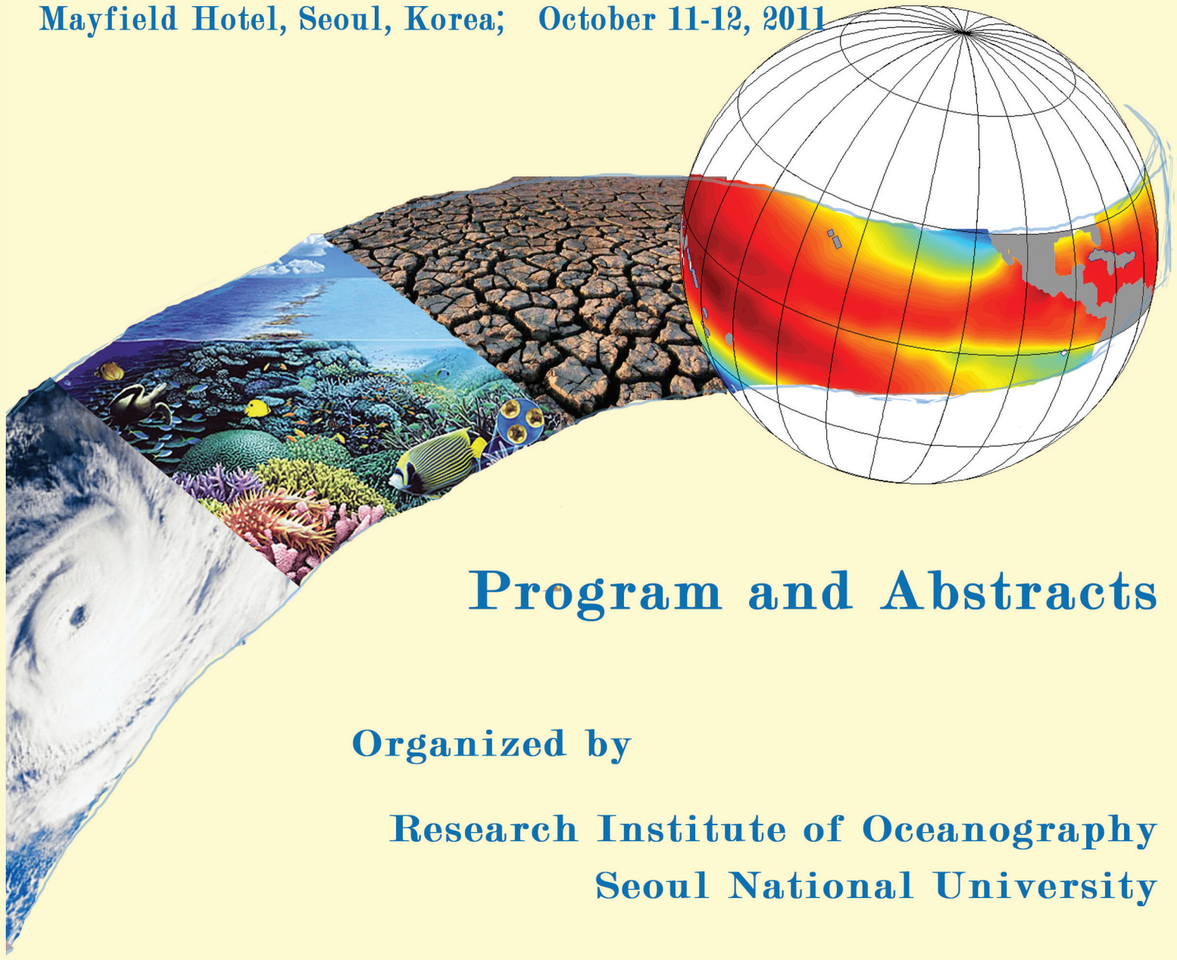

Program and Abstracts

Organized by

Research Institute of Oceanography
Seoul National University

Sponsors

MLTM
Ministry of Land, Transport and Maritime Affairs

RIO

PICES

ICES
CIEM

International Workshop

Development and Application of Regional Climate Models

General Information

Both global and regional numerical climate models are important tools in understanding physical mechanisms involved in and controlling climate change and variability at multiple spatio-temporal scales. They may also provide the unique possibility to construct physically based future climate projections, the starting point for many socio-economic impact and adaptation considerations to future climate change. Global and regional modellings complement each other. While the global coupled general circulation models (GCMs) may be capable of capturing the large-scale mean climate behavior, especially those related to anthropogenic forcing, they often cannot be directly used for assessing regional climate impacts mainly due to their coarse spatial scale. Furthermore, they are usually not successful in capturing regionally important physical processes and reproducing higher order statistics and extreme events. Regional climate modeling has been introduced to fill the gap between the GCMs and the growing demand of climate predictions and scenarios on highly-resolved spatio-temporal scales. Various approaches and parameterizations have been adopted in existing regional climate models (RCMs). This two-day workshop will provide a platform to discuss various aspects of regional coupled or ocean climate modelling such as different approaches, downscaling, parameterizations, and coupling to the GCMs. It will also encompass the coupling of RCMs to ecosystem models.

Dates and venue

The workshop will be held on October 11 – 12, 2011, at Mayfield Hotel, Seoul, Korea.

Conveners

Kyung-Il Chang (POC/PICES)
School of Earth and Environmental Sciences, Seoul National University
E-mail) kichang@snu.ac.kr
Michael Foreman (POC/PICES)
Fisheries and Oceans Canada, Institute of Ocean Sciences
E-mail) mike.foreman@dfo-mpo.gc.ca
Chan Joo Jang (POC/PICES)
Korea Ocean Research & Development Institute

E-mail) cjjang@kordi.re.kr

Myron Peck (ICES)

Institute for Hydrobiology and Fisheries Science, University of Hamburg

E-mail) myron.peck@uni-hamburg.de

Angelica Pena (BIO/PICES)

Fisheries and Oceans Canada, Institute of Ocean Sciences

E-mail) Angelica.Pena@dfo-mpo.gc.ca

Sponsors

Ministry of Land, Transport and Maritime Affairs, Korea

North Pacific Martine Science Organization

International Council for the Exploration of the Sea

Research Institute of Oceanography, Seoul National University

Location

How to get to Mayfield Hotel (http://www.mayfield.co.kr)

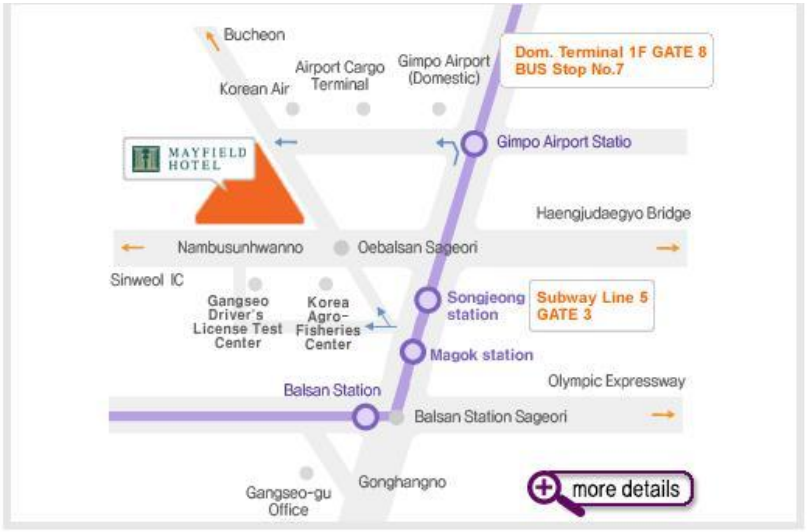

ADDRESS : 426 Balsan-dong, Gangseo-gu, Seoul, Korea 157-290
TEL : 82-2-2660-9000
FAX : 82-2-2660-9001

i) From Incheon International Airport to Hotel: KAL Limousine Bus

ii) From Kimpo Airport to Hotel: Hotel Shuttle Bus

Program

October 11 (Tuesday), 2011

08:30-09:30 **Registration**

09:30-10:00 **Opening**

Prof. Kyung-Ryul Kim (President, RIO/SNU)

(Director General for Marine Environment Policy, MTLM)

Session I. Global and Regional Coupled Models

Chan Joo Jang, Presiding

10:00-10:30 ***Hiroyasu Hasumi (invited)***

Development of a coupled climate model with a two-way nested ocean component

10:30-11:00 ***Hyun-Suk Kang (invited)***

Global and regional climate projections based on the RCP emission scenarios for IPCC AR5

11:00-11:20 *Tea/Coffee Break*

11:20-11:50 ***Tianjun Zhou (invited)***

Air-sea interaction and northwestern summer monsoon variability: A comparison of AGCM and regional ocean-atmosphere coupled model simulations

11:50-12:20 ***Hyodae Seo (invited)***

Regional coupled downscaling: mesoscale air-sea interaction and regional climate change

12:20-14:00 *Lunch Break*

Session II. Regional Ocean Projections

Kyung-Il Chang and Angelica Pena, Presiding

14:00-14:30 ***Bjorn Adlandsvik (invited)***

Dynamical downscaling of future climate in the Barents and North Seas

14:30-15:00 ***Gianmaria Sannino (invited)***
PROTHEUS: The regional climate model for the Mediterranean region

15:00-15:20 ***Cheol-Ho Kim***
Comparison of the sea surface height distribution in the different grid-resolution circulation models

15:20-15:40 ***MinHo Kwon***
Two types of North Pacific variability of ocean: a future projection

15:40-16:10 ***Dong-Hoon Kim (invited)***
Investigation on steric and nonsteric effect on sea level rise projections of the Northwestern Pacific Ocean

16:10-16:30 *Tea/Coffee Break*

16:30-17:00 ***Michael Foreman (invited)***
A regional climate model for the British Columbia continental shelf

17:00-17:30 ***Enrique Curchitser (invited)***
Up-and down-scaling effects of upwelling in the California Current System

17:30-17:50 ***Yang-Ki Cho***
Development of a regional ocean climate model for northwest Pacific marginal seas

18:30-20:30 Welcoming Reception

October 12 (Wednesday), 2011

Session III. Analysis of Climate Models

Kwang-Ryul Kim, Presiding

09:00-09:20 ***Inkweon Bang***
Climate change in the Northwestern Pacific seen in the CSEOF analysis of the SRES A1B simulations of AR4 models

09:20-09:40 ***Chan Joo Jang***
Evaluation of regional ocean simulation from CMIP3 models: a case for

the North Pacific Ocean mixed layer depth

09:40-10:00 ***Hyoun-Woo Kang***

Indonesian throughflow transport change in a warming climate

Session IV. Ecosystem Modeling

Kyung-Il Chang and Corinna Schrum, Presiding

10:00-10:30 ***Myron Peck (invited, ICES)***

New ICES working group on integrative physical, biological and ecosystem modeling: An overview and an invitation

10:30-11:00 ***Icarus Allen (invited)***

Regionally downscaled climate modeling: physics to fisheries

11:00-11:20 *Tea/coffee break*

11:20-11:50 ***Angelica Pena (invited)***

Development a regional plankton ecosystem model for the pacific coast of Canada

11:50-12:20 ***Corinna Schrum (invited)***

Climate change downscaling to marine ecosystems, lessons learnt from downscaling exercises of AR4 and AR5 GCM scenarios

12:20-14:00 *Lunch Break*

14:00-16:00 Poster Presentations

16:00-18:00 Wrap-up and Recommendations

Myron Peck and Michael Foreman, Presiding

What are the big questions in the regional downscaling ?

- Parameterizations
- Boundary conditions
- ??

How to tackle those questions ?

Establishment of ICES/PICES Joint WG

Regular workshop, 2012 Yeosu Sympo. (S3), 2013 Seoul ?

Poster presentations

Qionggiong Cai: The assessment of MJO simulation in the NCEP climate forecast system reanalysis

Sung-Tae Jang: Comparisons of experiments for a nested grid regional forecast model

Hera Kim: Mixed layer depth variability and its associated chlorophyll-a concentration changes in the North Pacific

Jingwei Liu: The extreme summer precipitation over East China during 1982-2007 simulated by LASG/IAP regional climate model

Gyundo Pak: The Japan/East Sea circulation in the MIROC-hires climate model

Taewook Park: Interannual surface salinity variability in the Yellow and East China Seas in response to ENSO

Ok Hee Seo: A numerical experiment on the typhoon intensity change on a warmed ocean using a coupled typhoon-ocean model

Jihyeon So: Mixed layer depth variability & its associated chlorophyll-a concentration changes in the East sea

Dan Sun: Simulation of the East Asian Intraseasonal Oscillation in 1998 with the variable-resoultion model LMDZ

Liwei Zou: Development and evaluation of a regional ocean-atmosphere coupled model with focus on Western North Pacific summer monsoon simulation: Impacts of different atmostpheric components

Affiliation/Country of Presenters

Invited Speakers

BjØ rn Å dlandsvik
Institute of Marine Research, Norway (bjorn@imr.no)
Icarus Allen
Plymouth Marine Laboratory, UK (jia@pml.ac.uk)
Enrique Curchitser
Rutgers University, USA (enrique@marine.rutgers.edu)
Mike Foreman
Institute of Ocean Sciences, Canada (mike.foreman@dfo-mpo.gc.ca)
Hiroyasu Hasumi
University of Tokyo, Japan (hasumi@ccsr.u-tokyo.ac.jp)
Hyun-Suk Kang
Korea Meteorological Administration, Korea (hyunsuk@korea.kr)
Dong-Hoon Kim
Korea Meteorological Administration, Korea (mail@dhkim.info)
Myron Peck
Institute for Hydrobiology and Fisheries Science, Germany (myron.peck@uni-hamburg.de)
Angelica Pena
Institute of Ocean Sciences, Canada (Angelica.Pena@dfo-mpo.gc.ca)
Gianmaria Sannino
Italian National Agency for New Technologies, Energy and Sustainable Economic Development, Italy (Gianmaria.sannino@enea.it)
Corinna Schrum
University of Bergen, Norway (Corinna.Schrum@gfi.uib.no)
Hyodae Seo
Woods Hole Oceanographic Institution, USA (hseo@whoi.edu)
Tianjun Zhou
Chinese Academy of Science, China (zhoutj@lasg.iap.ac.cn)

Contributors

Inkweon Bang
Seoul National University, Korea (Inkweon.bang@gmail.com)
Qiongqiong Cai
Chinese Academy of Science, China (qiongqiongcai@mail.iap.ac.cn)
Yang-Ki Cho
Seoul National University, Korea (choyk@snu.ac.kr)
Chan Joo Jang
Korea Ocean Research & Development Institute, Korea (cjjang@kordi.re.kr)
Sung-Tae Jang
Geosystem Research, Corporation, Korea (stjang@geosr.com)
Hyoun-Woo Kang
Korea Ocean Research & Development Institute, Korea (hwkang@kordi.re.kr)
Chel-Ho Kim
Korea Ocean Research & Development Institute, Korea (chkim@kordi.re.kr)
Hera Kim
Korea Ocean Research & Development Institute, Korea (herassemu@gmail.com)
MinHo Kwon
Korea Ocean Research & Development Institute, Korea (mhkwon@kordi.re.kr)
Jingwei Liu
Chinese Academy of Science, China (liujingwei@mail.iap.ac.cn)
Gyun-Do Pak
Seoul National University, Korea (gdpak@curl.snu.ac.kr)
Taewook Park
Korea Ocean Research & Development Institute, Korea (twpark.kr@gmail.com)
Ok Hee Seo
Korea Ocean Research & Development Institute, Korea (okioki9941@kordi.re.kr)
Jiheon So
Korea Ocean Research & Development Institute, Korea (sojhwlgus@gmail.com)
Dan Sun
Chinese Academy of Science, China (sundan@lasg.iap.ac.cn)
Liwei Zou
Chinese Academy of Science, China (zouliwei@gmail.com)

Development of a coupled climate model with a two-way nested ocean component

Hiroyasu Hasumi[1], Masao Kurogi[2], and Hiroaki Tatebe[2]

[1] Atmosphere and Ocean Research Institute, The University of Tokyo
(hasumi@ccsr.u-tokyo.ac.jp)
[2] Japan Agency for Marine-Earth Science and Technology

1. Background

Since coupled atmosphere-ocean general circulation models (CGCMs) came into practical use for projecting future climate changes, a lot of efforts have been made to improve models and to reduce uncertainties in projection. Increase of resolution is one of the main foci of such efforts. Most of the CGCMs contributing to the second assessment report of the Intergovernmental Panel on Climate Change (IPCC) [*IPCC*, 1995] adopt horizontal resolution of several hundreds of kilometers both for the atmosphere and the ocean, while typical horizontal resolution of 100–200 km has been attained among those contributing to the IPCC fourth assessment report [AR4; *IPCC*, 2007]. Further increase of resolution is still required for both uncertainty reduction and practical application. As for the latter, people's interest in future climate changes has shifted from global views to regional aspects and extreme events such as frequency of hurricanes or torrential rainfall, which necessitate an order of magnitude higher atmospheric horizontal resolution.

For ocean models, horizontal resolution of ~100 km, which is often called coarse-resolution, is unsatisfactory even when looking at large-scale features. Oceanic large-scale circulation is made up of a number of narrow, swift currents. For example, western boundary currents, such as the Kuroshio and the Gulf Stream, occupy only small portion of the ocean (~100 km width for each), while they account for an essential part of oceanic poleward heat transport. Proper modeling of such western boundary currents requires, at least, so-called eddy-permitting horizontal resolution, which is typically 20–30 km at mid-latitudes. For example, the actual Kuroshio separates from the eastern coast of Japan around 35°N and continues to flow eastward as the Kuroshio Extension. Separation of the Kuroshio tends to be realistically simulated under a horizontal grid size of 20 km at ~30°N, while the Kuroshio in coarse-resolution models is know to "overshoot" to the north, flowing along the east coast of Japan to ~40°N [*Hasumi et al.*, 2010]. Their future behavior and/or their influence on future climate

changes can never be appropriately discussed without CGCMs comprised of eddy-permitting ocean models. Upper ocean currents are primarily wind-driven, and recent studies indicate that eddy-permitting ocean resolution, not just an increase of atmospheric resolution, leads to significant improvement of surface winds in CGCMs [*Roberts et al.*, 2004; *Suzuki et al.*, 2005]. In this respect, too, high-resolution ocean models are required for reliable future projection of the ocean.

There already have been some attempts on climate modeling under the regime of eddying ocean. One of the CGCMs participating in IPCC AR4 future climate projection, which is referred to as "MIROC-hires" in the document, employed an eddy-permitting ocean component. Using its result, *Sakamoto et al.* [2005] showed that the Kuroshio and the Kuroshio Extension are significantly accelerated under global warming as a consequence of intensification of the Westerlies. Although a number of successful results have been obtained by ocean-eddy-permitting climate models, it is also obvious that eddy-permitting resolution is not yet satisfactory. Here, an example is also taken from the Kuroshio. Its path south of Japan is known to take two different forms, large-meandering and non-large meandering (Figure 1), and each type of path persists for a few years to a decade [Hasumi, 2010]. The path of the Kuroshio affects not only the climate over the Pacific region but also the fishery environment there as it transports eggs and larvae of some fishery important species. Its future change is of great concern for us. Even with high enough horizontal resolution to reproduce the Kuroshio separation from Japan's coast, however, models tend to have problems in capturing its path and variability south of Japan.

One of the essential treatments for realistically reproducing the Kuroshio path and its variability south of Japan is higher resolution: some modeling studies have shown that the horizontal grid size of at least 10 km is required. It is not currently impossible to globally adopt the 10 km horizontal resolution in CGCMs and conduct climate-oriented simulations, but it is not easy, either. And it is unimaginable that our quest for higher ocean resolution in CGCMs will stop at 10 km. On the other hand, many of the climate-controlling intense oceanic phenomena, including behavior of the Kuroshio, are highly localized. We do not have to apply very high resolution to the entire ocean in dealing with such phenomena. One solution to incorporate the effect of such phenomena into CGCMs is to selectively raise oceanic resolution only in target regions. For that purpose, we have been developing a coupled climate model with a two-way nested ocean component.

2. Model configuration

Results from two types of simulation are reported here. One is an ocean-only simulation targeted at the problem of Kuroshio path variability, and the other is a

CGCM simulation. The nested-grid ocean model utilized in both types of simulation is based on COCO [Hasumi, 2006], which is a z-coordinate ocean general circulation model and horizontally formulated on the generalized curvilinear coordinate. A regional model of relatively high resolution (an inner model) is nested into a global model of relatively low resolution (an outer model). The data exchange between the two models is two-way: the outer model provides data at lateral boundaries of the inner model, and the data of the outer model is overwritten by the inner model data in the overlapping region. The outer model employs a tripolar grid system: the region to the south of 60°N is covered by the regular longitude-latitude coordinate which has one singular point (pole) at the South Pole, and the region to the north is covered by a different curvilinear coordinate which has two singular points on 60°N (Figure 2).

For the ocean-only simulation, the horizontal resolution of the outer model in the longitude-latitude coordinate region is $0.5° \times 0.5° \cos\phi$ (zonal and meridional, respectively, where ϕ is latitude), and that of the inner model, whose domain covers 116°E-180°E and 15.6°N-53.6°N, is $0.1° \times 0.1° \cos\phi$. Both inner and outer models have 50 vertical levels, whose thickness is 2.5 m for the top level, increases with depth, and takes 250 m for the deepest level. The model is initiated by climatological temperature and salinity fields (WOA2001) and forced by climatological surface fluxes (CORE normal year forcing). Model integration is continued for 40 years.

For the CGCM simulation, the nested-grid ocean model described above is embedded in a coupled climate model MIROC [Hasumi and Emori, 2004]. Horizontal resolution of the atmospheric model is about 60 km. A control climate simulation is conducted where the external forcing (solar constant, atmospheric composition, and land use) is fixed at that of the preindustrial condition.

3. Results

The ocean-only simulation exhibits repeated emergence of the two major types of the Kuroshio path south of Japan (Figure 3). Duration of each path, a few years to a decade, is fairly realistic, and the transition processes characterized by growth of small meander and eddy separation are consistent with observed features. To our knowledge, this is the first successful simulation of spontaneous repetition of the two types of path. Some previous attempts succeeded in simulating the transition of path from non-large-meandering to large-meandering and then back to non-large-meandering with realistic transition processes, but duration of the large-meandering path was too short and only one transition event was simulated [Miyazawa et al., 2004; Tsujino et al., 2006].

Observations have shown that no stable large-meandering path has been realized since 1990, and a modeling study of an idealized setup suggests an influence of global

warming [Kurogi and Akitomo, 2006]. We also conducted another simulation by modifying the sea surface boundary condition to roughly incorporate warming of the upper ocean over past decades. Its result indicates that the large-meandering path becomes difficult to appear. We will report its detail in the presentation, together with the result of the CGCM simulation

References

IPCC (1995), *Climate change 1995*: *The Science of climate change*, edited by J. T. Houghton, L. G. Meira Filho, B. A. Callender, N. Harris, A. Kattenberg, and K. Maskell, 572 pp., Cambridge Univ. Press, Cambridge.

IPCC (2007), *Climate change 2007–The Physical Science Basis*. contribution of Working Group I to the Fourth Assessment Report of the IPCC, edited by S. Solomon, D. Qin, M. Manning, 996 pp., Cambridge Univ. Press, Cambridge.

Hasumi, H. (2006), CCSR Ocean Component Model Version 4.0, *CCSR Report*, **25**, http://www.ccsr.u-tokyo.ac.jp/~hasumi/COCO/.

Hasumi, H., and S. Emori (2004), K-1 coupled model (MIROC) description, *K-1 Technical Report*, **1**, 34 pp., Center for Climate System Research, University of Tokyo.

Hasumi, H., T. Tatebe, T. Kawasaki, M. Kurogi, and T. T. Sakamoto (2010), Progress of North Pacific modeling over the past decade, *Deep-Sea Res. II*, **57**, 1188-1200.

Kurogi, M., and K. Akitomo (2006), Effects of stratification on the stable paths of the Kuroshio and on their variation, *Deep-Sea Res. I*, **53**, 1564-1577.

Miyazawa, Y., X. Guo, and T. Yamagata (2004), Roles of mesoscale eddies in the Kuroshio paths, *J. Phys. Oceanogr.*, **34**, 2203-2222.

Roberts, J. M, H. Banks, N. Gendney, J. Gregory, R. Hill, S. Mullerworth, A. Pardaens, G. Rickard, R. Thorpe, and R. Wood (2004), Impact of an eddy-permitting ocean resolution on control and climate change simulations with a global coupled GCM, *J. Climate*, **17**, 3–20.

Sakamoto, T. T., H. Hasumi, M. Ishii, S. Emori, T. Suzuki, T, Nishimura, and A. Sumi (2005), Responses of the Kuroshio and the Kuroshio Extension to global warming in a high-resolution climate model, *Geophys. Res. Lett.*, **32**, L14617, doi:10.1029/2005GL023384.

Suzuki, T., T. T. Sakamoto, T. Nishimura, N. Okada, S. Emori, A. Oka, and H. Hasumi (2005b), Seasonal cycle of the Mindanao Dome in the CCSR/NIES/FRCGC atmosphere-ocean coupled model, *Geophys. Res. Lett.*, **32**, L17604 doi:10.1029/2005GL023666.

Tsujino, H., N. Usui, and H. Nakano (2006), Dynamics of Kuroshio path variations in a high-resolution general circulation model, *J. Geophys. Res.*, **111**, C11001,

doi:10.1029/2005JC003118.

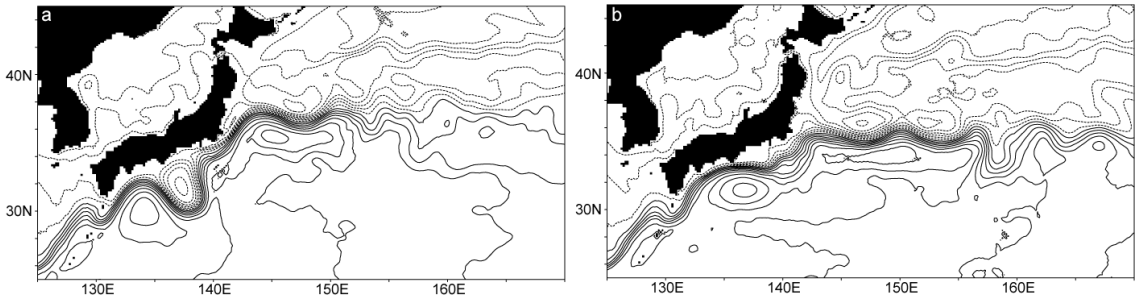

Figure 1. Annually averaged sea surface height, whose contours coincide well with streamlines of surface currents, in the Kuroshio region simulated by an eddy-permitting ocean model for (a) large-meandering and (b) non-large-meandering cases. Contour interval is 0.1 m.

Figure 2. An example for grid cell configuration of the nested-grid ocean model. White lines indicate grid cells, and the inner model domain is bonded by red lines.

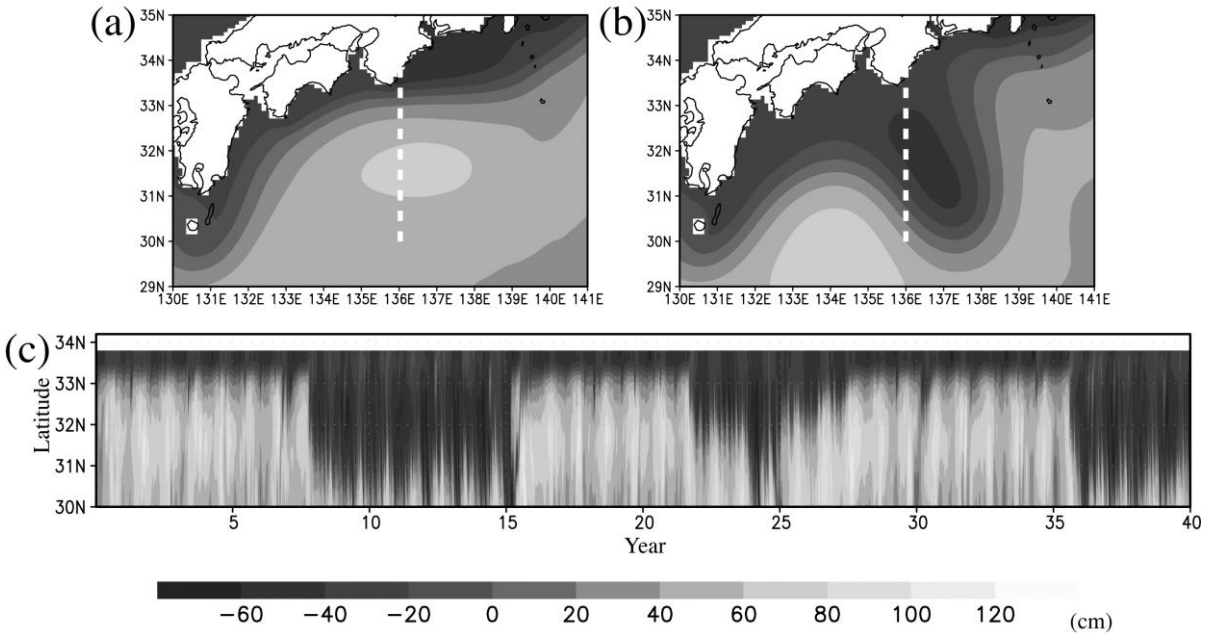

Figure 3. (a) Sea surface height averaged from year 30 to 35 and (b) from year 36 to 40 of the ocean-only simulation. (c) Time evolution of the sea surface height along 136.05°E (dotted lines in (a) and (b)).

Global and Regional Climate Projections based on RCP Emission Scenarios for IPCC AR5

Hyun-Suk Kang, Suhee Park, In-Hye Lee, and Chunho Cho

with many colleagues at

Climate Research Laboratory, National Institute of Meteorological Research
Korea Meteorological Administration
(hyunskang@korea.kr)

1. Introduction

Estimation and assessment of potential anthropogenic climate change in the future have been an important component of the Intergovernmental Panel on Climate Change (IPCC) working groups' activities. Since the latest assessment report (AR4) in 2007, IPCC is now preparing to update new scenarios for a possible Fifth Assessment Report (AR5) based on Representative Concentration Pathways (RCP) emission scenarios by 2013. In order to meet this timeline, global and regional climate modeling communities organized common frameworks to produce climate projection datasets, which are called CMIP5 and CODEX, respectively. Korea Meteorological Administration (KMA) is participating both the CMIP5 and CORDEX research programs by collaboration with Met Office Hadley Centre of UK, not only for contributing IPCC AR5 but also for supporting national policy of the Korean government on climate change. In this talk, fundamental features obtained from the global and regional climate projections based on RCP 4.5 and 8.5 emission scenarios are introduced.

2. RCP Emission Scenarios

According to the IPCC expert meeting report (Moss et al., 2008), RCPs are referred to as ***pathways*** to emphasize that it is to provide time-dependent projections of atmospheric greenhouse gas concentrations, which means that it is not only a specific long-term concentration but also the trajectory taken over time to reach a specific level. RCPs are ***representative*** since they are one of several different scenarios that have similar radiative forcing and emissions characteristics. Table 1 summarizes the RCP's CO_2 concentration compared with that of SRES (Special Report on Emission Scenarios), which was used for the AR4. Because the incoming solar radiation at top of the atmosphere (TAO) is about 238 Wm^{-2}, the amount of changes in radiative forcing for the RCP 8.5, 6.0, 4.5, and 2.6 corresponds 3.6, 2.5, 1.9, and 1.1%, respectively.

Table 1. Types of representative concentration pathways (adapted from Moss et al., 2008)

Name	Radiative forcing[1]	Concentration[2](ppm)	Pathway type	SRES
RCP 8.5	> 8.5 Wm^{-2} in 2100	> 1370 CO_2-eq in 2100	Rising	A2(830)~A1FI(970)
RCP 6.0	~ 6.5 W/m^2 (at stabilization after 2100)	~ 850 CO_2-eq (at stabilization after 2100)	Stabilization w/o overshoot	B2(600)~A1B(720)
RCP 4.5	~ 4.5 W/m^2 (at stabilization after 2100)	~ 650 CO_2-eq (at stabilization after 2100)	Stabilization w/o overshoot	B1(550)
RCP 3-PD[3]	Peak at ~ 3W/m^2 before 2100 and then decline	Peak at ~490 CO_2-eq before 2100 and then decline	Peak and decline	N/A

Notes:
[1] Approximate radiative forcing levels were defined as ±5% of the standard level in W/m2. Radiative forcing values include the net effect of all anthropogenic GHGs and other forcing agents.
[2] Approximate CO_2 equivalent (CO_2-eq) concentrations, which were calculated with the simple formula Conc = 278* exp(forcing/5.325). Note that the best estimate of CO_2-eq concentration in 2005 for long-lived GHGs only is about 455 ppm, while the corresponding value including the net effect of all anthropogenic forcing agents (consistent with the table) would be 375 ppm CO_2-eq.
[3] PD = peak and decline

3. Models and Simulation Design

The HadGEM2-AO (Collins et al., 2008) and HadGEM3-RA (Moufouma-Okia et al., 2011) are used to produce global and regional climate projections, respectively. HadGEM2-AO is a fully atmosphere-ocean-sea ice coupled model, in which the spatial resolution is about 130 km in the horizontal and 38 layers in the vertical with the top of 80 km-level from the surface. Meanwhile, the HadGEM3-RA for regional downscaling is the regional version of atmospheric component of the HadGEM3. Particularly, HadGEM3-RA for regional downscaling was applied for two domains: one of them covers quite huge area of Asia with the horizontal grid distance of 50 km, and the other one mainly covers Korean peninsula with the grid distance of 12.5 km. Please note that configuration of model domain and physics are made as close as possible in accordance with the frameworks of CMIP5 (http://cmap-pcmdi.llnl.gov/cmip5) and CORDEX (http://www.meteo.unican.es/en/projetcs/CORDEX).

Prior to integrate the global coupled model for representing current climate, spin-up period to reach an equilibrium status of the model climatology is essential. Therefore, the HadGEM2-AO was run for 200 years with the preindustrial GHG forcings as of 1850. In this preindustrial run, 200-year-long integration for spin-up is definitely not sufficient for a coupled model to reach an equilibrium status; however, it can be considered as an ensemble member of climate projections (500-year-long and 700-year-long preindustrial simulations are also on going.) Historical run is made with the observed GHG forcings for the period of 1850-2005, and then RCP 8.5 and 4.5 forcings are given to derive climate projections for the period of 2006-2100. Regional downscaling simulations also consist of three experiments; one is the evaluation run in which the lateral boundary forcing are given by observed reanalysis, another is the

historical run forced by HadGEM2-AO's historical outputs, and the other is the projection runs forced by HadGEM2-AO's RCP outputs.

4. Results

4.1 Global Projections

Global projection in terms of global mean temperature and precipitation by the end of the 21st Century obtained from the HadGEM2-AO RCP 4.5 and 8.5 scenarios are summarized in Table 2. It shows that increases in global mean temperature are about 2.8°C and 4.8°C for RCP 4.5 and 8.5 scenarios, respectively. Meanwhile, precipitation increases are about 4.5 and 6.0% for the 4.5 and 8.5 scenarios. Temperature increase is profound in entire globe especially for the region of northern hemispheric land area, while the precipitation increase is limited in some particular regions. Decrease of precipitation appears in Australia, southern Europe, north and south Africa. Increase of temperature and precipitation over land of East Asia including Korea peninsula are 3.6°C (RCP4.5), 6.5°C (RCP8.5) and 12.3% (RCP4.5), 15.2% (RCP8.5), respectively, which are greater than those of the global mean (see Fig. 1). A few more concerns such as sea-ice melting, soil moisture which is associated with changes in precipitation and temperature, and some extreme climate events are also analyzed.

Table 2. Global mean projection by the end of the 21th Century.

RCP		4.5 (540 ppm[1])	8.5 (940 ppm[1])
Global mean	Temperature[2] (°C)	2.8	4.8
	Precipitation (%)	4.5	6.0
	Sea level rise[3] (cm)	21.9	29.7

[1] CO2 concentration in 2100
[2] 30 years (2070-2099) average compared to current 30 years (1971-2000)
[3] Caused by thermal expansion

4.2 Regional Projections

In this section, major results from the evaluation runs using the HadGEM3-RA are briefly introduced in order to give an insight on the overall performance of the regional model. Results from the historical and projection runs will be discussed in the presentation. In terms of 20-year-long annual mean, precipitation and surface air temperature distributions for the East Asia domain are comparable between ERA-Interim and HadGEM3-RA. However, the model shows systematic cold and wet biases of which the values are about -1.41°C and 0.23 mm day^{-1} for surface temperature and precipitation, respectively, particularly over land area (Fig. 2). In order to investigate how effectively the regional model adds regional details, we compare the results simulated by HadGEM3-RA (12.5 km resolution's over Korea) and HadGEM2-AO for

the period of 1989-2008. It is found that the HadGEM3-RA simulates well small-scale mean climate, climate variability, especially around mountain and coastal regions. Though 50 km domain's simulation represents similar to HadGEM2-AO for climate annual cycle in East Asia domain, those from 12.5 km domain's simulation is much better than that of HadGEM2-AO for climate annual cycle of precipitation and surface air temperature in South Korea. Particularly, local maxima/minima of precipitation and surface air temperature simulated by the 12.5 km's domain coincides pretty well compared with the observed features (Fig. 3). This feature implies that the RCM simulates current climate more realistically than the GCM over complicated topography and coastal area. Also, the RCM is much better at simulating and projecting changes to extremes, such as annual maximum daily precipitation amount and daily maximum temperature. More detailed results including projected regional climate change will be discussed in the presentation.

References

Moufouma-Okia et al., 2011: Predicting and understanding African climate drivers using the HadGEM3 modelling system, CORDEX conference, Trieste, Italy, 24 March 2011

Collins W. J., and co-authors, 2008: *Evaluation of the HadGEM2 model*, Hadley Centre Technical Note, 74, Met Office.

Moss, R. and co-authors, 2008: *Towards new scenarios for analysis of emissions, climate change, impacts, and response strategies*, IPCC, Geneva, 132pp.

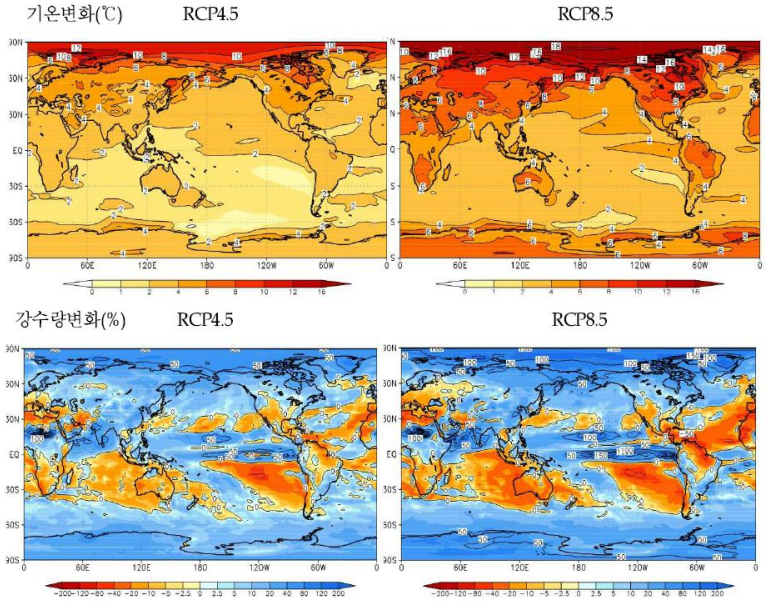

Figure 1. Changes in surface air temperature (^{o}C, upper) and precipitation (%, lower) at the end of the 21th Century (2070-2099) compared with the current climate (1979-2000).

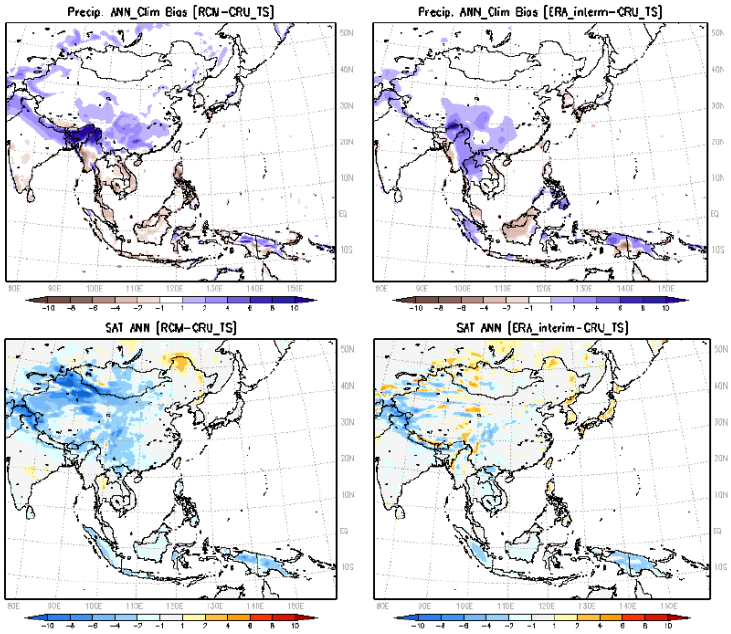

Figure 2. Difference of 20-yr mean annual precipitation (upper) and surface air temperature (lower) from observations.

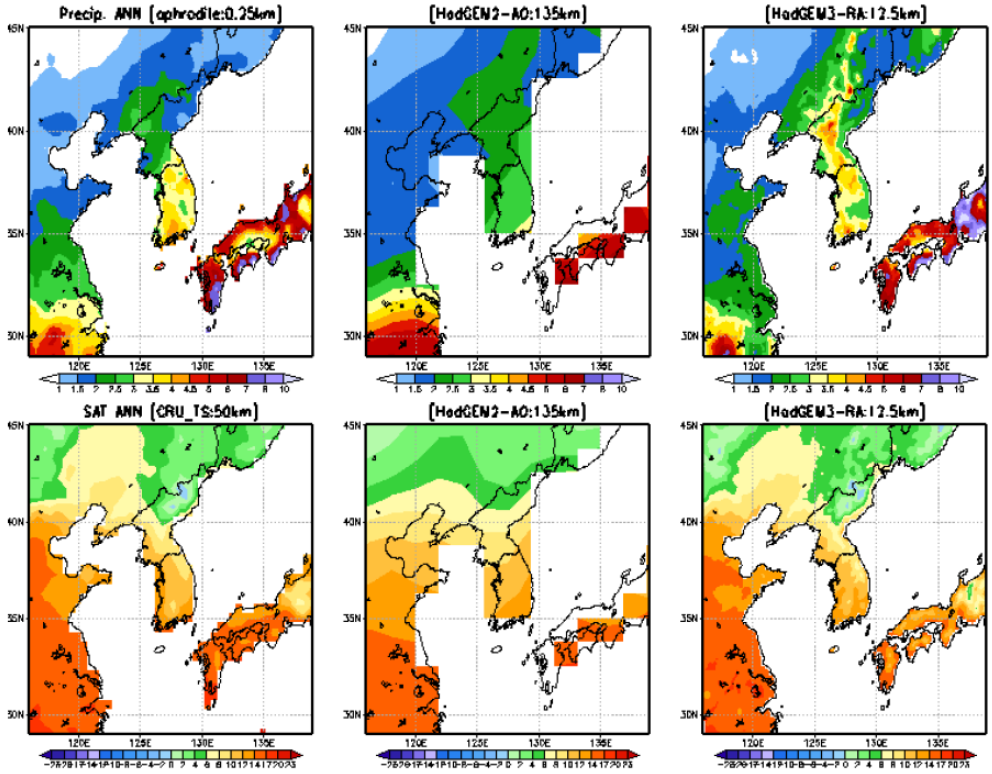

Figure 3. 20-yr mean annual precipitation and surface air temperature (1989~2008).

Air-Sea Interaction and Northwestern Summer Monsoon Variability: A Comparison of AGCM and Regional Ocean-Atmosphere Coupled Model Simulations

ZHOU Tianjun, ZOU Liwei, WU Bo, WANG Lu

LASG, Institute of Atmospheric Physics, Chinese Academy of Sciences,
Beijing, China
(zhoutj@lasg.iap.ac.cn)

ABSTRACT

The Asian-Australian monsoon (AAM) region, spanning from about 40ºE to 160ºE and from 30ºS to 40ºN, covers one-third of the global tropics and subtropics. The economy and society across the region are critically influenced by the evolution and variability of the monsoon. However, numerical simulation and prediction of the AAM interannual variability based on Atmospheric General Circulation Model (AGCM) has been a challenge. The difficulty in simulating and predicting AAM rainfall is partially related to the strategies of the AGCM-alone simulation.

Previous studies suggested that local monsoon-warm pool ocean interactions should be considered in the prediction of summer monsoon rainfall. The poor performance in simulation of Asian summer monsoon variability with AGCMs forced by observed SST is attributed to the experimental design, in which the atmosphere is forced to respond to the specified SSTs, while in nature the SSTs are also partly forced by the atmosphere. In the absence of the monsoon-ocean interaction, the SST-rainfall correlations yielded by AGCMs are at odds with observations in some portions of the AAM domain, in particular the northwestern Pacific. Thus an accurate simulation and prediction of the northwestern Pacific summer monsoon may depend on either global or regional ocean-atmosphere coupled models.

With the motivation to understand the relationships between air-sea interaction and the northwestern summer monsoon variability, and also to improve the skill of northwestern summer monsoon simulation, the authors have devoted great efforts to the modeling studies of the broad Asian-Australian monsoon system. In this presentation, the authors will address the following questions:

1. How well do Atmospheric General Circulation Models capture the leading modes of the interannual variability of Asian-Australian Monsoon?

Observational analysis has identified two statistically distinguished modes of AAM

that represent the highly predictable part of AAM precipitation variability. The two leading modes account for about 38% of the total interannual variances of AAM rainfall for the period 1979-1999. The observed leading modes of the AAM system are revealed by applying the S-EOF analysis to CMAP rainfall seasonal anomalies (1979-1999). The seasonal evolutions of the spatial patterns of AAM rainfall anomalies associated with S-EOF1 are shown in Fig. 1a. The notable feature of S-EOF1 (Fig. 1a) is two seasonal anti-cyclonic anomalies, the South Indian Ocean (SIO) and the western North Pacific (WNP) anticyclones (AC). During JJA (0), an anomalous AC ridge extends from maritime continent to the southern tip of India with enhanced monsoon westerly extends from India to the western Pacific. From SON(0) to D(0)JF(1), the SIO AC slightly weakens, meanwhile a new AC forms over the Philippine Sea. Associated with the anomalous circulation patterns, the dry and wet centers exhibit prominent seasonal evolutions (Fig. 1a). During JJA(0), there are less rainfall over the maritime continent and equatorial eastern Indian Ocean. An enhanced rainfall is evident over the equatorial western Pacific and the Philippine Sea. During D(0)JF(1), the center of dry anomalies shifts to the Philippine Sea.

The spatial patterns of S-EOF2 in observation are shown in Fig. 1b. A large-scale cyclonic anomaly forms over the WNP in the summer to fall, followed by a continuous southeastward movement and strengthening through the following winter and next spring. Following the seasonal evolution of the WNP cyclonic wind anomalies, excessive rainfall occurs over the WNP in JJA(0), and then shifts equator-ward in SON(0). Dry anomalies develop in the northern Indian Ocean and South China Sea in D(0)JF(1), and over the eastern Indonesia and northern Australia in MAM (1).

To answer the question whether these leading modes can be captured by AGCM with prescribed SST forcing, eleven AGCMs that participated in the AMIP, which used observational SST to drive AGCMs for the period 1979-1999, are evaluated by comparing with the observation. The results of Multi-Model Ensemble (MME) are shown in Figure 2. Significant skills are found. The main findings are listed below.

(1) The MME of AMIP simulation captures most part of the realistic features of the spatial structure, seasonal evolution, temporal variations, and the relationship with ENSO in terms of the two major modes of AAM rainfall. The MME reasonably estimates both the biennial tendency and low frequency of the leading modes (Figure 2). While the first mode generally concurs with the turnabout of El Nino, the second mode is a response to La Niña forcing at decaying stage.

(2) The prominent feature of the first leading mode of AAM variability is two seasonal anti-cyclonic anomalies, the SIO and the WNP ACs (Figures 1-2). There exists a phase-shift in the simulated first dominant mode. The seasonal evolution of both SIO and WNP ACs in AMIP simulation strictly matches that of El Nino remote forcing, while in observation it is not absolutely in phase with ENSO forcing. The reasonable part of AMIP simulation in reproducing the main features of the first leading mode indicates the dominance of remote El Nino forcing in driving interannual variability of AAM, meanwhile the deficiency of AMIP simulation in reproducing the seasonal phase of SIO and WNP ACs suggests the essential role of ocean-atmosphere coupling (Figure 3).

(3) The first two leading modes of the interannual variability of AAM mainly reflect rainfall variations over the tropical regions, especially the maritime continent, tropical eastern Indian Ocean and western Pacific. The MME reasonably captures the

two major modes, with results comparable to or even slightly better than those of reanalysis in the tropical regions. Since the two modes explain a high variance of the tropics, the MME presents a high skill in reproducing the total rainfall variability in the region. Over the extra-tropical western North Pacific and South China Sea, where ocean-atmosphere coupling may be critical for modeling the monsoon rainfall, the MME shows barely any skill, but the reanalysis has higher skill due to the inclusion of part of ocean-atmosphere coupling from the 6-12 hrs updating cycle.

(4) The performance of AMIP simulation in reproducing the leading modes of AAM rainfall is seasonally dependent. The skills of DJF, SON, and MAM are better than that of JJA. This seasonal difference suggests that treating the atmosphere as a response to ocean forcing in DJF and transitional seasons is more reasonable than that in JJA.

(5) The MME shows comparable or even slightly better skill than the reanalysis in capturing the tropical signals associated with the two major modes. Although the superiority of MME relative to re-analysis data may stem from the ensemble technique, the GFDL AM2, HadGEM1 and ECHAM5 models are superior to other AGCMs in capturing the leading modes of AAM. Accurate model climatology generally coincides with good anomaly patterns associated with the leading modes.

2. How to improve the performance of LASG/IAP Regional Ocean Atmosphere coupled model over the northwestern summer monsoon domain: Sensitivity of the model to convection parameterization?

With the motivation to improve the simulation of Western North Pacific (WNP) summer monsoon, the regional climate model RegCM3 is coupled with the Princeton ocean model (POM2000) through the coupler OASIS3.0 (Ocean Atmosphere Sea Ice Soil 3.0). The performance of the regional ocean-atmosphere couple model (hereafter **LASG/IAP ROAM**) is assessed by doing case simulation of 1998 summer monsoon. The cold bias of simulated sea surface temperature (SST) is evident as previous ROAM simulations over Asian-Australian summer monsoon region. Five sets of sensitivity experiments with convection suppression criterion based on the averaged relative humidity from cloud base to cloud top are designed to improve the performance of ROAM. The results of SST bias improvement are shown in Figure 4.

The results show that the column averaged cloud fraction is reduced in convection suppression experiments. A reduction of column averaged cloud cover, which is dominated by the decrease of convective cloud cover, increases the solar shortwave radiation reaching in sea surface, then warms the SST. A reduction of convective rainfall is followed by an increase of large scale rainfall which results from an increasing cloud water. When the critical value is set to 0.70, the rainfall is partly improved in terms of the spatial distribution and root mean square error. The percentage of convective rainfall over WNP is also improved. The authors show evidence that the SST cold bias, which are evident in many regional ocean-atmosphere coupled models in Asian-Australian summer monsoon region, may partly stem from the overestimation of convection frequency by the atmospheric model.

3. How well does LASG/IAP Regional Ocean-Atmosphere coupled model capture the interannual variability of northwestern summer monsoon?

To examine the performance of LASG/IAP ROAM in the simulation of the interannual variability of Western North Pacific Summer Monsoon (WNPSM), a continuous long-term simulation covering the period of 1983-2007 was done by using the regional ocean-atmosphere coupled model. A comparison of model simulations against the observation is shown in Figure 5.

The results highlight the importance of air-sea coupling in simulating the interannual variability of WNPSM. Compared with control simulation forced with observed SST, the ROAM simulation shows improvement in the simulation of climatology and interannual variability of rainfall. The leading mode of rainfall variability and associated anomalies of circulation are more reasonably simulated in ROAM simulation than those in the control simulation without regional air-sea coupling. In observation, corresponding to the negative rainfall anomalies over WNP region, the anomalous anticyclone and associated subsidence are evident in lower troposphere. The subsidence leads to the decrease of cloud, and then increases the net shortwave radiation reaching at sea surface. The RegCM3 simulation forced by observed SST shows an anomalous cyclone north of 20°N since the climatology of summer-mean rainfall in RegCM3 simulation is weaker than that in observation. Due to the colder SST and weaker SST anomalies in couple simulation, the ROAM partly reproduces the anomalous anticyclone at lower troposphere and associated physical mechanism, while the anomalous anticyclone shows westward shift and is weaker than that in observation. The resemblance between regional coupled simulation and the simulation forced by the SST derived from coupled simulation confirms that the weaker forcing of SST improves the response of RegCM3 to the driving fields at the lateral boundary.

In addition to above results, the results of CMIP3 global coupled models in the simulation of the leading modes of the interannual variability of Asian-Australian monsoon may also be shown, pending on the time limit of the presentation.

REFERENCES

Zhou, T., B. Wu, and B. Wang, 2009: How well do Atmospheric General Circulation Models capture the leading modes of the interannual variability of Asian-Australian Monsoon? ***Journal of Climate***, **22**, 1159-1173

Zhou, T., R. Yu, H. Li, and B. Wang, 2008: Ocean forcing to changes in global monsoon precipitation over the recent half century, ***Journal of Climate***, **21** (15), 3833–3852

Zhou, T., B. Wu, A. A. Scaife, S. Bronnimann, et al., 2009: The CLIVAR C20C Project: Which components of the Asian-Australian Monsoon circulation variations are forced and reproducible? ***Climate Dynamics***, **33**, 1051-1068, DOI 10.1007/s00382-008-0501-8

Li, B., and **T. Zhou** (2011), El Niño–Southern Oscillation–related principal interannual variability modes of early and late summer rainfall over East Asia in sea surface

temperature-driven atmospheric general circulation model simulations, ***J. Geophys. Res.***, 116, D14118, doi:10.1029/2011JD015691

Zou, L., and **T. Zhou**, 2011: Sensitivity of a Regional Ocean-Atmosphere Coupled Model to Convection Parameterization over Western North Pacific, ***J. Geophys. Res.***, Accepted and In Press

Zou, L., and **T. Zhou**, 2011: Interannual variability of northwestern summer monsoon simulated by LASG/IAP Regional Ocean-Atmosphere coupled model. ***Journal of Climate***, to be submitted.

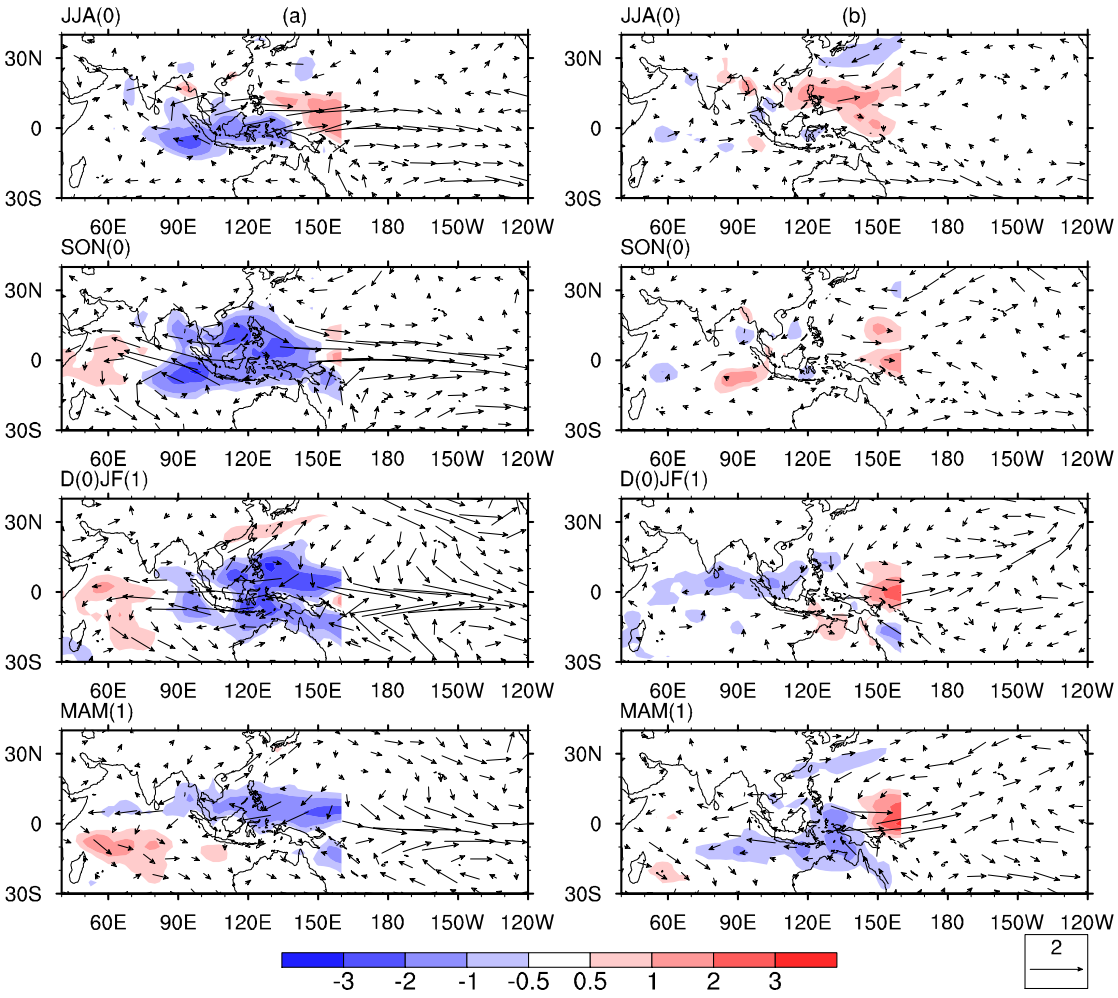

Figure 1. (a) Spatial patterns of the first S-EOF mode of seasonal precipitation anomalies from JJA(0) to MAM(1) (color shading, units of mmday^{-1}) and the NCEP-2 850 hPa wind anomalies (vectors, unit of ms^{-1}), which were linearly regressed against the corresponding principal component. (b) Same as in (a) except for the 2nd S-EOF mode.

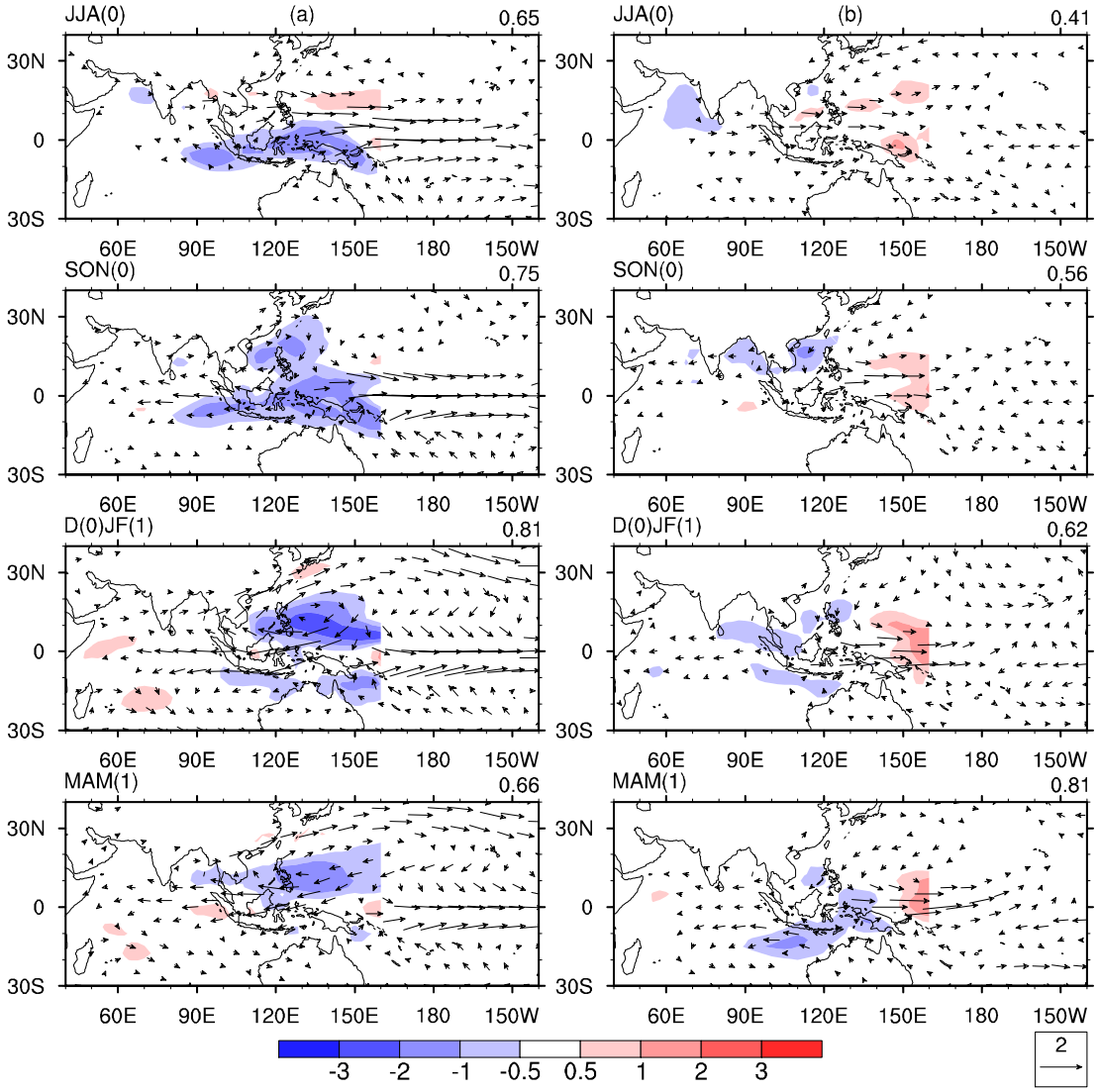

Figure 2. Same as **Figure 1** except for MME of AMIP2 models. Spatial pattern correlations of rainfall anomalies with the observation are marked at the right upper corner of each panel.

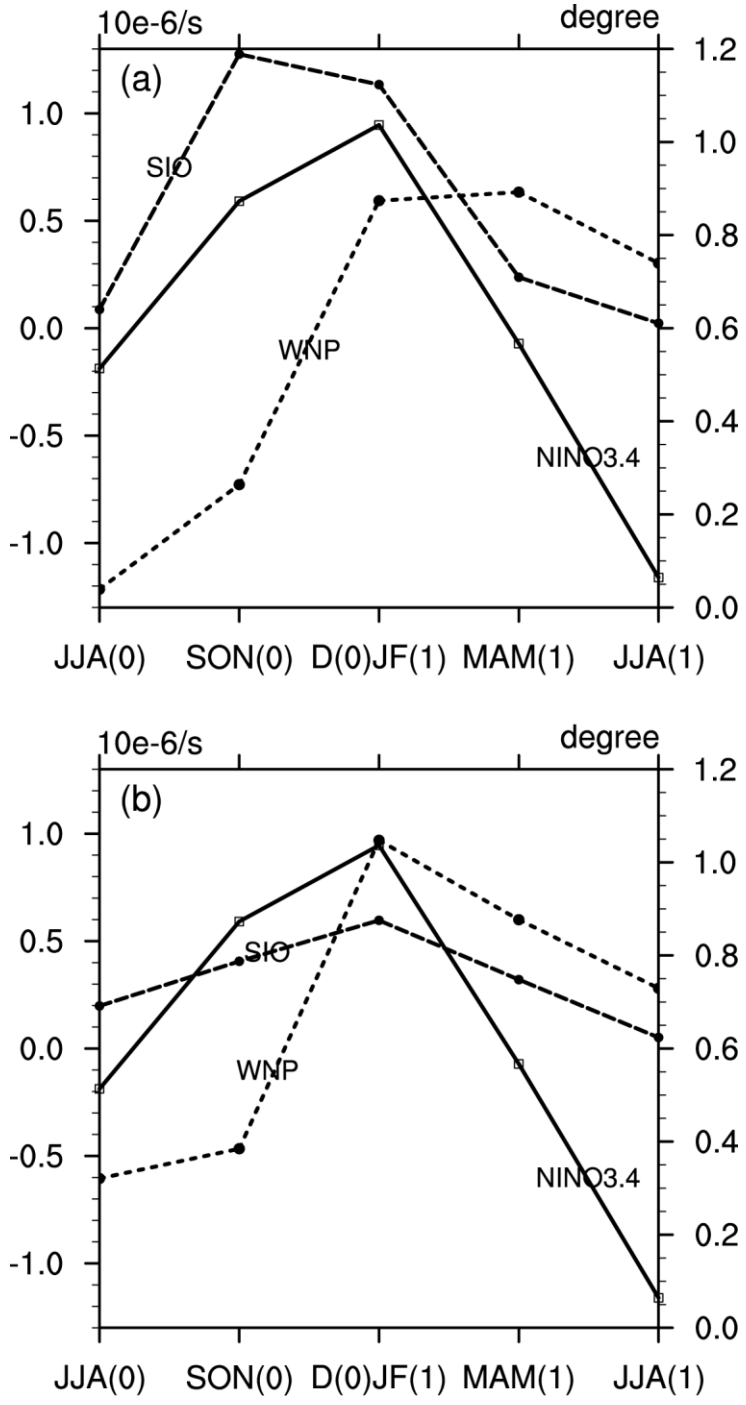

Fig 3. Seasonal variations of the anomalous SIO anticyclonic vorticity averaged over the region of 5ºS–20ºS, 60ºE–100ºE, and the anomalous WNP anticyclonic vorticity averaged over the region of 5ºN–20ºN, 120ºE–160ºE. The sign of WNP vorticity is reversed for easy comparison. Shown also are the regressed NINO3.4 SST anomalies with respect to the first principal component of the S-EOF mode. (a) NCEP-2 Reanalysis, (b) AMIP MME.

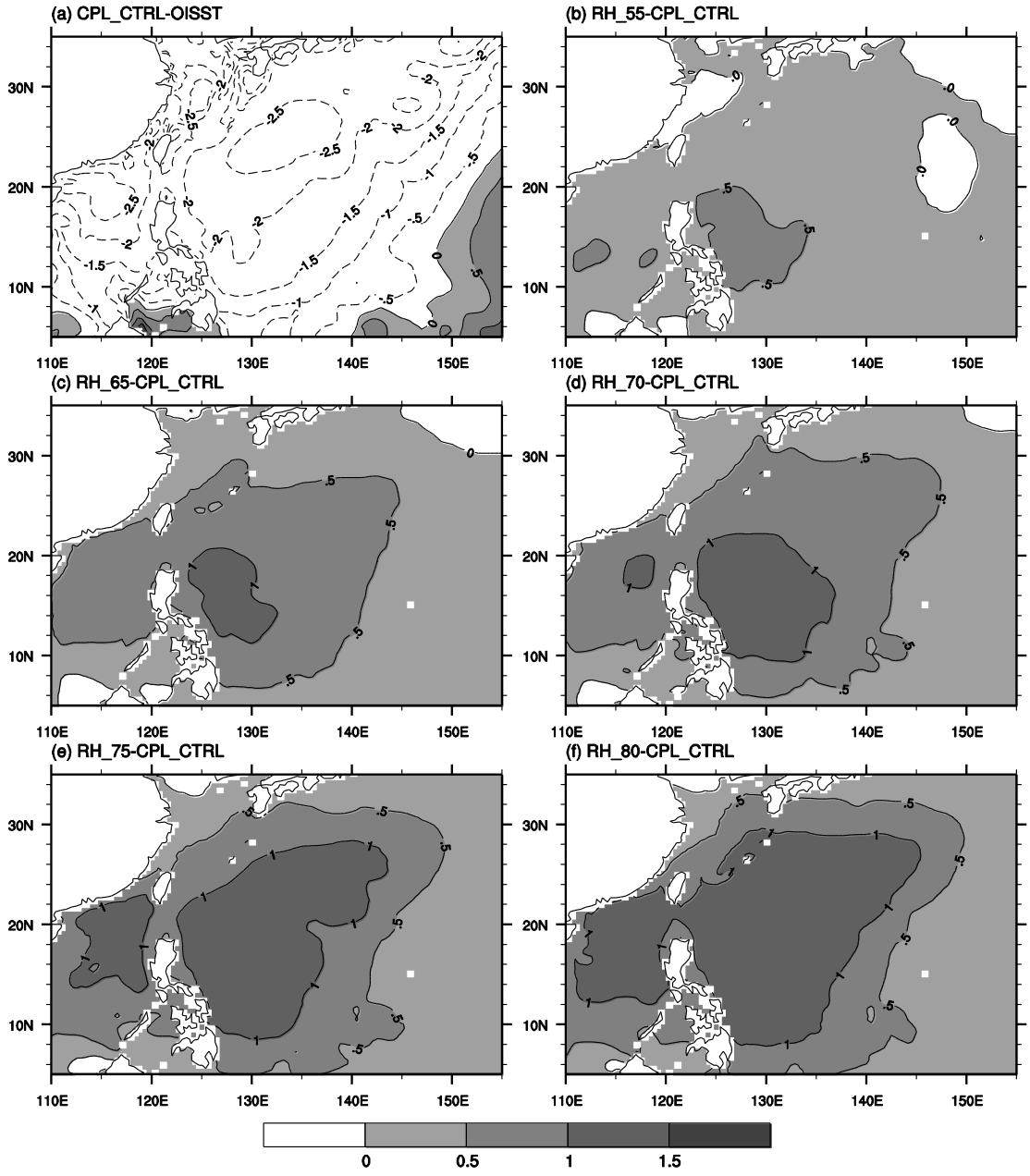

Figure 4. (a) Spatial distribution of SST difference (℃) between the control run of LASG/IAP ROAM and OISST averaged from May to August of 1998. (b-f) the SST difference (℃) between sensitivity experiments and the control run. Five sets of sensitivity experiments are designed and the convection suppression criterion of mean Relative Humidity (RH) is set to 0.55, 0.65, 0.70, 0.75 and 0.80, receptively. These 5 sets of sensitivity experiments are termed as "RH_55", "RH_65", "RH_70", "RH_75" and "RH_80", respectively.

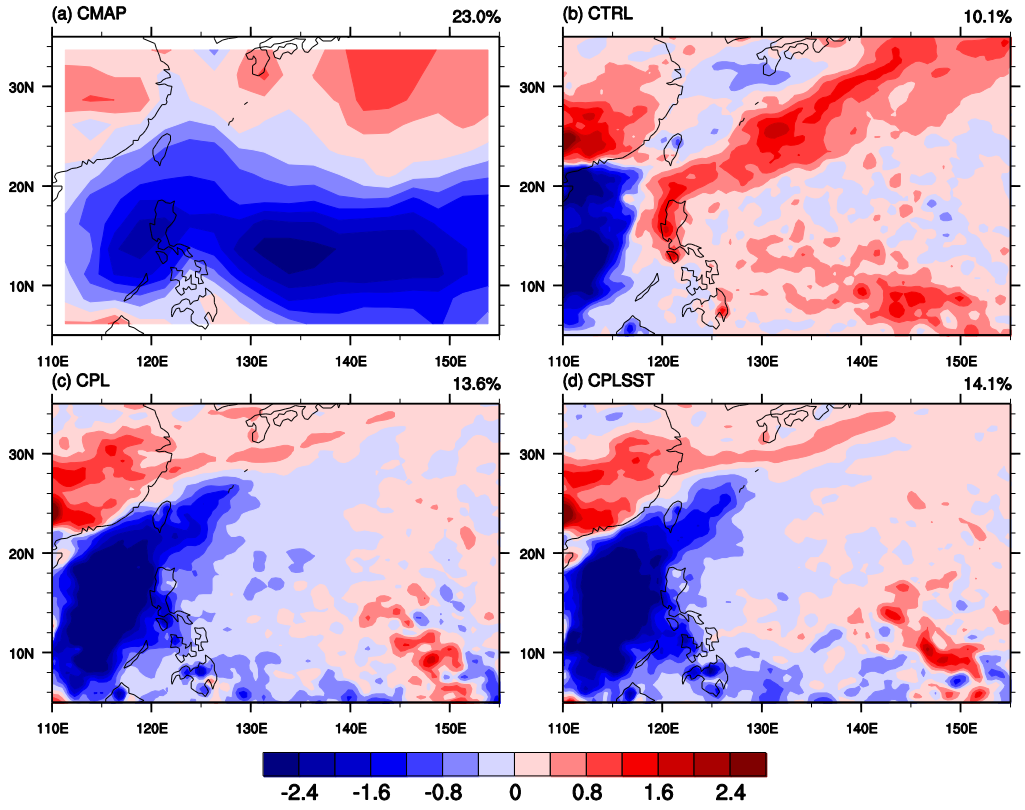

Figure 5. The 1st EOF mode of summer rainfall during 1983-2007 derived from: (a) CMAP data, (b) RegCM3 run forced by historical SST, (c) ROAM, and (d) RegCM3 run forced by the SST predicted by ROAM.

Regional coupled downscaling:

mesoscale air-sea interaction and regional climate change

Hyodae Seo

Woods Hole Oceanographic Institution, MA 02543
(hseo@whoi.edu)

1. Introduction

Processes at the air-sea interface are key for understanding the circulation in both the ocean and atmosphere. Variations in wind forcing drive ocean circulations and the changes in heat, momentum and moisture fluxes influence the large-scale atmospheric circulations. In the large-scale climate scenarios (e.g., Pacific Decadal Oscillation), it has been traditionally thought that the atmospheric variability drives the ocean circulations, where for example the increase in westerlies lead to the decreased SST on interannual and longer timescales via turbulent heat flux and ocean mixing. The recent satellite and in-situ observations however indicate that the ocean and atmosphere are also strongly coupled on spatial scales that are much smaller (10-100 km), and on this spatial scale, it is the ocean that primarily drives the atmosphere (Chelton et al. 2004; Xie 2004; Small et al. 2009; Chelton and Xie, 2010). On the scale of ocean eddies and fronts, the sea surface temperature is ubiquitously positively correlated with the surface wind speed throughout the global oceans, opposite to the conventional view that strong wind speeds are found over cooler ocean surfaces.

Understanding the physical processes behind such relatively smaller-scale ocean-atmosphere interactions are of great interest to the climate modeling communities (Bryan et al. 2010) as these unresolved coupled processes in the Atmosphere-Ocean General Circulation Models (AOGCMs) possibly rectifies the large-scale circulations through the upscaling effects. Although the AOGCMs are beginning to increase their resolutions to attempt to resolve increasingly smaller-scale processes, high-resolution regional coupled ocean–atmosphere models, if properly driven by the large-scale circulation, could provide additional advantages in the study of the detailed patterns of air–sea interactions involving oceanic mesoscale eddies.

The regional coupled downscaling technique can also provide a unique opportunity to understand the processes for the regional climate variability and to assess the range of possible future climate changes. This has an important implication for developing appropriate regional adaptation and mitigation strategies under various climate change scenarios. This article will briefly introduce the regional coupled modeling system and

discuss the one particular example, in which the small-scale coupled processes have large impact on the mean states in a changing climate.

2. The Scripps Coupled Ocean-Atmosphere Regional Model

SCOAR is originally a coupling of two regional models, the atmospheric Regional Spectral Model (RSM, Juang and Kanamitsu 1994) and the Regional Ocean Modeling System (ROMS, Haidvogel et al., 2000; Shchepetkin and McWilliams 2005). The RSM is a regional extension to the Global Spectral Model (GSM) used in the NCEP/Department of Energy (DOE) Re-analysis (RA2; Kanamitsu et al. 2002a). The RSM is a primitive-equation hydrostatic model on terrain-following sigma coordinates, and the large- scale (low wavenumber) components of the flow are specified in the model by the RA2 downscaling procedure or by any GSM simulation. Details about the model physics can be found in Kanamitsu et al. (2002b). The ROMS solves the incompressible and hydrostatic primitive equations with a free surface on horizontal curvilinear coordinates and utilizes stretched generalized sigma coordinates in order to enhance vertical resolution near the sea surface and bathymetry. A radiation method is used along the open boundaries in order to allow for stable, long-term integrations together with a flow-adaptive nudging term for relaxation toward the prescribed lateral boundary conditions. That is, the nudging is stronger (time scale of 1 day) if the flow is inward and weaker (time scale of 1 year) for outflow (Marchesiello et al. 2001). Implicit diffusivity associated with third-order upstream horizontal advection is used in the lateral plane as opposed to explicit diffusivity. Mixed layer dynamics are parameterized using a K- profile parameterization (KPP) scheme (Large et al. 1994).

The flux-coupler (Seo et al., 2007a) couples the RSM and ROMS in a sequential fashion, and the air-sea interface is based on either RSM's surface and planetary boundary layer schemes, or on the bulk aerodynamic formula of Fairall et al., (1996). ROMS, in turn, provides SST and surface currents to the atmospheric model, where the wind stress can be calculated by taking into account the relative motion of wind and ocean current with the modified bulk formula. This version of SCOAR has been widely used in the Pacific (Seo et al., 2007a, Putrasahan et al., 2011a,b), the Atlantic (Seo et al., 2006, 2007b, 2008a, Seo and Xie 2011), in the Indian Ocean (Seo., 2008b, 2009) and this study.

A recent update of SCOAR includes coupling the Weather Research and Forecast (WRF) model (Skamarock et al., 2008) to ROMS based on the identical flux-SST coupler. The WRF-ROMS version of SCOAR are currently being used for several applications including the study of the Madden Julian Oscillations in a tropical channel mode, and the results will be reported in the near future.

3. Atlantic Tropical Instability Waves under global warming

Despite the regional and potentially global importance, it is unclear how the equatorial Atlantic variability will respond to the increased anthropogenic greenhouse gas concentrations in a changing climate. Like the Pacific, the equatorial Atlantic ocean's

response to global warming would heavily rely upon ocean dynamical processes and heat transport that generate the non-uniform warming pattern in the upper ocean in spite of the uniform radiative heating (Xie et al., 2010). Models adopted so far for climate projection omit some potentially important ocean processes. One example is tropical instability waves (TIWs, Fig. 1). They are generated from instabilities of equatorial zonal currents and fronts (e.g., Philander, 1976) and are the most energetic mesoscale variability in the equatorial oceans. Observations reveal TIWs as westward propagating wave-like oscillations with peak-to-trough SST differences up to 5-6C, sufficient to trigger significant atmospheric anomaly patterns propagating together with TIWs. Associated with the large amplitude anomalies in SST and currents, TIWs are recognized as key organizers in heat and momentum balances in the equatorial oceans.

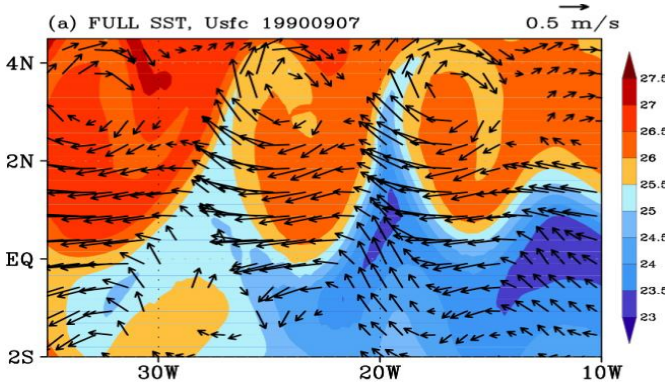

Fig. 1 Simulated Atlantic TIWs showing SST (color) and surface ocean currents (vector, m/s).

Considering the multi-scales and the air-sea interactions involved in TIWs, explicitly resolving them in the coupled climate models is important for simulation and prediction of tropical climate (Shaffrey et al., 2009; Ham and Kang, 2010). Most Intergovernmental Panel on Climate Change (IPCC)-class models, however, do not produce TIWs, hence their potential impacts have been left unexplored. The current study uses the SCOAR model to demonstrate the typical mesoscale air-sea interaction patterns associated TIWs and to infer their potential role in a warming climate.

3.1 Atmospheric boundary layer response to TIWs

The ½ ° RSM, downscaling the NCEP2 for the atmosphere, is coupled to ¼ ° ROMS over the entire tropical Atlantic sector (30°S-30°N, 74°W-20°E) using the lateral boundary conditions (LBCs) from the Simple Ocean Data Assimilation (SODA). The greenhouse gas concentrations in RSM are set to the present-day value to match those used in the NCEP2. This control simulation (CTL) is then integrated for 28 years from 1980 to 2007. Fig. 1 illustrates the typical SST/current patterns associated with TIWs. The simulated TIWs in the model are qualitatively similar to the observations, with the cusps of cold SST north of the equator along the equatorial front and the associated anti-cyclonic vortices.

Fig. 2 shows the first mode of the combined EOF of (a) SST and surface wind and SST and (b) latent heat flux from the Pacific TIW simulations, illustrating that the perturbations wind speed fields tend to co-propagate with the undulating SST anomalies. The winds are stronger (more southeasterly) over warmer SST and weaker (more northwesterly) over the cold SST. Latent heat flux tends to be out of phase with the SST due to the higher wind

speed and higher saturation water vapor mixing ratios associated with high SSTs (Fig. 2b), providing a thermal negative feedback to TIWs (Thum et al. 2002) Do these substantial atmospheric responses feed back to the ocean? Seo et al. (2007) reported a dominant negative correlation of the TIW-induced wind stress anomalies with the TIW-induced current anomalies (Fig. 3), suggesting that the TIW-currents are always slowed down by the overlying wind response to the TIW SST anomalies. The net impact has been estimated to be roughly 10% of the barotropic energy conversion rate in the equatorial ocean, acting as a significant sink term in the eddy kinetic energy budget (Small et al. 2009).

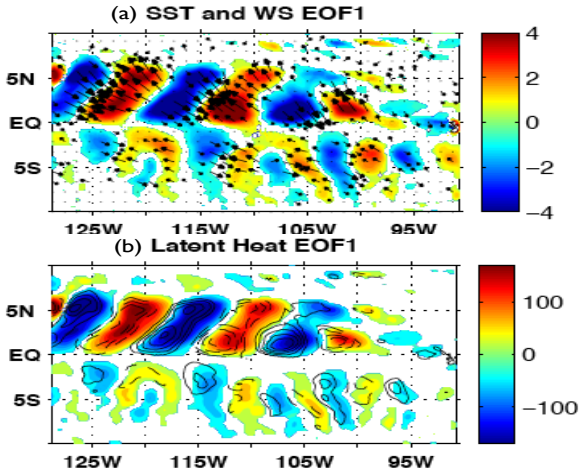

Fig. 2 The first mode of the combined EOF in (a) SST (C, color) and wind speed (m/s, vector), (b) latent heat flux (W/m^2, positive into the ocean, color) and SST (contours, negative dashed).

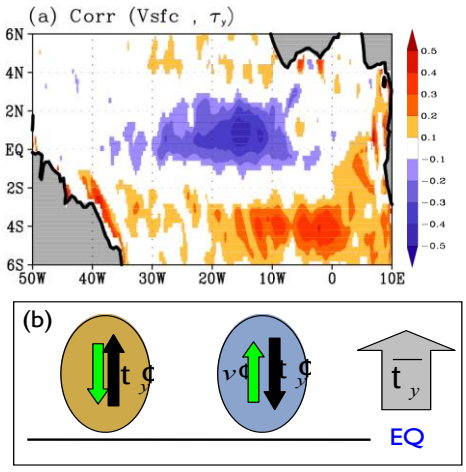

Fig. 3 (a) A map of correlation coefficients between high-passed meridional wind stress and currents. (b) Schematic diagram of SST anomalies (color), meridional wind stress vectors (black), surface current vectors (green) and the background wind stress (gray).

3.2. Global warming response

The global warming (GW) anomalies have been inferred from the CM2.1 simulations and added to the lateral boundary conditions in CTL. CO_2 concentration in GW run is increased to 521.75 PPM to match that in CM2.1. With an identical setup otherwise, GW run is also performed for the same period of time. Fig. 4 shows the simulated annual mean zonal equatorial currents (contours) and difference (color, GW-CTL). In the present-day condition, the Equatorial Undercurrent (EUC) in SCOAR is found at the depth of 75 meters with a narrow meridional scale and the speed exceeding 80 cm/s, features that are similar to the observations (not shown). Both the observed northern and southern branches of the South Equatorial Current (SEC) at the surface are also well captured in the downscaled model. CM2.1 generally underestimates the amplitudes of EUC and SEC, with much

broader scales of EUC core and no distinction of two branches of SEC. Overall, downscaling produces a much more realistic equatorial currents and the cold tongue structure, which is a critical requirement for studying dynamic instability and energetics.

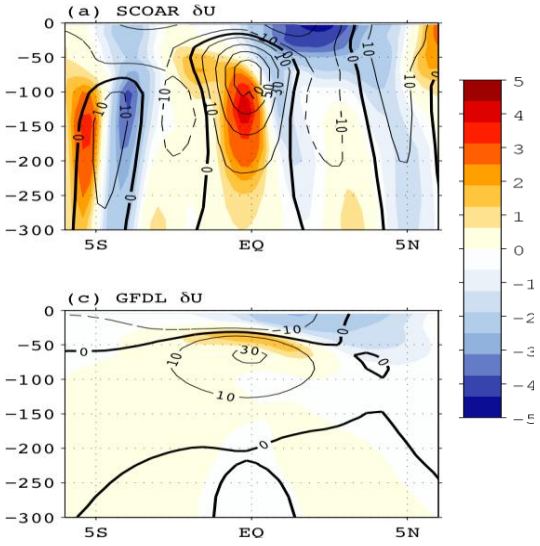

Fig. 4 Annual mean (1998-2007) difference (δ, shade) in zonal currents (cm s^{-1}) from (top) SCOAR and (bottom) CM2.1 averaged over 30°W-10°. The present-day climatological values are superimposed in black contours in each panel with CI=10 cm s^{-1}.

Under global warming (GW-CTL), both CM2.1 and SCOAR tend to suggest a spin-up of the SEC and EUC, but SCOAR shows a much greater strengthening of currents. This is associated with the increase in cross-equatorial southerly wind in SCOAR, primarily driven by the large-scale change in atmospheric circulations, giving rise to the increased in convection in northeast Atlantic and decrease in south Atlantic (not shown). The strengthening of SEC/EUC and the increased shear in SEC/NECC affects dynamical instabilities that energize TIWs, leading to strengthened TIW variability. EKE, defined as $EKE = \frac{1}{2}(u'^2 + v'^2)$, where the prime denotes a 20-40 day band-pass filtered field are enhanced by 31% from CTL to GW. EKE increase is largest during the boreal summer upwelling season that eddy variability is most enhanced (May-September).

3.3. Eddy temperature advections

TIWs significantly contribute to the heat budget of the equatorial ocean through eddy heat transport (e.g., Hansen and Paul, 1984). This section examines the change in eddy temperature advection terms $-u\partial T/\partial x - v\partial T/\partial y - w\partial T/\partial z$ in the mixed-layer heat budget. In CTL, the simulated eddy heat temperature advections are consistent with the results from the previous studies. For example, TIWs significantly warm the equatorial cold tongue by moving the warmer off-equatorial waters to the equator by meridional eddy motions (Fig, 5b, $-v\partial T/\partial y$). TIWs also warm the region from the equator to 2°N through $-u\partial T/\partial x$ (Fig 5a), which is comparable in magnitude to $-v\partial T/\partial y$. This sizable warming by TIW zonal advection is primarily due to strong current anomalies acting on relatively stronger zonal SST gradient on TIW-eddy scales (Fig. 1). This is hence due to the zonal inhomogeneity in equatorial currents on the scale of TIWs. The net warming by zonal temperature advection tends to be offset by $-w\partial T/\partial z$. This cooling by $-w\partial T/\partial z$ (Fig. 5c) occurs over the regions of

strong shear due to TIW current anomalies, where the turbulent mixing/entrainment is large (Moum et al., 2009). Furthermore, in the warm phase of TIWs, the perturbation wind speed increases (Fig. 2), enhancing the mechanical energy for turbulent mixing at the center of TIW vortices having large vertical motion. Overall, the total three-dimensional eddy temperature advection leads to a net warming of the equator (Fig. 5d).

As TIWs are energized under global warming, each element of the eddy temperature advection also strengthens. Note that the zonal advection shows the largest warming. This is primarily due to the aforementioned structure of the SST gradient and the current anomalies of TIWs in the present-day condition, which are both more strengthened under global warming due to the stronger front and the westward SEC. The stronger currents, shears, and SST anomalies associated with TIWs also increase the vertical temperature advection by TIWs, which tend to offset the warming effect by the horizontal eddy advection. Overall, the change in net eddy advection significantly warms the equatorial mixed layer. The full heat budget analysis does suggest that this net warming by eddy motions are the most dominant source of equatorial warming, counteracting the cooling effect due to the change in large-scale circulation changes (not shown).

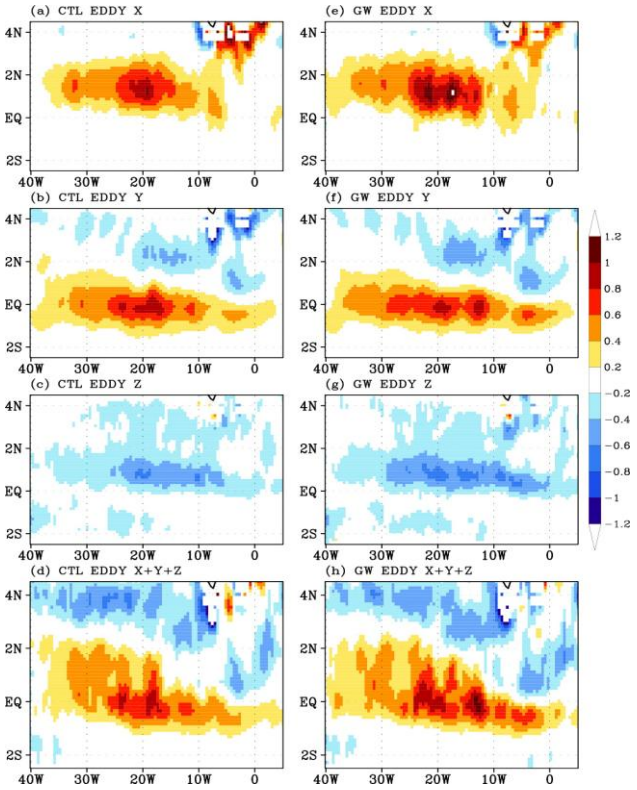

Fig. 5 Each component of the annual mean eddy temperature advections (℃ month^{-1}) in (left) CTL and (right) GW averaged from 1998-2007. (a,e) Zonal, (b,f) meridional, (c,g) vertical, and (d,h) the sum. The contour intervals are 0.2 ℃ month^{-1}.

4. Summary

The main goal of this paper is to demonstrate that having TIWs in the equatorial oceans may bring advantage to the interpretation of warming patterns since they produce sizable eddy heat flux that interacts with the climate feedback processes. In order to better resolve TIWs, it is necessary to have the realistic equatorial wind and currents, the sharp thermocline, and the strong air-sea interactions, which are under-represented in the climate models. In this study, we deliver a new regional coupled dynamical downscaling technique

to the climate modeling community for assessing the regional aspects of global climate change. With better representation of the equatorial oceanic processes including explicitly resolving TIWs, the regional coupled models do provide a useful guidance to improving parameterization of the effect of TIWs in the GCMs and simulation of the equatorial climate thereof.

References

Bryan, F.O, R. Thomas, J. Dennis, D. Chelton, N. G. Loeb, and J. L. McClean, 2010: Frontal scale air-sea interaction in high-resolution coupled climate models. *J. Climate*, 23(23), 6277-6291

Chelton, D.B., M. Schlax, M.H. Freilich and R.F. Milliff, 2004: Satellite measurements reveal persistent small-scale features in ocean winds. Science, **303**, pp. 978–983.

Chelton, D.B., and S.-P. Xie, 2010: Coupled ocean-atmosphere interaction at oceanic mesoscales. *Oceanogr*., 23, 52-69

Fairall, C. W., E. F. Bradley, D. P. Rogers, J.D. Edson and G.S. Young, 1996: Bulk parameterization of air-sea fluxes for Tropical Ocean-Global Atmosphere Coupled-Ocean Atmosphere Response Experiment. J. Geophys. Res., **101**, pp. 3747– 3764.

Haidvogel, D. B., H. G. Arango, K. Hedstrom, A. Beckmann, P. Malanotte- Rizzoli, and A. F. Shchepetkin, 2000: Model evaluation experiments in the North Atlantic Basin: Simulations in nonlinear terrain-following coordinates. *Dyn. Atmos. Oceans*, 32, 239–281.

Ham, Y.-G., and I. S. Kang, 2011: Improvement of seasonal forecasts with inclusion of tropical instability waves on initial conditions, Clim. Dyn., 36, 7-8, 1277-1290.

Juang, H. M. H., and M. Kanamitsu, 1994: The NMC nested regional spectral model. *Mon. Weather Rev*., 122, 3–26

Kanamitsu, M., W. Ebisuzaki, J. Woollen, S. K. Yang, J. J. Hnilo, M. Fiorino, and G. L. Potter, 2002a: NCEP-DOE AMIP-II Reanalysis (R-2). *Bull. Am. Meteorol. Soc.,* 83, 1631–1643

Kanamitsu, M., A. Kumar, H.-M. H. Juang, W. Wang, F. Yang, J. Schemm, S.-Y. Hong, P. Peng, W. Chen, and M. Ji: 2002b: NCEP Dynamical Seasonal Forecast System 2000. *Bull. Amer. Met. Soc.*, **83**, 1019-1037

Large, W. G., J. C. McWilliams, and S. C. Doney, 1994: Oceanic vertical mixing: A review and a model with a nonlocal boundary layer parameterization. *Rev. Geophys*., 32, 363–404.

Marchesiello, P., J. C. McWilliams, and A. Shchepetkin, 2001: Open boundary conditions for long-term integration of regional oceanic models. *Ocean Modell*., 3, 1–20.

Moum, J. N., A. Lien, A. Perlin, J. D. Nash, M. C. Gregg, and P. J. Wiles, 2009: Sea surface cooling at the equator by subsurface mixing in trop- ical instability waves. *Nat. Geosci.,* 2, 761–765.

Philander, S. G. H., 1976: Instabilities of zonal equatorial currents, J. Geo- phys. Res., 81, 3725–3735,

Putrasahan, D., A. J. Miller and H. Seo: Air-sea Interactions and Local Impact of

Mesoscale Sea Surface Temperature on the Atmospheric Boundary Layer in the Southeast Pacific. *In prep.*

Putrasahan, D., A. J. Miller and H. Seo: Mesoscale Atmospheric Forcing Impact on the Humboldt Current System. *In prep.*

Seo, H., M. Jochum, R. Murtugudde, A. J. Miller, 2006: Effect of Ocean Mesoscale Variability on the Mean State of Tropical Atlantic Climate. *Geophys. Res. Lett., 33,* L09606.

Seo, H., A.J. Miller, J.O. Roads, 2007a: The Scripps Coupled Ocean-Atmosphere Regional (SCOAR) model, with applications in the eastern Pacific sector. *J. Climate,* 20, 381-402.

Seo, H., M. Jochum, R. Murtugudde, A.J. Miller and J.O. Roads, 2007b: Feedback of Tropical Instability Wave - induced Atmospheric Variability onto the Ocean. *J. Climate,* 20, 5842-5855.

Seo, H., R. Murtugudde, M. Jochum and A.J. Miller, 2008a: Modeling of mesoscale coupled ocean-atmosphere interaction and its feedback to ocean in the western Arabian Sea. *Ocean Modell.*, 25, 120-131.

Seo, H, M. Jochum, R. Murtugudde, A. J. Miller, J. O. Roads, 2008b: Precipitation from African Easterly Waves in a Coupled Model of the Tropical Atlantic. *J. Climate, 21*, 1417-1431.

Seo, H., S.-P. Xie, R. Murtugudde, M. Jochum, and A. J. Miller, 2009: Seasonal effects of Indian Ocean freshwater forcing in a regional coupled model. *J. Climate.* 22, 6577-6596

Seo, H. and S.-P. Xie, 2011: Response and Impact of Equatorial Ocean Dynamics and Tropical Instability Waves in the Tropical Atlantic under Global Warming: A regional coupled downscaling study. *J. Geophys. Res.-Oceans,* 116, C03026

Shaffrey, L., et al., 2009: U.K. HiGEM: The new U.K. high resolution global environment model—Model description and basic evaluation, J. Clim., 22, 1861–1896.

Shchepetkin, A. F., and J. C. McWilliams, 2005: The regional oceanic modeling system (ROMS): A split-explicit, free-surface, topography-following-coordinate ocean model. *Ocean Modell*., 9, 347–404

Skamarock, W. C., J. B. Klemp, J. Dudhia, D. O. Gill, D. M. Barker, M. G. Duda, X. Huang, W. Wang, and J. G. Powers, 2008: A description of the advanced research WRF version 3. Rep. NCAR/TN–475+STR, Natl. Cent. for Atmos. Res., Boulder, Colo.

Small, R.J., S. de Szoeke, S.-P. Xie, L. O'Neill, H. Seo, Q. Song, P. Cornillon, M. Spall and S. Minobe, 2008: Air-sea interaction over ocean fronts and eddies. *Dynam. Ocean. Atmos*., 45, 274-319.

Small, R. J., K. J. Richards, S.-P. Xie, P. Dutrieux, and T. Miyama, 2009: Damping of tropical instability waves caused by the action of surface currents on stress. *J. Geophys. Res.*, 114, C04009

Thum, N., S. K. Esbensen, D. B. Chelton, and M. J. McPhaden, 2002: Air–sea heat exchange along the northern sea surface temperature front in the eastern tropical Pacific. *J. Climate*, 15, 3361–3378.

Xie, S.-P., C. Deser, G. A. Vecchi, J. Ma, H. Teng, and A. T. Wittenberg, 2010: Global warming pattern formation: Sea surface temperature and rainfall. *J. Climate*, 23, 966–986

Xie, S.-P., 2004: Satellite observations of cool ocean–atmosphere interaction. *Bull. Amer. Meteor. Soc.*, 85, pp. 195–209.

Dynamical Downscaling of Future Climate in the Barents and North Seas

Bjørn Å dlandsvik,

Institute of Marine Research, Bergen, Norway,
Bjerknes Centre for Climate Research, Bergen, Norway

1.Introduction

The marine ecosystems in the Norwegian Sea, the North Sea and the Barents Sea support some of the largest fisheries in the world and Norway's second largest export industry (after petroleum which also is affected be marine climate). In the long run, with proper management, traditional fisheries and aquaculture may provide an important source of food and income in the future. As the ecosystems are heavily affected by changes in the marine climate, it is important to obtain regional marine climate projections.

To study the effects of future climate change, we need consistent and realistic ocean climate projections for the seas around Norway. The ocean components of the global climate projections are consistent, but not realistic for the productive shelf seas. This is due to low resolution, not resolving the topography, exchange processes between deep ocean and shelves, freshwater-driven coastal currents, eddies, and lack of important shelf physics like tidal mixing. Dynamical downscaling, where a regional ocean model is forced from the atmosphere and at the lateral boundaries with results from a global coupled climate model is tried as an alternative.

At IMR we have used two different set-ups for downscaling, both using the Regional Ocean Model System (ROMS) as regional ocean circulation model. The first, documented by Å dlandsvik and Bentsen (2007) and Å dlandsvik (2008), uses a model domain for the North Sea and deep ocean outside with average resolution 8 km. The other setup covers the whole North Atlantic, the Polar Ocean and the ice-infected parts of the Pacific with a stretched grid with resolution approximately 10 km in the Barents Sea. This setup is described by Melsom et al. (2009). Both domains are shown in Fig. 1.

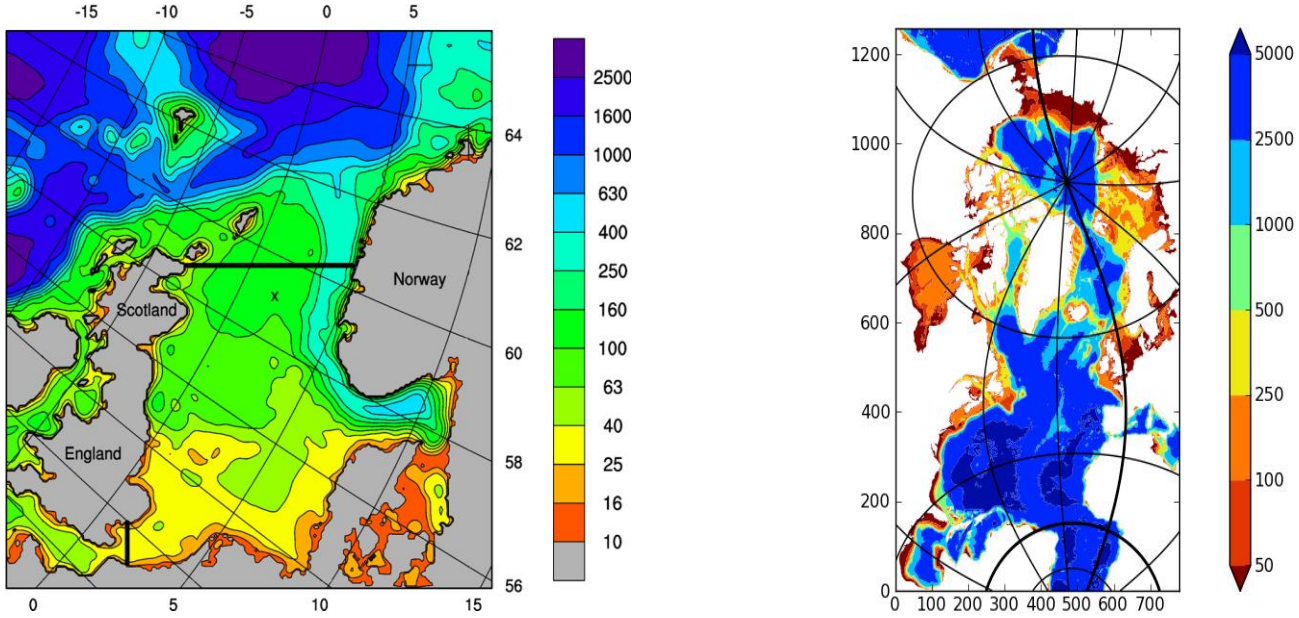

Figure 1. Model domains with topography, left: North Sea, right: Atlantic-Arctic

The global models are taken from the runs for the IPCC AR4, using the Norwegian BCCR BCM model for the North Sea domain and American models NASA GISS AOM and NCAR CCSM for the Atlantic-Arctic domain, with the end of the 20C3M runs as control, and A1B as future scenario, see table 1 for a summary.

Downscaling	Global Climate Model	Control	Scenario
North Sea	BCCR BCM	20C3M 1981-1999	A1B 2081-2099
AA-GISS	NASA GISS AOM	20C3M 1986-2000	A1B 2051-2065
AA-NCAR	NCAR CCSM3	20C3M 1986-2000	A1B 2051-2065

Table 1: Overview of IMR downscalings

The choice of the models for the AA downscaling, was guided by the analysis in Overland and Wang (2007) which showed that these models are among the best models from the IPCC AR4 runs for sea ice coverage in the Barents Sea and the central Arctic Ocean.

2.Results

Fig. 2 gives an example of how downscaling works for the North Sea. The left panel shows the circulation from the BCM global model. This gives a smooth picture of the circulation in the area, not bad given the resolution of approx. 80 km. The downscaled situation in the right panel shows a much richer flow fields with intensification at the

shelf slope, a realistic inflow to the North Sea and some mesoscale features.

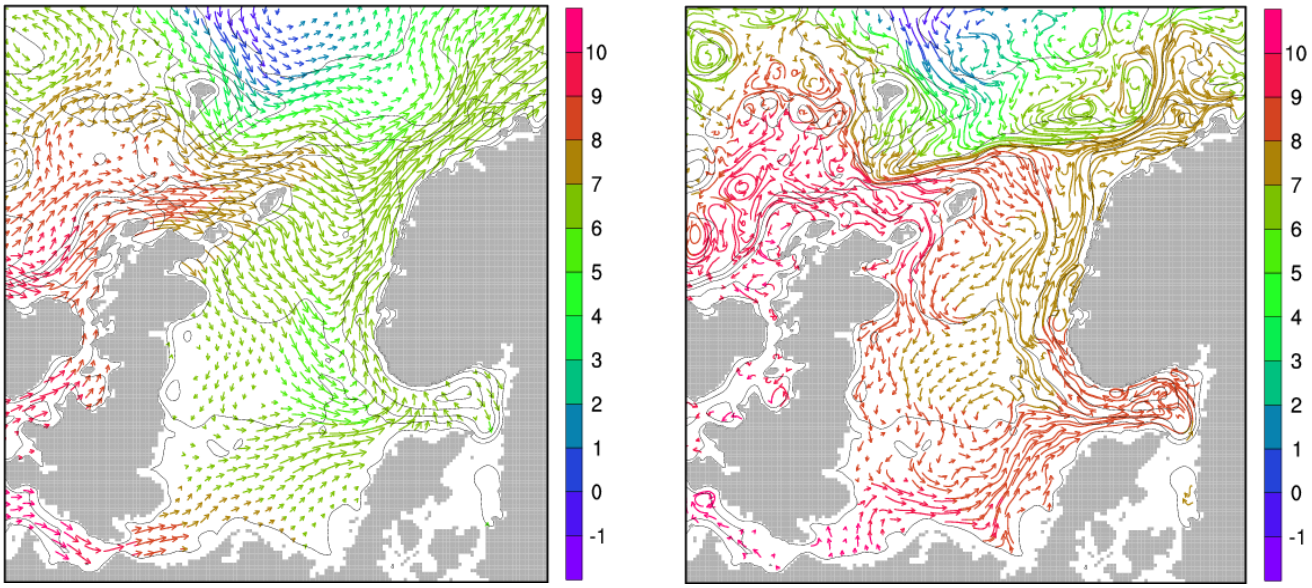

Figure 2. Current at 25 m, January 1979, left: BCM interpolated to regional grid, right: downscaled. Colours show temperature.

Figure 3 shows the ice coverage in the Barents Sea from the control run. The global GISS model
clearly has to much sea ice. The downscaling is a strong improvement giving more open water and realistic ice-edge consistent with the bottom topography. The global NCAR model does quite well on the sea ice, but also here the downscaling improves the regional details. But both downscalings has too much sea ice in the eastern Barents Sea.

This illustrates a fundamental problem with regionalisation at high latitudes. If the global model has too extensive sea ice coverage, the atmosphere becomes too cold over the ice, strongly cooling the regional model. Straightforward downscaling is only capable of improving the ice coverage to a certain degree.

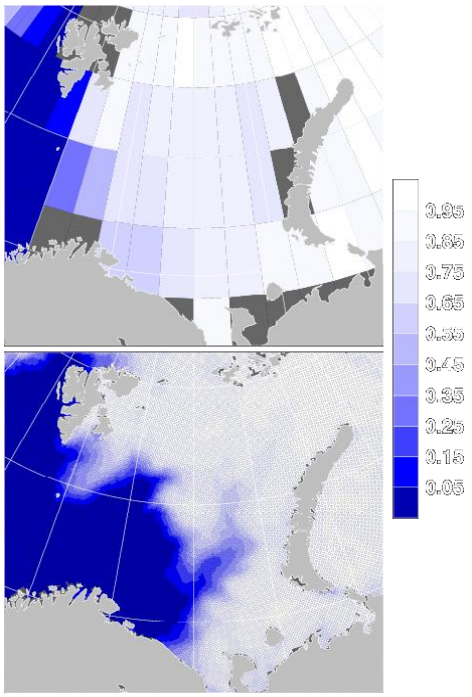

Figure 3. Ice coverage in control run, May average. Upper left GISS global, lower left downscaled GISS, upper midle NCAR global, lower midle downscaled NCAR, right NCEP reanalysis

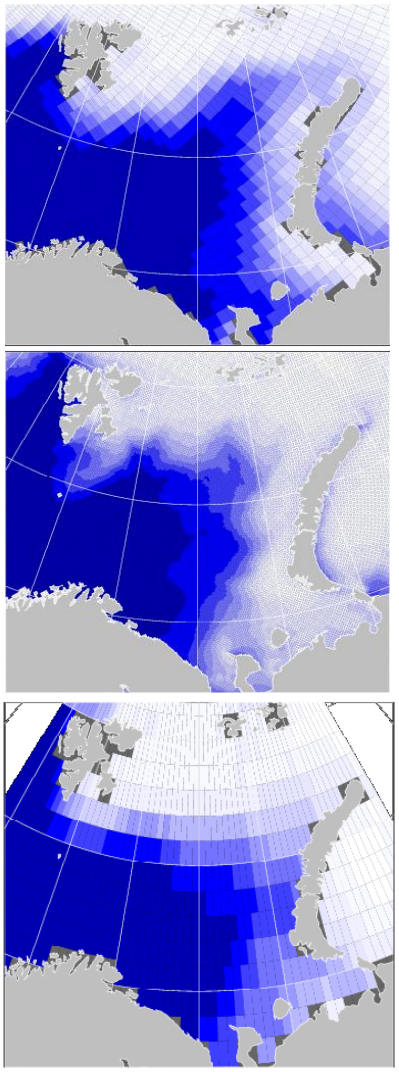

Figure from A.Melsom

3.Regional future scenarios

The projected change in temperature 65 years ahead with the downscalings for the North Sea is given in figure 4. The GISS based downscaling shows a weak warming, yearly mean of 0.3 degrees while the NCAR based gives a warming of 1.1 degrees, averaged over the volume of the central North Sea.

For the Barents Sea, figure 5 shows the control, future scenario and difference August mean temperature at 100 m depth. The GISS based downscaling shows a warming in the south-eastern
Barents Sea. The CCSM based downscaling has a cold bias to start with in the Atlantic Water. It shows a stronger warming in the eastern Barents Sea. Volume averaged for the Barents Sea, the
GISS downscaling gives a yearly mean warming of 0.6 degrees and the NCAR based 1.4 degrees.

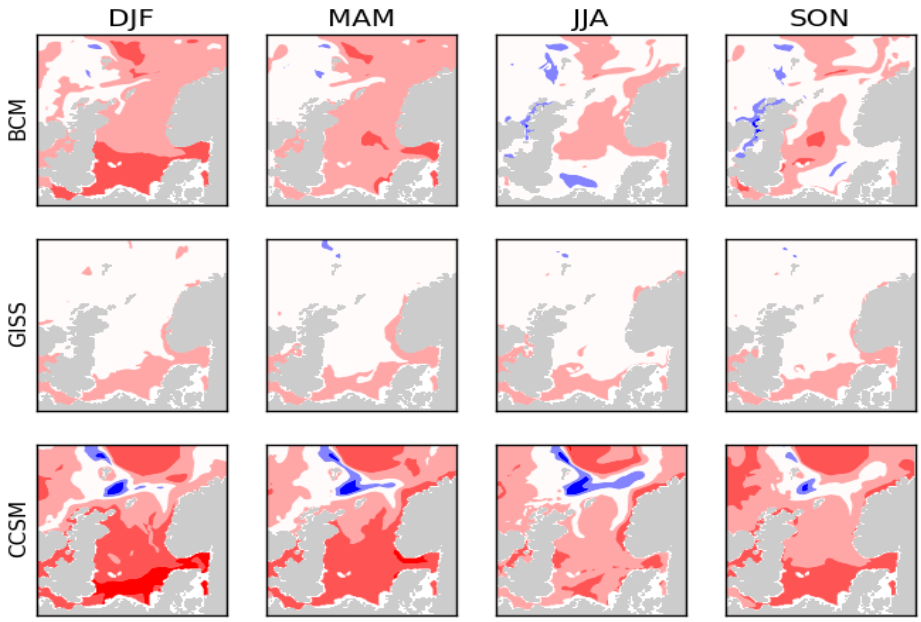

Figure 4. Seasonal temperature change for the three downscalings for the North Sea

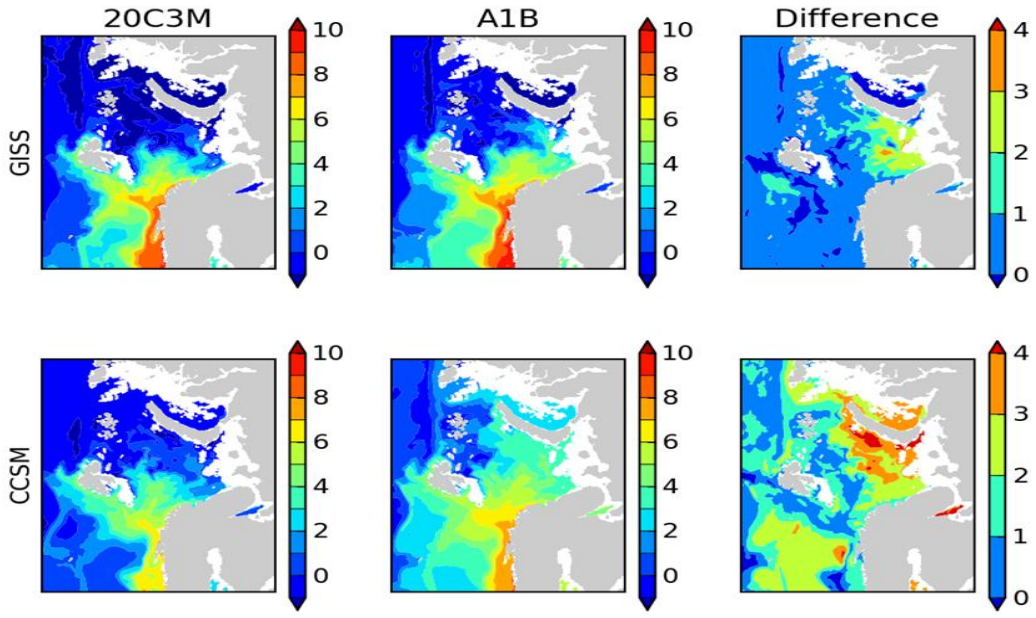

Figure 5. Control, scenario and difference in August mean temperature at 100 m in the Barents Sea

4.Conclusions

Downscaling global coupled climate models with regional ocean circulation model provides added value, at least for shelf seas. This goes to improved circulation pattern, mesoscale features, improved inflow to the shelves and more realistic stratification.

The downscalings shows different warming from 2000 to 2065 from less than 0.5 to more than 1.5 degrees. Both seas have shallow areas in south with stronger warming. Errors in the ice coverage in the control run gives unrealistic strong warning in parts of the eastern Barents Sea.

5.Future work

IMR is now leading a new downscaling project at the Centre for Climate Dynamics at the Bjerkens Centre. In addition to downscaling some of the new IPCC runs for the AR5, the project will work on method improvement. In particular, a regional coupled atmosphere-ocean-ice model will be developed to address the sea ice problems.

Acknowledgement

The results presented include work by my colleagues W. Paul Budgell, Vidar Lien, Anne Britt Sandø at IMR and Arne Melsom at the Norwegian Meteorological Institute.

References

B. Å dlandsvik, 2008, Marine downscaling of a future climate scenario for the North Sea Tellus, 60A, 451-458.

B. Å dlandsvik and M. Bentsen, 2007, Downscaling a 20th century global climate simulation to the North Sea Ocean Dyn., 57, 453-466.

A. Melsom, V.S. Lien and W.P. Budgell, 2009, Using the Regional Ocean Modeling System (ROMS) to improve the ocean circulation from a GCM 20th century simulation Ocean Dyn., 59, 969-981.

PROTHEUS: The regional climate model for the Mediterranean region

Gianmaria Sannino and Adriana Carillo

UTMEA-CLIM, ENEA C.R. Casaccia, Roma, Italy

Extremely complex coastlines and topographical features, such as the Alpine, Apennine, Pyrenees and Balkan mountain chains, the Italian and Hellenic peninsulas and large islands, characterize the Euro-Mediterranean region (Figure 1). From the atmospheric point of view this morphological complexity leads to the formation of intense weather phenomena that strongly affect the Mediterranean ocean circulation.

The Mediterranean Sea is a semi-enclosed basin displaying an active thermohaline circulation (MTHC) that is sustained by the atmospheric forcing and controlled by the narrow and shallow Strait of Gibraltar (Sannino et al. 2009). The atmospheric forcing drives the Mediterranean basin toward a negative budget of water and heat, and toward a positive budget of salt. Over the basin, evaporation exceeds the sum of precipitation and rivers discharge, while through the surface a net heat flux is transferred to the overlying atmosphere. Mass conservation in the basin represents the last ingredient necessary to activate the MTHC (Figure 2). Within the Strait of Gibraltar the MTHC takes the form of a two-way exchange: at surface fresh and relatively warm Atlantic water spreads in the Mediterranean basin, while at the bottom colder and saltier Mediterranean water sinks as a tongue in the North Atlantic at intermediate depths becoming one of the factors preconditioning the surface water column of the convective cells in the North Atlantic.

Within the framework of the EU CIRCE project (www.circeproject.eu), 5 regional coupled ocean-atmosphere models dedicated to the study of the future climate of the Mediterranean region have been developed. The five models simulated the same study of the future climate of the Mediterranean region have been developed. The five models simulated the same period 1951-2050 following the A1B hypothesis, for the GHG and aerosols concentration, after year 2000. Among these five models PROTHEUS is the coupled model developed at ENEA, the Italian National Agency for New Technologies, Energy and Sustainable Economic Development.

The PROTHEUS system is composed of the RegCM3 atmospheric regional model and the MITgcm ocean model. The coupling of RegCM3 and MITgcm models is accomplished using the OASIS3 coupler (Valcke and Redler (2006)) that performs both the synchronization of the two models and the interpolation of coupling fields from a source to a target grid. The oceanic model transfers SST to the atmospheric model and receives wind stress components and total heat and salt fluxes. Coupling fields are exchanged every 6 hours. No relaxation to climatology is applied (Figure 3).

RegCM3 is a 3-dimensional, sigma-coordinate, primitive equation, hydrostatic RCM. It was originally developed by Giorgi et al. (1993a, b) and then successively upgraded as described by Giorgi and Mearns (1999) and Pal et al. (2007). RegCM3

includes different physics options. In this study we employ the CCM3 radiative transfer scheme (Kiehl et al. 1996) with specified GHG concentrations, the planetary boundary layer scheme of Holtslag et al. (1990), the Biosphere–Atmosphere Transfer Scheme (BATS1E) of Dickinson et al. (1993), the resolvable precipitation scheme of Pal et al. (2000) and the cumulus convection scheme of Grell (1993) with the Fritsch and Chappell (1980) closure assumption. Air–sea exchanges are treated using the parameterization of Zeng et al. (1998). This scheme was implemented to improve some of the problems found in the original BATS package, most noticeably the excessive evaporation from warm ocean surfaces (Pal et al. 2007). In experiments over the continental US and adjacent ocean water the Zeng scheme lead to a considerable improvement of evaporation and precipitation over the Gulf of Mexico and the tropical western Atlantic (Pal et al. 2000). The configuration used here has a uniform horizontal grid spacing of 30 km on a Lambert conformal projection, 18 sigma-levels are used. The simulation is performed on an area going from 20 N° to 60 N° including the entire Mediterranean Sea. Lateral boundary conditions are supplied every 6 hour by interpolating horizontal wind components, temperature, specific humidity and surface pressure from the global atmospheric model.

The ocean component is based on the MITgcm developed by Marshall et al. (1997a,b); here the model is used in its hydrostatic, implicit free-surface, partial step topography formulation (Adcroft et al. (1997)). The model has a resolution of 1/8°x1/8° equivalent to rectangular meshes of variable resolution with the meridional side of about 14 Km and the zonal one ranging from about 9 Km in the northern part of the domain to about 12 Km in the southern part. The model has 42 vertical Z-levels with a resolution varying from 10 m at the surface to 300 m in the deepest part of the basin, and an intermediate resolution of about 40-50 m between the depths 200-700 m. Horizontal viscous and diffusive terms are modeled with a bi-harmonic formulation with diffusivity and viscosity coefficients equal to 1.5×10^{10} m^4 s^{-1}. Vertical eddy diffusivity is modeled via a Laplacian formulation with diffusivity coefficient ranging from 3.0×10^{-5} m^2 s^{-1} at surface to 10^{-7} m^2 s^{-1} at the bottom, while the viscous coefficient is hold constant to 1.5×10^{-4} m^2 s^{-1} over the whole water column (see Sannino et al. (2009b)). Deep convection is simulated through the enhancement of the vertical diffusivity to 1 m^2 s^{-1} in regions where the stratification becomes unstable.

Surface natural boundary conditions, that is P+R-E (Precipitation plus runoff minus evaporation) are treated as real fresh water flux are used. Monthly river discharges computed from the RegCM3 total runoff are used by the oceanic model. Catchment basins for 148 rivers falling into the Mediterranean Sea have been reconstructed using Total Runoff Integrated (TRIP) database. The Black Sea contribution has been computed interactively from the E-P-R budget. To obtain a realistic estimate of the freshwater flux that reaches the Mediterranean Sea, the value of the discharge computed has been rescaled, using coefficients derived from a previous RegCM3 stand-alone run forced by reanalysis, to match the monthly climatology presented by Stanev (Stanev et al. (2000)). Monthly values of the discharge of the Black Sea are then applied as a further river.

The initial conditions for the oceanic run are derived from a stand-alone ocean model run. During such run T and S values were 3D relaxed towards MEDATLAS (MEDAR Group (2002)) climatology with a relaxation coefficient of 5 days. At the surface, the model was forced perpetually by heat and water fluxes derived from year

1958 of the ERA40 dataset. Velocity field was kept free to evolve adjusting to the imposed T,S fields. The spin-up was run as long as the kinetic energy 3D integrated over the whole domain reached a stable value.

The two-way exchange through the Strait of Gibraltar is achieved by means of 3D relaxation of salinity and temperature toward the climatological monthly Levitus data (Levitus (1982)), in a box composed by 30 grid points located west of Gibraltar.

It has been demonstrated in Artale et al. 2010 that PROTHEUS is able to simulate present-climate in a hindcast experiment using the ERA40 reanalyses as boundary and initial conditions. Numerical results are compared to available observational datasets, with the corresponding atmospheric stand-alone RegCM simulations and with the ERA40 fields. PROTHEUS has been recently used also to asses the sea-level projection under the A1B SRES scenario (Carillo et al. 2011).

The present presentation will be mainly focalized on the description of the PROTHEUS components, its skill in reproducing the present climate, and results obtained for the sea-level projection. The presentation will show also future improvements on the oceanic component to solve one of the main issue in reproducing correctly the Mediterranean thermohaline circulation: the Strait of Gibraltar.

Bibliography

Adcroft, A., C. Hill, and A. J. Marshall. 1997. Representation of topography by shaved cells in a height coordinate ocean model. *Monthly Weather Review* 125 (9): 2293–2315.

A. Carillo, G. Sannino, V. Artale, P.M. Ruti, S. Calmanti, A. Dell'Aquila, Steric sea level rise over the Mediterranean Sea: present climate and scenario simulations, Climate Dynamics, Under review 2011.

Dickinson R, Henderson-Sellers A, Kennedy P (1993) Biosphereatmosphere transfer scheme (BATS) version 1e as coupled to the NCAR community climate model. Technical report, National Center for Atmospheric Research

Fritsch JM, Chappell CF (1980) Numerical prediction of convectively driven mesoscale pressure systems. Part 1: convective parameterisation. J Atmos Sci 37:1722–1733

Giorgi F, Bates G, Nieman S (1993a) The multi-year surface climatology of a regional atmospheric model over the western United States. J Clim 6:75–95

Giorgi F, Marinucci M, Bates G (1993b) Development of a second generation regional climate model (RegCM2) I: boundary layer and radiative transfer processes. Mon Weather Rev 121:2794–2813

Giorgi F (2006a) Regional climate modeling: status and perspectives. J Phys IV 139:101–118

Giorgi F (2006b) Climate change hot-spots. Geophys Res Lett 33:L08707. doi:10.1029/2006GL025734

Giorgi F, Mearns LO (1999) Introduction to special section: regional climate modeling revisited. J Geophys Res 104:6335–6352

Grell GA (1993) Prognostic evaluation of assumptions used by cumulus parameterizations. Mon Weather Rev 121:764–787

Holtslag A, de Bruijn E, Pan H-L (1990) A high resolution air mass transformation model for short-range weather forecasting. Mon Weather Rev 118:1561–1575

Kiehl J, Hack J, Bonan G, Boville B, Breigleb B, Williamson D, Rasch P (1996) Description of the NCAR community climate model (CCM3). Technical report NCAR/TN-420?STR, National Center for Atmospheric Research

Marshall, J., A. Adcroft, C. Hill, L. Perelman, and C. Heisey. 1997a. A finite-volume, incompressible navier stokes model for, studies of the ocean on parallel computers. *J. Geophys. Res.* 102 (C3): 5753–5766.26

Marshall, J., C. Hill, L. Perelman, and A. Adcroft. 1997b. Hydrostatic, quasi-hydrostatic, and nonhydrostatic ocean modeling. *J. Geophys. Res.* 102 (C3): 5733–5752.

Marsland, G. A., H. Haak, J. H. Jungclaus, M. Latif, and Rske F. 2003. The max planck institute global/sea-ice model with orthogonal curvilinear coordinates. *Ocean Model* 5: 91–127.

Pal JS, Small E, Eltahir E (2000) Simulation of regional-scale water and energy budgets: representation of subgrid cloud and precipitation processes within RegCM. J Geophys Res Atmos 105(D24):29579–29594

Pal JS, Giorgi F, Bi X, Elguindi N, Solmon F, Gao X, Rauscher SA, Francisco R, Zakey A, Winter J, Ashfaq M, Syed FS, Bell JL, Diffenbaugh NS, Karmacharya J, Konare´ A, Martinez D, da Rocha RP, Sloan LC, Steiner AL (2007) Regional climate modeling for the developing world: the ICTP RegCM3 and RegCNET. Bull Am Meteorol Soc 88:1395–1409

Sannino, G., Pratt, L., Carillo, A., 2009a. Hydraulic Criticality of the Exchange Flow through the Strait of Gibraltar. J. Phys. Oceanogr. 39 (11), 2779–2799.

Sannino G, Herrmann M, Carillo A, Rupolo V, Ruggiero V, Artale V, Heimbach P (2009b) An eddy-permitting model of the Mediterranean Sea with a two-way grid refinement at the Strait of Gibraltar. Ocean Model 30:56–72. doi:10.1061/j.ocemod.2009. 06.2002

Stanev, E. V., P. Y. Le Traon, and E. L. Peneva. 2000. Sea level variations and their dependency on meteorological and hydrological forcing: Analysis of altimeter and surface data for the black sea. *J. Geophys. Res.* 105 (C7): 17203–17216. doi:10.1029/1999JC900318.

Valcke S, Redler R (2006) OASIS3 User guide. PRISM support initiative report no 4, 60 pp

Zeng X, Zhao M, Dickinson RE (1998) Intercomparison of bulk aerodynamic algorithms for the computation of sea surface fluxes using TOGA COARE and TAO data. J Clim 11:2628–2644

Figure 1. Euro-Mediterranean map (from: http://it.wikipedia.org/wiki/File:Mediterranean_Sea_political_map-it.svg)

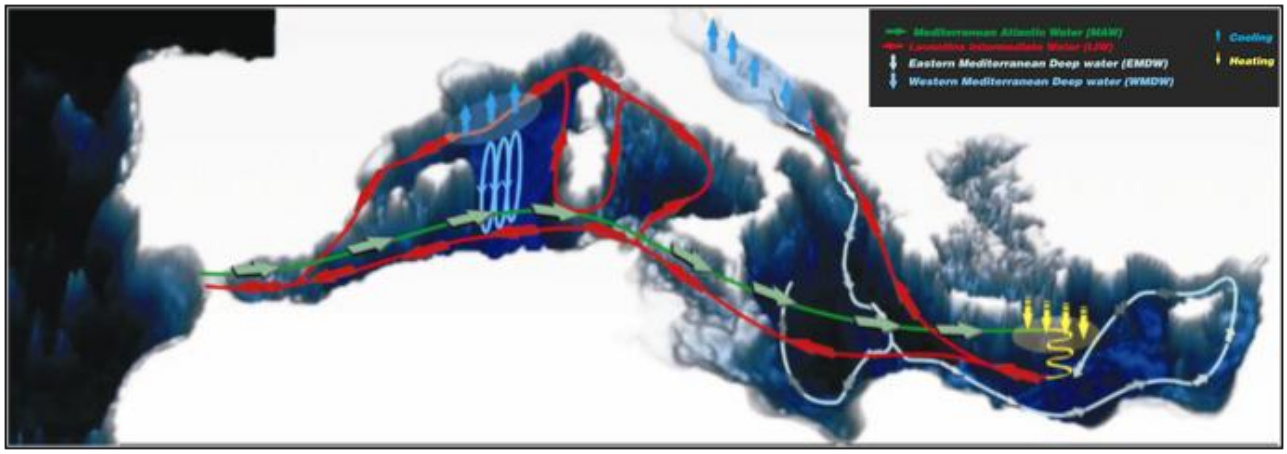

Figure 2: A simplified scheme for the Mediterranean thermohaline circulation.

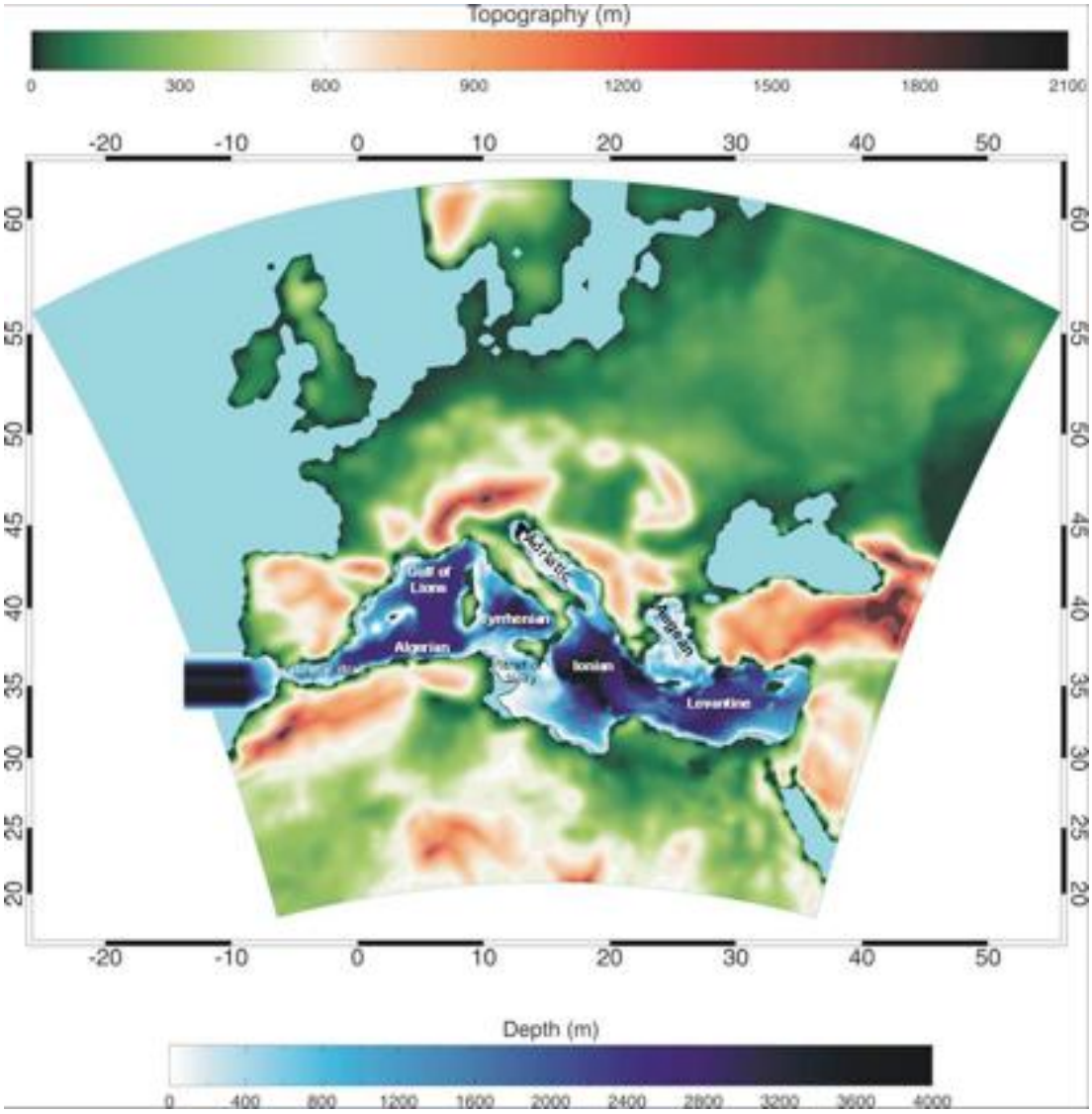

Figure 3: Domain for the PROTHEUS simulation with corresponding topography and bathymetry. Units are m.

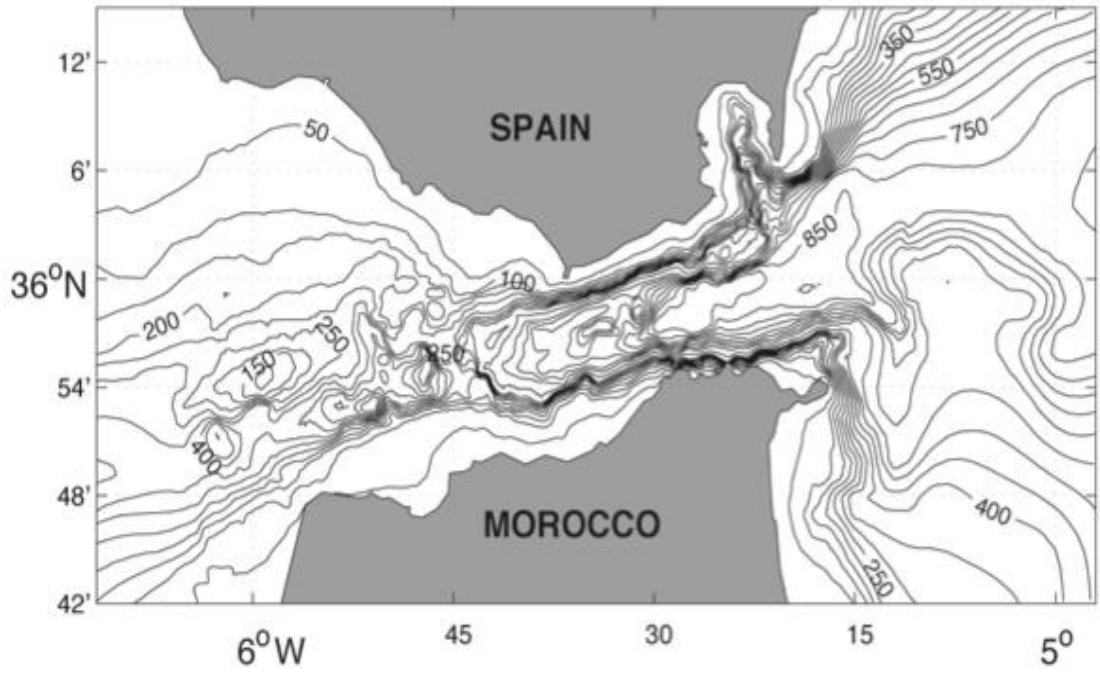

Figure 4. Bathymetry of the Strait of Gibraltar

Comparison of the sea surface height distribution in the different grid-resolution circulation models

Cheol-Ho Kim[1], Chan Joo Jang[1], Minwoo Kim[1], and Hyun Soo Cho[1]

Korea Ocean Research & Development Institute, Ansan, Korea

1. Introduction

Subtropical gyre in the North Pacific ocean and its major current, the Kuroshio are one of the most important dynamic factors affecting the circulation and the sea surface height distribution in the East Asian Marginal Seas; the Kuroshio not only supplies heat and salt to the seas surrounding the Korean Peninsula and the Japanese Island, but also sustains high sea level state off the East China Sea shelf through the geostrophic balance. The North Pacific subtropical gyre and the Kuroshio region show the highest sea level in the global ocean. In this study we have conducted a series of numerical experiments to set up the ocean circulation model for simulating the realistic sea level variation and the circulation in the Northwest Pacific.

2. Model configurations of the global and regional ocean circulation models

The general circulation model used in this study is the GFDL MOM4p1. To escape the lateral boundary condition problems in regional circulation model (RCM) we have set up global circulation model (GCM) together with RCM. The GCMs have three versions of horizontal resolution; 2 degree x 1 degree, 1 degree (about 1/3 degree in equatorial region) x 1 degree, 0.5 degree(about 1/3 degree in equatorial region) x 0.5 degree in latitudinal and longitudinal direction, respectively. The North Pacific RCM has a grid resolution of 0.5 degree in both latitude and longitude. The vertical grid of the GCMs and the North Pacific RCM is composed of 50 vertical levels, resolving the actual bottom topography.

Major numerical schemes adopted in these global and regional models are psom scheme for tracer advection, isopycnal mixing scheme for horizontal diffusion of tracer, and kpp scheme for vertical diffusion. To simulate the distribution of sea surface elevation by density variation, pressure-coordinate system together with the non-boussinesq equation (equation of mass conservation) is adopted. For the thermohaline boundary condition at sea surface restoring condition using WOA (2005) climatology is applied with damping time scale of 10 days for temperature, and 60 days for salinity. As for the momentum boundary condition NCEP wind climatology are used. Heat flux is given using a bulk formula based on this climatologic wind.

3. Numerical experiments

GCM with 2 degree x 2 degree grid-resolution (GCM_2) was integrated for 40 years, and 1 degree x 1 degree version (GCM_1) was integrated for 500 years in model integration time. GCM_1 showed a generally increasing trend in sea surface height in the Pacific from the

initial stage to about 200 years. From 200 years to 500 years, however, it showed no remarkable increase in sea surface height, indicating that the model approached the quasi-steady state as for the sea surface height. It is shown that the sea level variation in the Southern Ocean approached the steady state after 50 years of a relatively short integration time. We examined the sea level variation obtained at 30 years of integration in the two GCMs for the consistent comparison though they are still in the spin-up stage.

The common features found in GCM_2 and GCM_1 are that the highest sea level is formed in the Kuroshio region of the North Pacific and the lowest sea level in the Southern Ocean (Fig. 1 and Fig. 2). In the GCM_2 the highest sea level of +1.2 m is obtained at the southwest off Japan and the lowest sea level of -2.5 m in the Southern Ocean both in August (Fig. 1). The subtropical and the subarctic gyre in the North Pacific show the maximum and the minimum sea surface height respectively, in the western part of the basin; in the subtropical gyre maximum of +1.2 m in summer and in the subarctic gyre minimum of -0.4 m in winter.

In the GCM_1 the maximum sea surface height of +1.0 m appears at the east off Philippine in August and the minimum of -3.0m in the Ross Sea close to the Antarctic continent in the same month (Fig. 2). The North Pacific subarctic gyre shows the minimum of -0.3m in sea surface elevation in winter.

In the RCM the maximum sea surface height is +0.6m in August at the east off Philippine, and the local minimums are -1.0 m in the coastal region of Okhotsk Sea and -0.6 m in the center of subarctic gyre in February (Fig. 3).

4. Discussion

The sea surface height simulated in the global model is generally determined by the spatial distribution of wind stress curl, heat and fresh water flux through sea surface, distribution of currents by basin-scale circulation, and the internal density field given as an initial condition, which is especially important in the spin-up stage. In this study we have found that the two GCMs and the RCM composed of the same surface boundary conditions, initial condition and the same numerical schemes but with different horizontal grid-resolution show different features of sea surface height distribution among them.

The GCM_2 simulated the sea surface height much higher than the GCM_1 in the subtropical gyre of the North Pacific and the Southern Ocean as a whole for the same period of model integration. The maximum and the minimum value of sea surface height obtained in the GCM_2 at 30 years correspond to those of GCM_1 for the period of 300 ~ 500 years of integration time (i.e., the maximum of 1.2 m in the North Pacific subtropical gyre and the minimum of -2.6 m in the Southern Ocean). This result implies that the spin-up time of the GCM_1 is longer than the GCM_2.

The 0.5 degree-resolution RCM shows 40~60 cm lower than the two GCMs in the maximum sea surface height of the North Pacific subtropical gyre at the same integration time. Also the circulation pattern inferred from the sea level distribution in the RCM is quite different from the two GCMs in the Gulf of Alaska and in the east coast of North America; in the GCMs relatively high sea levels induced by the Kuroshio Extension are expanded along the east coast of America and Gulf of Alaska, but in the RCM relatively low sea levels by the North Pacific subarctic gyre, instead. Sea surface height in the subtropical gyre of the South Pacific is also much lower and its spatial scale is much smaller in the RCM compared with the ones simulated in the 0.5 x 0.5 degree-resolution GCM though in its initial stage, which seems to be related with the existence of artificial southern boundary in the RCM (Fig. 4).

For the realistic simulation of the sea surface height distribution in the global or basin-scale modeling it is suggested that the consideration of integration time enough to cover the spin-up stage in the finer-resolution model, and the proper treatment of lateral boundary condition in the RCM are very important.

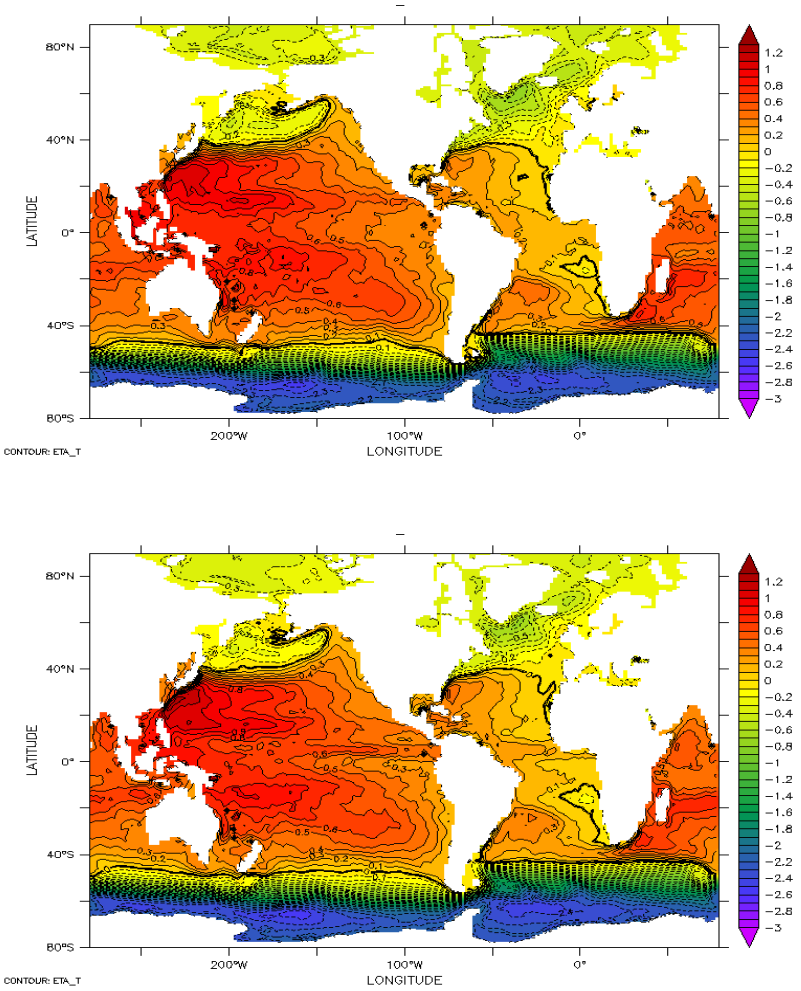

Fig. 1 Global sea surface height in GCM_2 in February (upper) and August (lower) at 30 years of integration

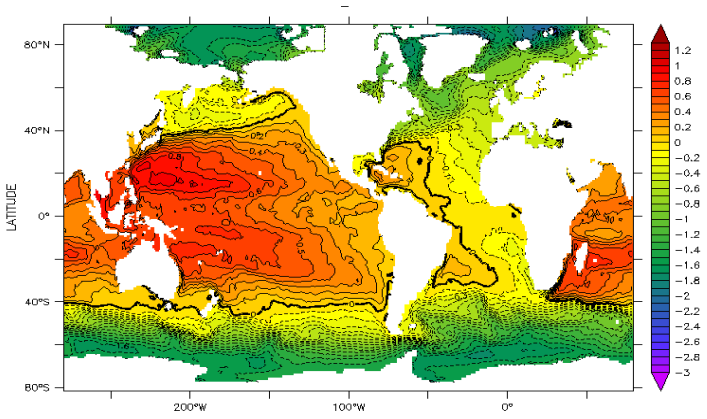

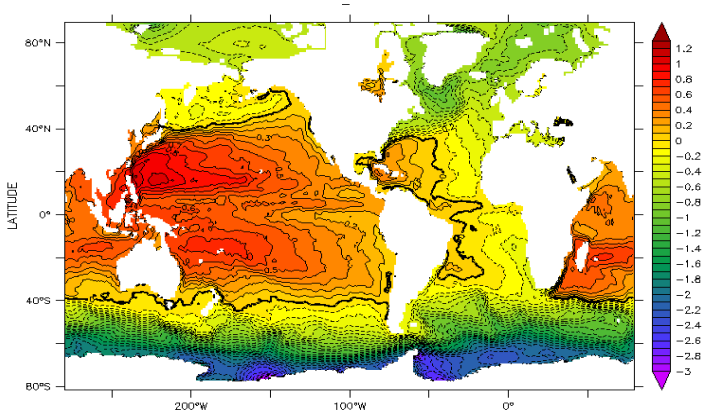

Fig. 2 Global sea surface height in GCM_1 in February (upper) and August (lower) at 30 years of integration

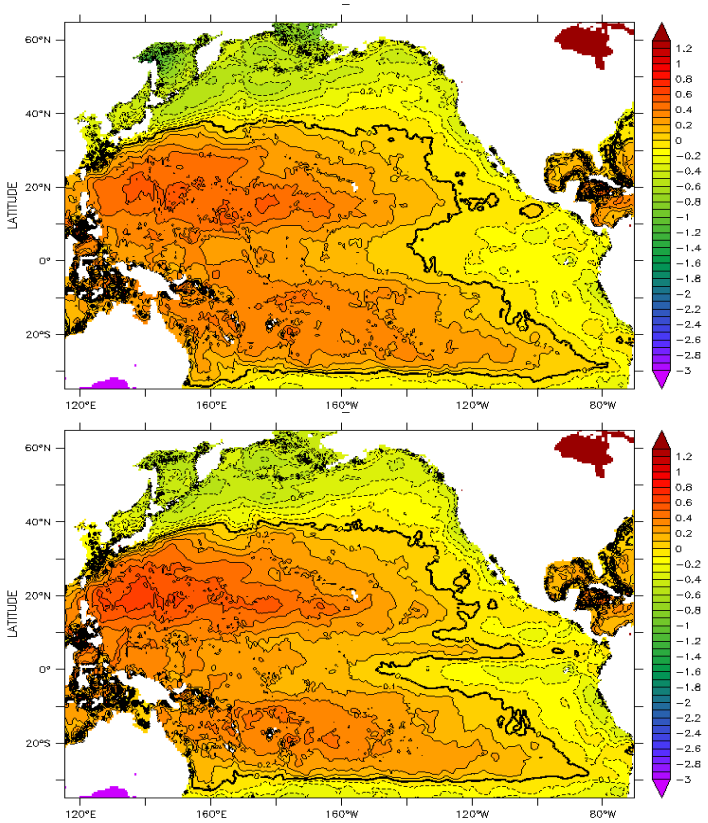

Fig. 3 Sea surface height of the Pacific Ocean in RCM in February (upper) and August (lower) at 30 years of integration

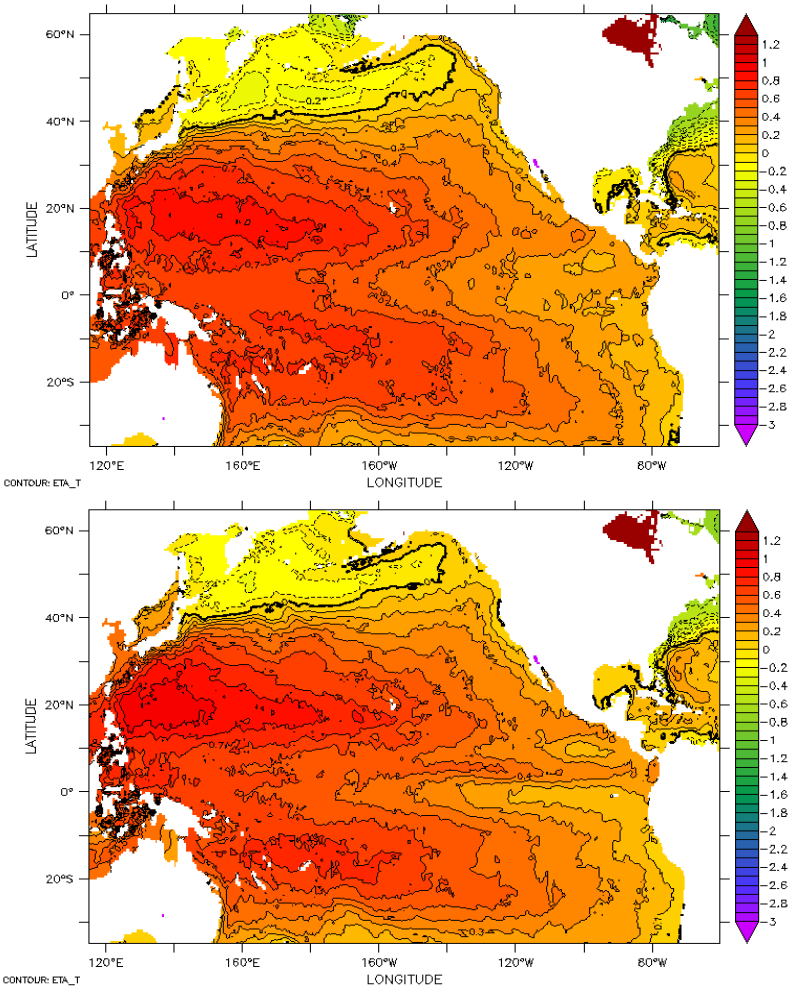

Fig. 4 Sea surface height of the Pacific Ocean in 0.5 degree-resolution GCM in February (upper) and August (lower) at 8 years of integration

Two Types of North Pacific Variability of Ocean: A Future Projection

Kwon, MinHo[1], Sang-Wook Yeh[2], and Chan Joo Jang[3]

[1]Korea Ocean Research & Development Institute, Ansan, Korea

[2]Hanyang University, Ansan, Korea

1. Introduction

Pacific decadal oscillation (PDO) has been described by some as a long-lived El Nino-like pattern of Pacific climate variability, which is the dominant empirical orthogonal functions (EOF) mode of unfiltered Pacific sea surface temperature anomaly in the north of 20N (Mantua et al., 1997). El Nino and southern oscillation (ENSO), which could affect all over the world, is known as the most prominent feature in the tropics on interannual time scale. Many researchers mentioned that PDO is related to ENSO as well as independent of ENSO. According to the previous studies, PDO contains two components such as North Pacific only mode induced by atmospheric noise and air-sea interaction and ENSO-related mode by atmospheric bridge (Frankignoul et al., 1997; Jin, 1997; Zhang et al., 1997; Mantua et al., 1997; Alexander et al., 2002; Newman et al., 2003; An and Wang, 2005). In addition, ENSO-related PDO has a significant effect to continental climate (e.g., Pavia et al., 2006). Recently, the impact of combined ENSO and PDO on the Pacific North Atlantic (PNA) climate was suggested using long-term simulations of coupled general circulation model (CGCM) (Yu and Zwiers, 2007).

Previous studies for North Pacific decadal variability suggested that there are two different modes of decadal sea surface temperature variability in the North Pacific (Deser and Blackmon, 1995; Miller and Schneider, 2000; Wu and Liu, 2003; Yeh and Kirtman, 2004). One is the SST variability around the subpolar front including the Kuroshio-Oyashio Extension (KOE) in the western part of the North Pacific basin. The other is the variability around the subtropical front associated with tropical and subtropical variability in the central part of the North Pacific.

The Fourth Assessment Report (AR4) of Intergovernmental Panel on Climate

Change (IPCC) has documented that global warming since the mid-last century is very likely due to the anthropogenic increase in greenhouse gas concentrations. The global warming forced by carbon dioxide can alter the characteristics of ENSO (e. g., Timmermann et al., 1999). AR4-IPCC GGCM results have diverse changes in characteristics of ENSO due to increase in greenhouse gas concentrations. For example, ENSO amplitude increases in the some coupled models by global warming scenario. It does not increase or decreases in the other models. In spite of the diversion of the model results, ensemble-means of the CGCMs could have consistent changes in oceanic and atmospheric characteristics of the greenhouse gas-induced coupled models. Currently, studies about two different modes of PDO and its changes causing by greenhouse gas increases are hardly found in the coupled model simulations. This study focuses changes of two modes of North Pacific variability due to global warming and its possible relationship with ENSO.

2. Data and Model Description

Monthly mean reanalysis SSTs provided by the National Centers for Environmental Prediction-National Center for Atmospheric Research (NCEP/NCAR) are utilized from 1850 to 2006 on 2.0 degrees latitude-longitude grid (Smith et al., 1996). The European Centre for Medium Range Weather Forecasting (ECMWF) reanalysis dataset (Uppala et al., 2005) provides atmospheric data for the period 1958-2002. The monthly means of these data have been entered into every grid with a horizontal resolution of 2.5 by 2.5 degrees.

CGCM results are used in order to assess future climate due to the global warming. AR4-IPCC model results are provided by the Program for Climate Model Diagnosis and Intercomparison (PCMDI). We used two scenarios, 20C3M and Special Reports for Emission Scenario A1B (SRES A1B) to compare 20 century climate with future climate forced by greenhouse gas increase. 20C3M was initialized from a point early enough in the pre-industrial control run to ensure that the end of all the perturbed runs branching from the end of this 20C3M run end before the end of the control. SRES A1B was initialized with conditions from the end of the 20C3M simulation and run to 2100, after which hold concentrations fixed as 720 ppm of the greenhouse gas concentration and continue run to 2200. We used 12 different coupled models such as CGCM3.1(T47), CNRM-CM3, GFDL-CM2.0, GFDL-CM2.1, GISS-ER, FGOALS-g1.0, INM-CM3.0, MIROC3.2(medres), MRI-CGCM2.3.2, PCM, UKMO-HadCM3, and UKMO-HadGEM1, which contain at least 100 years of commitment period. Our analysis is

confined to the commitment periods to understand characteristics of the greenhouse gas-stabilized climate of the coupled models.

3. Results

The detrended sea surface temperatures (SSTs) are used to decompose PDO modes from the coupled model results because the SSTs have strong trends even for commitment period of the scenarios 20C3M and SRES A1B. In addition, the wintertime-mean (December-January-February) SSTs are used because both ENSO and PDO have strong seasonal peaks during wintertime. Western PDO(WPDO) is defined by the first EOF mode of detrended DJF SST anomalies (SSTA) in the equatorial bands of western North Pacific Ocean (20N-70N, 120E-180) meanwhile central PDO (CPDO) is defined by the first EOF mode of detrended DJF SST anomalies (SSTA) in the equatorial bands of western North Pacific Ocean (20N-70N, 180-90W) in this model study. Figure 1a and 1b show two coherent modes of North Pacific SST variability. Interestingly, their corresponding principal component time series have different teleconnection patterns each other (Fig. 1c and 1d). WPDO is related to negative Indian Ocean sea surface temperature meanwhile CPDO is associated with warm anomalies of Indian Ocean. Also, CPDO is strongly correlated with ENSO.

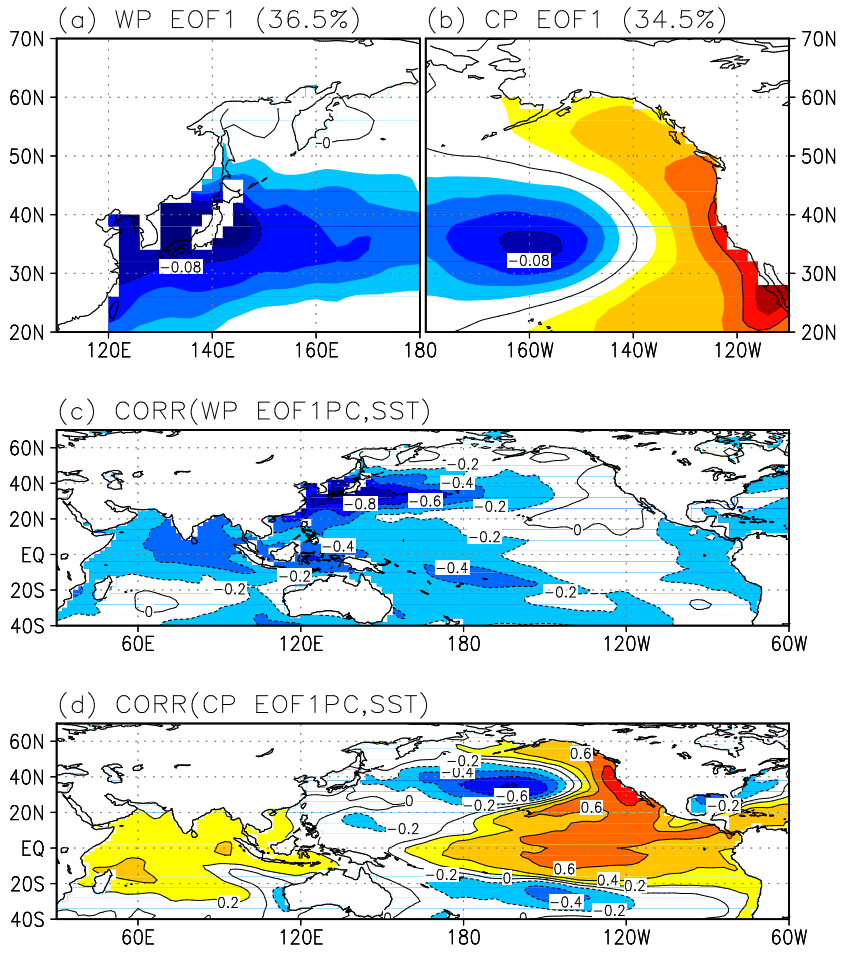

Figure 1. Dominant EOF modes of sea surface temperature in wintertime (December, January and February) in the two regions: (a) 20N-70N, 120E-180, (b) 20N-70N, 180-90W. Principal component regressed sea surface temperature anomalies of (a) and (b) for (c) western and (d) central North Pacific regions.

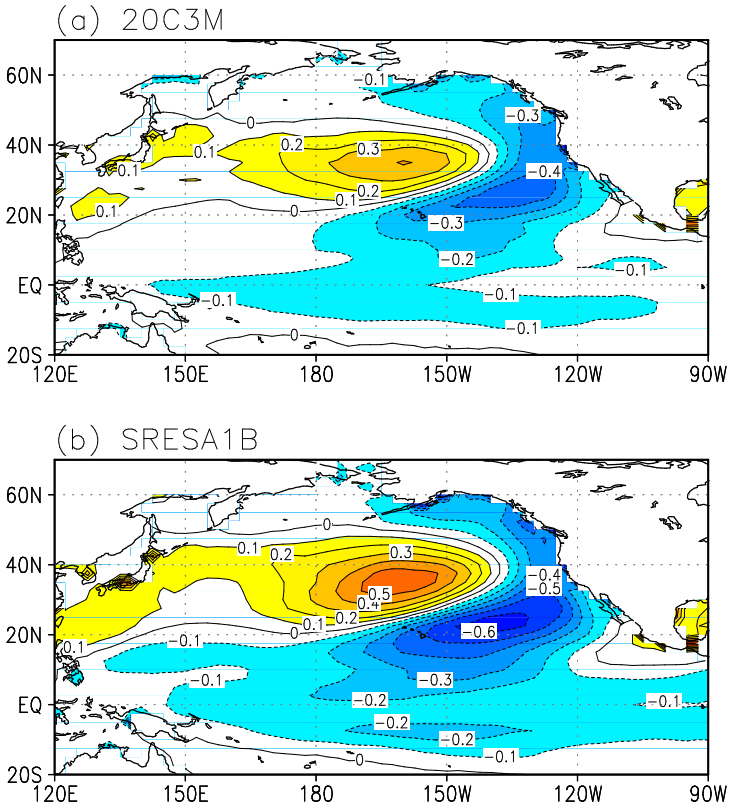

Figure 2. Maps of correlation coefficient between CPDO and sea surface temperatures in the North Pacific regions in (a) 20C3M and (b) SRES A1B scenarios in the coupled models.

Figure 2 shows that intensified CPDO variability associated with ENSO in the warmed climate state. It indicates that relationship between ENSO and PDO would be strengthened in the future scenario run. In order to investigate the ENSO and PDO relationship ENSO index is defined by principal component of EOF1 of equatorial Pacific sea surface temperatures. The ENSO index of the model is the corresponding principal component of EOF1 rather than NINO indices because the ENSOs simulated by the coupled model have diverse characteristics such as different positions of SSTA center during El Nino peak. ENSO index is also symbolized by ENSO in convenience. The maps of correlation coefficient between ENSO and SSTA exhibit different patterns in the scenarios 20C3M and SRES A1B for all models (Figure 3). There are some distinctive changes of the correlation map in SRES A1B comparing with that of 20C3M. First of all, ENSO-related PDO has stronger and its center shifts eastward in SRES A1B.

It is noteworthy that ENSO-related PDO of the models does not appear in the Kuroshio-Extension region. SST variability in the Kuroshio-Extension region is not

related to ENSO in observation. The correlation coefficients between ENSO and SSTA in the tropical Pacific region are smaller in SRES A1B than those of 20C3M.

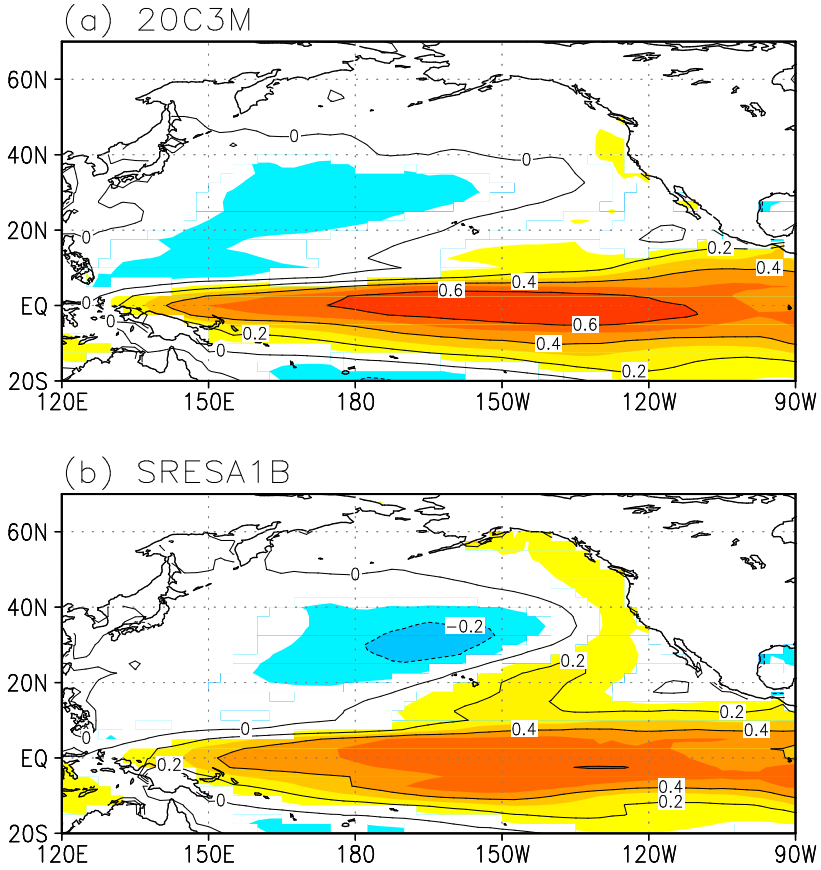

Figure 3. Maps of correlation coefficient between 12-model combined SSTA and ENSO index for (a) 20C3M and (b) SRESA1B

These relatively small correlation coefficients between ENSO and SSTA in tropics indicate that tropical SSTA has non-ENSO variability because ENSO is defined by the first EOF of tropical SSTA in Pacific in this study. Moreover, the eigenvalue for EOF1 in ENSO region decreases in dominant number of models, which are run in SREA A1B scenario, than that of 20C3M (figure not shown). As a matter of fact, the non-ENSO variability of the SSTA could be understood as modified ENSO due to tropics-subtropics interaction. SSTA in the subtropical region (160W-130W, 10N-20N) is highly correlated with ENSO. The negative relationship between that subtropical SSTA and SSTA in the mid-latitude region (180-150W, 20N-40N) increases in SRES A1B. All individual models exhibit the similar increase of the negative relationship between those

two time series except only 1 model, GISS-ER. The ENSO-correlated subtropical SSTA are associated with subtropics-expanded EOF of tropical SSTA in almost SRES A1B models (figure not shown). This implies that the interaction between ENSO and PDO could be more active in SRES A1B scenario.

References

Alexander, M., I. Bladé, M. Newman, J. R. Lanzante, N.-C. Lau, and J. D. Scott (2002), The atmospheric bridge: The influence of ENSO teleconnections on air–sea interaction over the global oceans, J. Climate, 15, 2205–2231.

An, S.-I., and B. Wang (2005), The forced and intrinsic low frequency modes in the North Pacific. J. Climate, 18, 876–885.

Deser, C., and M. L. Blackmon (1995), On the relationship between tropical and North Pacific sea surface temperature variations. J. Climate, 8, 1677-1680.

Frankignoul, C., P. Müller, and E. Zorita (1997), A simple model of the decadal response of the ocean to stochastic wind forcing, J. Phys. Oceanogr., 27, 1533–1546.

Jin, F.-F. (1997), A theory of interdecadal climate variability of the North Pacific ocean–atmosphere system, J. Climate, 10, 1821–1835.

Mantua, N. J., S. R. Hare, Y. Zhang, J. M. Wallace, and R. Francis (1997), A Pacific interdecadal climate oscillation with impacts on salmon production, Bull. Amer. Meteor. Soc., 78, 1069–1079.

Miller, A. J., and N. Schneider (2000), Interdecadal climate regime dynamics in the North Pacific Ocean: Theories, observations and ecosystem impacts. Progress in Oceanography, Vol. 27, 257-260.

Newman, M., G. P. Compo, and M. A. Alexander (2003), ENSO-forced variability of the Pacific decadal oscillation, J. Climate, 16, 3853–3857.

Pavia, E., F., Graef, J. Reyes (2006), PDO-ENSO effects in the climate of Mexico, J. Climate, 19, 6433-6438.

Timmermann, A., J. Oberhuber, A. Bacher, M. Esch, M. Latif, and E. Roeckner (1999), Increased El Nino frequency in a climate model forced by future greenhouse warming, Nature, 398, 694-696.

Uppala, S. M., and coauthors (2005), The ERA-40 re-analysis, Q. J. R. Meteorol. Soc., 131, 2961-3012.

Wu, L., and Z. Liu (2003), Decadal Variability in the North Pacific: The Eastern North Pacific Mode. J. Climate. 16, 3111–3131.

Yeh, S.-W., and B. P. Kirtman (2004), The impact of internal atmospheric variability on the

North Pacific SST variability, Clim. Dyn., 22, 721– 732.

Yu, B., and F. Zwiers (2007), The impact of combined ENSO and PDO on the PNA climate: a 1,000-year climate modeling study, Clim. Dyn., 29, 837-851.

Zhang, Y., J. M. Wallace, and D. S. Battisti (1997), ENSO-like interdecadal variability, J. Climate, 10, 1004–1020.

A Regional Climate Model

for the British Columbia Continental Shelf

M.G.G. Foreman[1], D. Masson[1], W. Callendar[1], J. Morrison[1],

I. Fain[1], W.J. Merryfield[2], B. Pal[2],

[1]Institute of Ocean Sciences, Fisheries and Oceans Canada,
P.O. Box 6000, Sidney B.C., V8L 4B2, Canada
[2]Canadian Centre for Climate Modelling and Analysis, Environment Canada,
University of Victoria, P.O. Box 3065 STN CSC, Victoria B.C., V8W 3V6, Canada

The ocean circulation model used to estimate future circulation and water properties along the British Columbia shelf was developed by Masson and Fain (2011). It is an application of the Regional Ocean Modeling System (ROMS, Haidvogel et al., 2008) with 3 km horizontal resolution, 30 sigma layers in the vertical, and the coverage shown in Fig 1. The model is forced with tides, daily wind and heat flux from the North American Regional Reanalysis (NARR), freshwater runoff from twenty rivers, and lateral boundary salinities and temperatures from the Simple Ocean Data Assimilation (SODA) project. With initial temperatures and salinities also taken from SODA, a model simulation over the period 1995 to 2008 has been shown to reproduce inter-annual sea surface temperature patterns, the major seasonal currents, and elevation time series from coastal tide gauges with reasonable accuracy. The interested reader is directed to Masson and Fain (2011) for more details.

In order to use this model for future projections, it need only be run with suitable future forcing and initial fields. As the gravitational forcing fields that determine the tides are completely predictable, that component can be easily forecast. The required atmospheric forcing can be obtained by applying downscaling techniques to output from global climate models (GCMs) and/or regional climate models (RCMs) that are available from either

- the Coupled Model Intercomparison Project phase 3 (CMIP3) multi-model data set of the World Climate Research Programme (WCRP), assembled at the Program for Climate Model Diagnosis and Intercomparison (PCMDI, http://www-pcmdi.llnl.gov/) to inform the IPCC Fourth Assessment, or
- the North American Regional Climate Change Assessment Program (NARCCAP, http://www.narccap.ucar.edu/).

As the NARCCAP data have a finer horizontal resolution (approximately 50 km) and thus should be better to able to capture spatial variations in i) terrestrial precipitation (both rainfall and snowfall) and ii) oceanic winds and heat fluxes, they were chosen. As a consequence, our model simulations focussed on the NARCCAP-defined ‘current’ and

'future' time periods of 1970-1999 and 2040-2069, respectively. Note that these NARCCAP future simulations assume the A2 emissions scenario (no leveling off of greenhouse gases). Initial conditions, boundary conditions and atmospheric forcing values were generally constructed for the future simulation by calculating anomalies between future and current RCM/GCM downscaled values and adding them to the ROMS hindcast values.

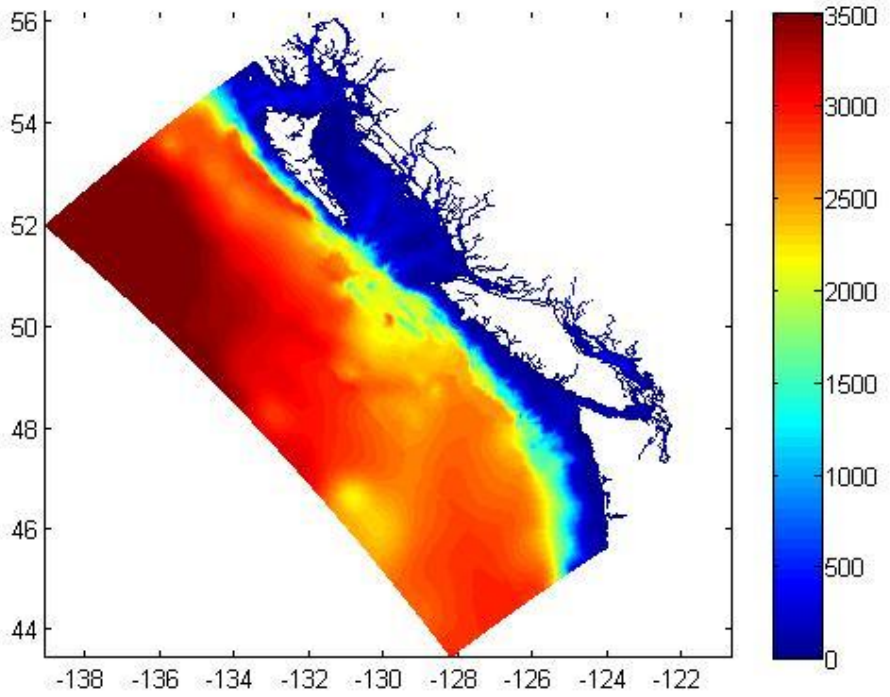

Fig 1. Extent and bathymetry (m) for the British Columbia regional climate model.

There are six RCMs within NARCCAP. Though we eventually aim to force our BC shelf model with the atmospheric anomalies from all six and compute ensemble averages from the associated results, our initial anomalies for air temperature, air pressure and humidity were calculated using only one, the Canadian Regional Climate Model (CRCM) which in turn was forced by the Canadian Global Climate Model (CGCM3). Since the CRCM has significantly lower resolution than our oceanic shelf model, there were regions that it defined as land and our model defined as water. As the values for air temperature, air pressure and humidity given by the CRCM in these regions were affected by being over land, new values for these coastal areas were calculated using Empirical Orthogonal Functions (EOFs). These EOFs were generated using NARR data over a 15 year period between 1995 and 2009 where 14 years were used to generate the EOFs and the remaining year was used to test the ability of the EOFs to generate coastal data based on offshore data. Ten EOFs were used to approximate the data and the regeneration of the test year was

accomplished with an average R-squared value of 0.95 and p-values with an order of magnitude 10^{-5}.

Dealing with the rest of the atmospheric forcing was less complex. As no land effects were noticeable in the CRCM precipitation output, these data were used as-is to calculate the necessary anomalies. Short-wave and long-wave radiation showed no significant difference between the current and future scenarios, so these forcings were left at their current scenario values.

As the CRCM is atmosphere only, anomalies for the initial oceanic temperature and salinity fields were calculated from CGCM3 output. As with the CRCM downscaling, the coarse CGCM3 resolution necessitated the use of special downscaling techniques. In this case, the number of points in the 3-D GCM grid made using EOFs prohibitive so latitudinally-averaged annual anomalies were found and applied to the current scenario fields over the entire grid. The results are shown in Fig 2. The same anomaly fields were applied to temperatures and salinities along the lateral boundaries of the model.

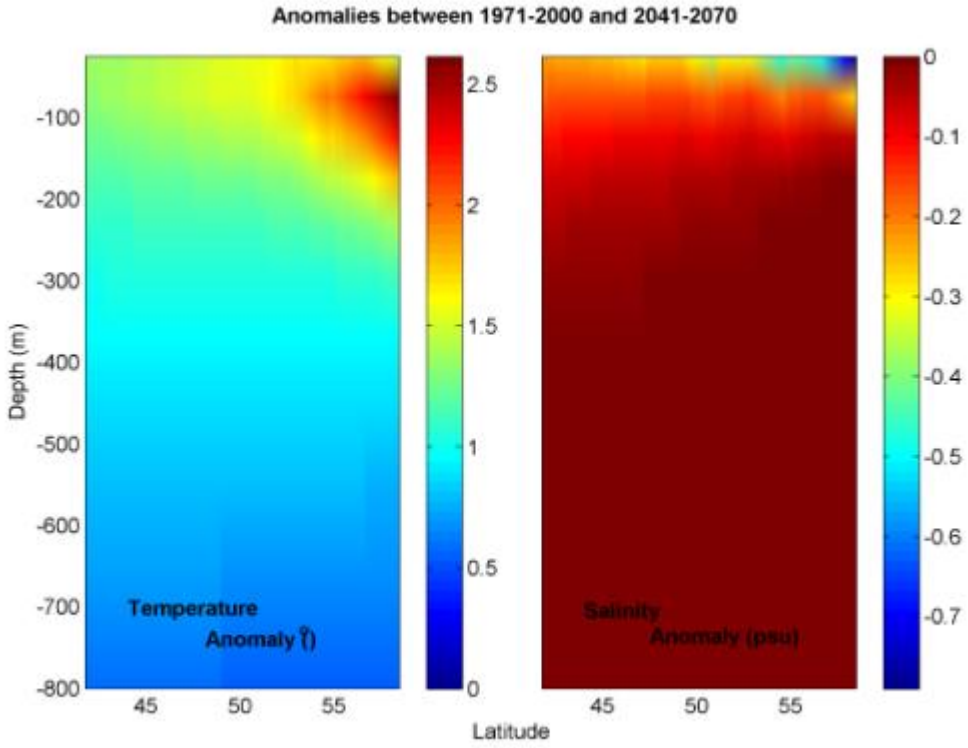

Figure 2. Temperature and salinity anomalies as functions of latitude and depth, and as computed from the CCCma CGCM3.1 T47 SRES A2 run #4.

As baroclinic flows along the BC shelf are largely determined by salinity rather than temperature gradients, freshwater discharges along the coast are important, not only for their direct role in generating coastal currents but also indirectly for transporting larvae and

nutrients and acting as possible barriers to cross-shelf transport, e.g. from shelf-edge upwelling. Fig 3 shows that watersheds along the BC coast are projected to become wetter in winter (DJF) and drier in summer (JJA). As a significant amount of the winter precipitation away from the coast itself is stored as snow-pack and released later in the year, drier summers do not necessarily mean less discharge.

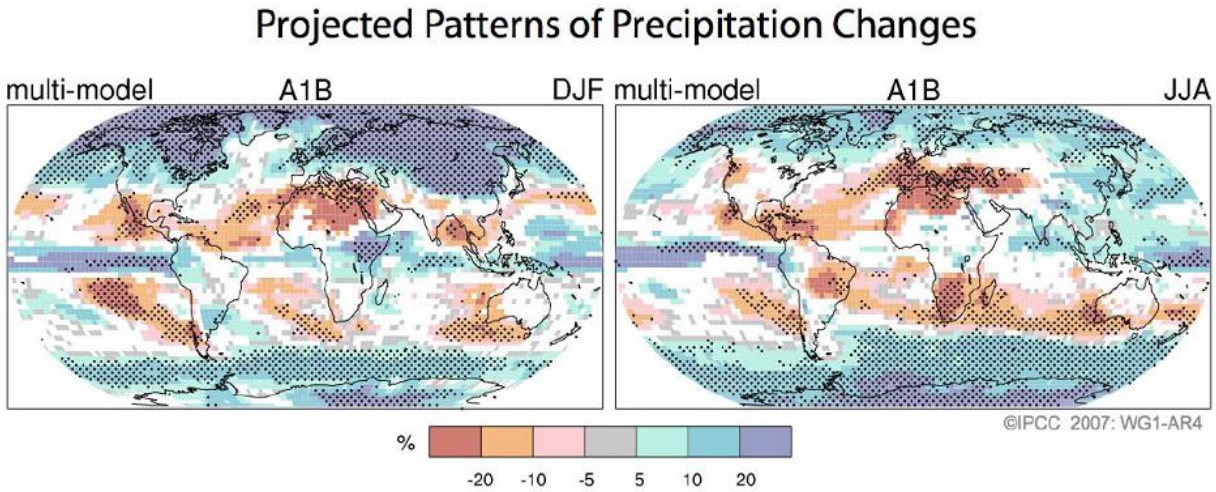

Figure 3. Percentage changes in precipitation for the period 2090–2099, relative to 1980–1999. Values are multi-model averages based on the A1B emission scenario. White areas are where less than 66% of the GCMs agree in the sign of the change and stippled areas are where more than 90% of the models agree in the sign of the change. DJF =winter, JJA=summer. This was Fig 7 in IPCC AR4 Summary for Policy Makers.

The main problem in estimating both historical and future freshwater discharge affecting the BC coast is that approximately 20% is ungauged. Morrison et al. (2011) developed a technique for estimating ungauged runoff based on the precipitation, temperature, terrain characteristics, and storage capacity within twenty-two basins (Fig 4) whose freshwater discharges affect coastal BC waters. The technique has been verified with historical observations and used to reconstruct time series for each of the twenty-two watersheds back to 1970. Though there was considerable annual variability, the total annual discharge averaged about 1000 km^3 and there was no statistically significant trend over this time period.

In order to employ the same technique to estimate future discharges, future precipitation, temperatures, and snowpack estimates were downscaled from the same CRCM model output that was used to provide the atmospheric forcing. An earlier study that was restricted to only the Fraser River watershed (Morrison et al., 2002) and projections from the CCCma IPCC AR3 global model predicted only a modest (5%) increase in the average total annual discharge over 2070-2099, but increased flow over the winter and an earlier (by 24 days) spring melt and 18% smaller peak discharge.

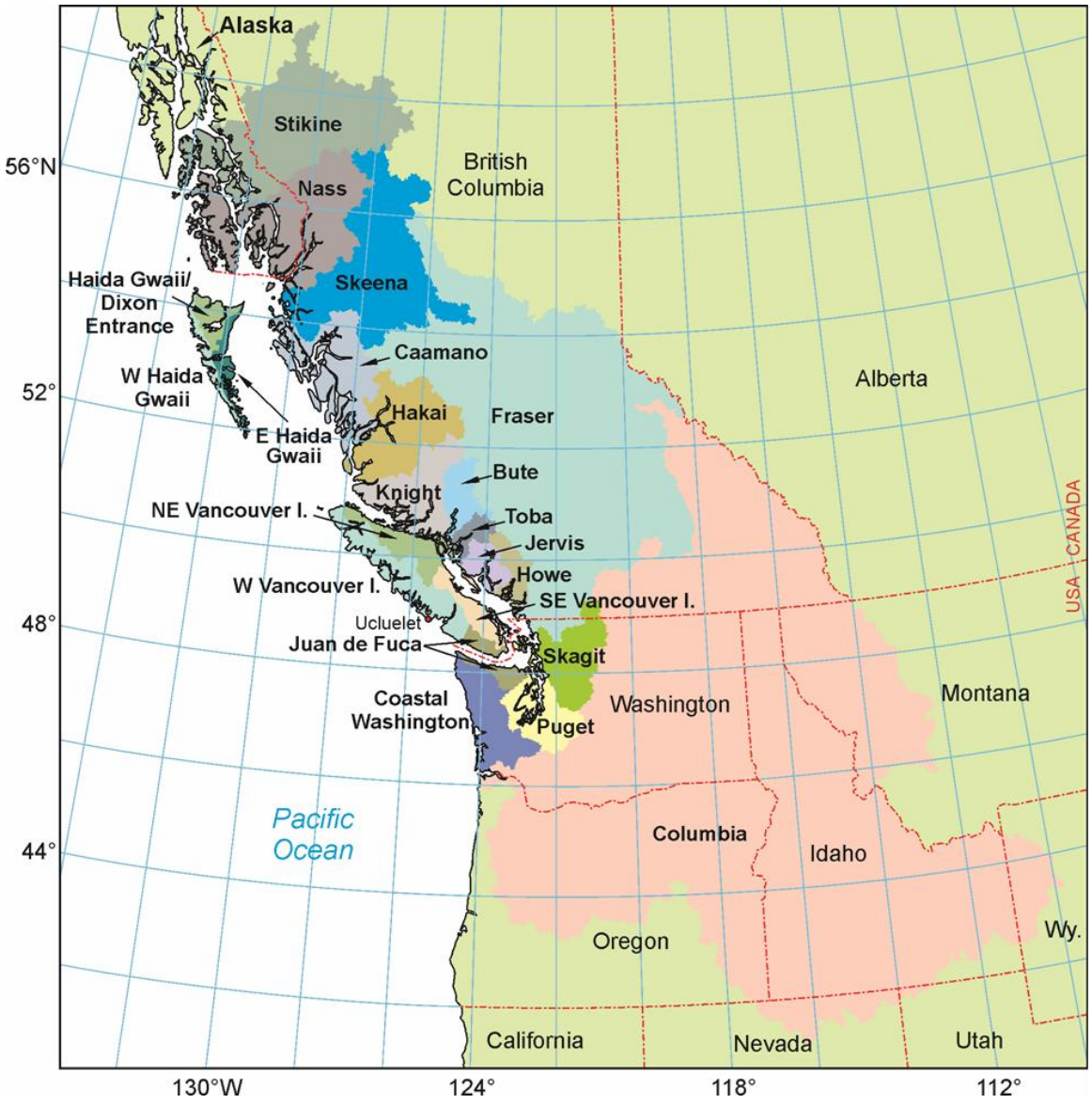

Figure 4. Water Survey of Canada drainage basins affecting British Columbia coastal waters.

Figure 5 shows the 1970-99 and 2040-69 discharges for the twenty-two basins affecting BC shelf waters and the nine that empty into the Salish Sea (Puget Sound, Juan de Fuca Strait, and the Strait of Georgia). Consistent with the projections shown in Fig 3, only for July and parts of June and August are the future discharges projected to be less than present-day values; for the rest of the year they are larger. And consistent with the Morrison et al (2002) result, in the Salish Sea where the Fraser River is the largest contributor to the total discharge, the peak discharge is seen to be occurring earlier in the year. However the peak value remains about the same.

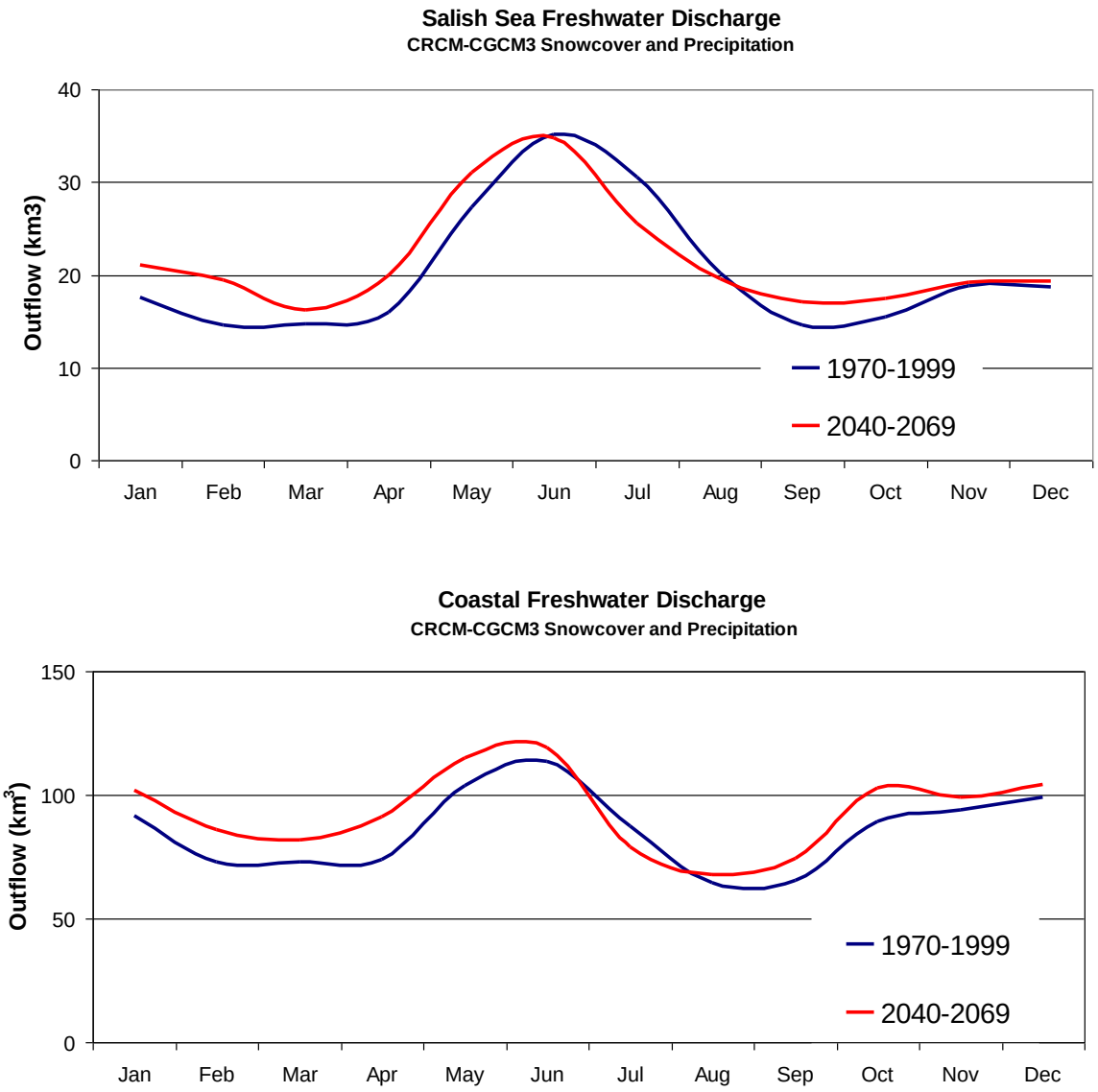

Figure 5. Contemporary and future freshwater discharges for a) the nine watersheds emptying in the Salish Sea, and b) all twenty-two watersheds impacting coastal BC waters, as estimated by output from the CRCM.

Our modelling strategy is to build-up the future forcing fields incrementally so that the impact of each can be assessed. At the time of writing this report, only simulations with future heat flux, tides and lateral boundary forcing had been completed. Future freshwater discharges are planned next and future winds will be the final addition; but for the results shown here, those forcings were kept the same as for the baseline period.

Sample results for the first set of simulations are shown in Figures 6 and 7. Average annual sea surface temperature anomalies for a 14-year future simulation with respect the 1995-2008 Masson and Fain (2011) hindcast are shown in Fig 6b. Warmer values are seen

everywhere along the thalweg (Fig 6a) traversing Juan de Fuca Strait, Haro Strait, and the Strait of Georgia, but due to a combination of tidal mixing and Fraser River discharges (which enters the Strait of Georgia at approximately kilometre 250), they are not spatially uniform. Figure 7 shows average annual temperature anomalies as a function of depth at a location which is approximately 300 km along the thalweg. Though positive anomalies of at least 0.65℃ are seen all the way down the water column, they are larger near the surface and have depth dependent maxima ranging between April and June.

Simulations with additional future forcing fields are planned and analyses of their results will be described in a manuscript that will be submitted to a peer-reviewed journal.

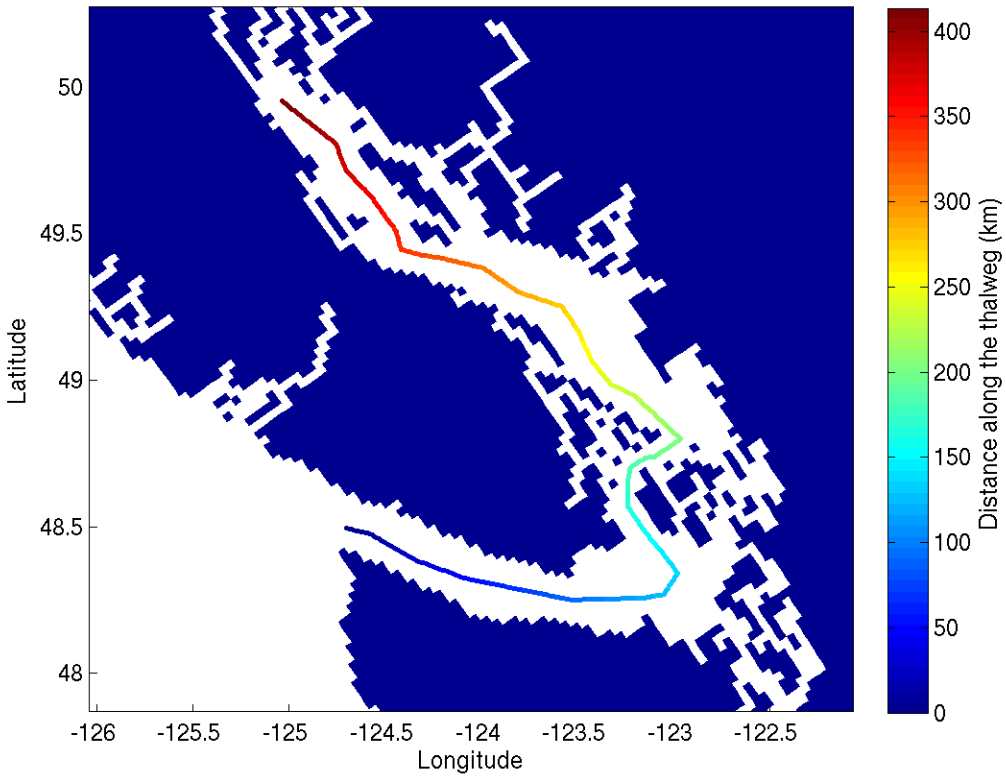

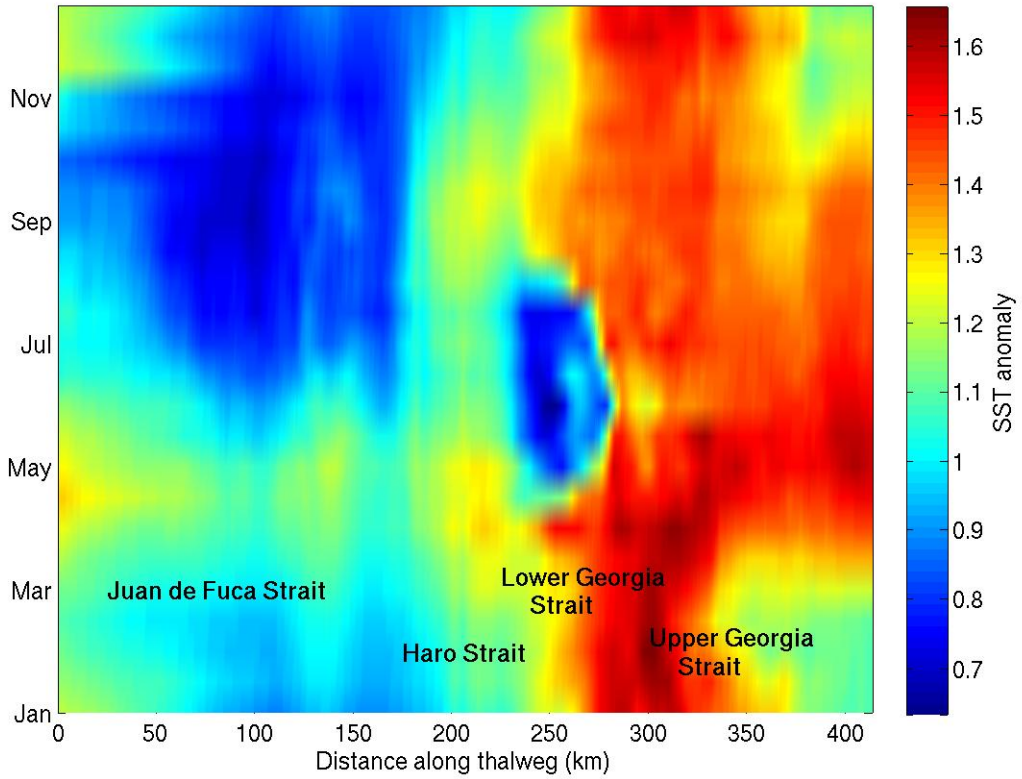

Figure 6. a) Model grid and thalweg along Juan de Fuca Strait, Haro Strait and Strait of Georgia, b) annual average sea surface temperature anomalies (℃) along the thalweg.

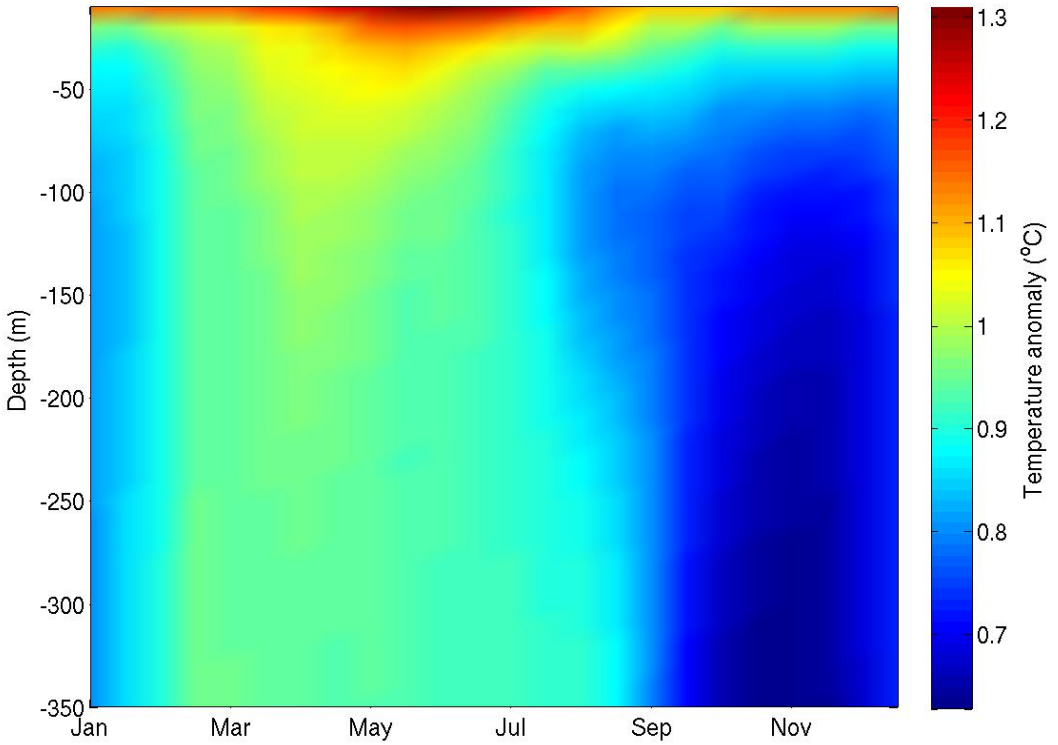

Figure 7. Average temperature (℃) anomalies (future-present) as a function of depth at a site 300km along the thalweg shown in Fig 6a.

Acknowledgments

We thank the Centre for Ocean Model Development for Application within Fisheries and Oceans Canada (FOC) for the funding to support the development of the BC shelf model, and to purchase the 256 processor computer on which that model runs. We also thank the Climate Change Science Initiative and Ecosystem Research Initiative within FOC for their financial support, and the Korean Ministry of Land, Transport and Maritime Affairs, the North Pacific Martine Science Organization, the International Council for the Exploration of the Sea, and Seoul National University for their support of this RCM workshop.

References

Haidvogel, D. B. , H.G. Arango, W.P. Budgell, B.D. Cornuelle, E. Curchitser, E. Di Lorenzo, K. Fennel, W.R. Geyer, A.J. Hermann, L. Lanerolle, J. Levin, J.C. McWilliams, A.J. Miller, A.M. Moore, T.M. Powell, A.F. Shchepetkin, C.R. Sherwood, R.P. Signell, J.C. Warner, J. Wilkin (2008), Ocean forecasting in terrain-following coordinates: formulation and skill assessment of the Regional Ocean Modeling System. Journal of Computational Physics, 227(7), 3041-3065.

Masson, D., and I. Fain (2011), A circulation model for the British Columbia continental shelf, in preparation.

Morrison, J., M.C. Quick, and M.G.G. Foreman (2002), Climate change in the Fraser watershed: Flow and temperature predictions. J. Hydrology, 263, 230-244.

Morrison, J., M.G.G. Foreman, and D. Masson (2011), A method for estimating monthly freshwater discharge affecting British Columbia coastal waters, accepted in Atmosphere-Ocean.

Up- and down-scaling effects of upwelling

in the California Current System

Enrique Curchitser[1], Justin Small[2], Kate Hedstrom[3,]

Michael Alexander[4] and William Large[2]

[1]Institute of Marine and Coastal Sciences, Rutgers University

[2]National Center for Atmospheric Research, Boulder, Colorado
[3]University of Alaska Fairbanks
[4]National Oceanic and Atmospheric Administration, Boulder, Colorado.

1.Background

Though global climate models can represent many identifiable features of the climate system, they also suffer from significant localized biases. Climate model biases are not uniform over the globe. For example, in the ocean, modeled sea surface temperature (SST) errors are often largest along the continental margins (see Figure 1). Many coupled climate models generate very large SST biases in the coastal upwelling regions of the California Current System (CCS), the Humboldt Current system (HCS) and the Benguela Current System (BCS), where simulated mean SSTs are much warmer than observed. Figure 1 (top left panel) shows that the NCAR-CCSM3 (spectral atmosphere) used in IPCC-AR4 was no exception, with biases in excess of 3oC in all three regions. Furthermore, these SST biases have significant remote effects on surface and subsurface temperature and salinity, and on precipitation and hence atmospheric heating and circulation (Collins et al. 2006). Large and Danabasoglu (2006) showed, in particular, with observed SSTs imposed along the BCS coast in an otherwise freely-evolving CCSM3 simulation there are significant improvements in precipitation in the western Indian Ocean, over the African continent and across the Equatorial Atlantic (see Figure 2). Imposed SSTs along the HCS coast reduce precipitation in the so-called double ITCZ region of the south tropical Pacific.

These errors often coincide with regions of importance to oceanic ecosystems and nearby human populations. In the Intergovernmental Panel on Climate Change (IPCC-AR4) Working Group 1 assessment report, where the reliability of the models used to make projections of future climate change is assessed, Randall et al. (2007) discuss the many improvements and the strengths of the current generation of coupled models of the physical climate system, but they also highlight a number of remaining significant model errors. Furthermore, they state "*The ultimate source of most such errors is that many important small-scale processes cannot be represented explicitly in models, and so must be included*

in approximate form as they interact with larger-scale features." Some of the reasons given for the deficiencies are limited computer power, data availability and scientific understanding. Conversely, regional models have shown significant skill in modeling coastal processes (e.g., Curchitser et al., 2005, Powell et al., 2007, Combes et al., 2009, Veneziani et al., 2009a,b). This creates the opportunity, and perhaps necessity, to develop multi-scale numerical solution schemes that adapt the resolution in specific areas of interest, such as the California Current System.

Figure 1 (top right) shows that the coastal winds in the latest CCSM4 with a 2o resolution (finite volume) atmosphere produce even larger SST biases than were apparent in CCSM3 (top left), despite many improvements to the physical model components. Improving the coastal winds by increasing the atmospheric resolution to 1o, however, significantly reduces the coastal SST biases (Figure 1, bottom). The implication is that the further reductions in the SSTs required to eliminate the coastal biases under present day conditions will likely also need to come from improvements to the ocean physics and the upwelling of cold water in particular. These improvements must be realized before the regional biogeochemistry and ecosystem models can be expected to behave accurately because of the sensitivity to temperature and the critical importance of upwelled nutrients for biological processes.

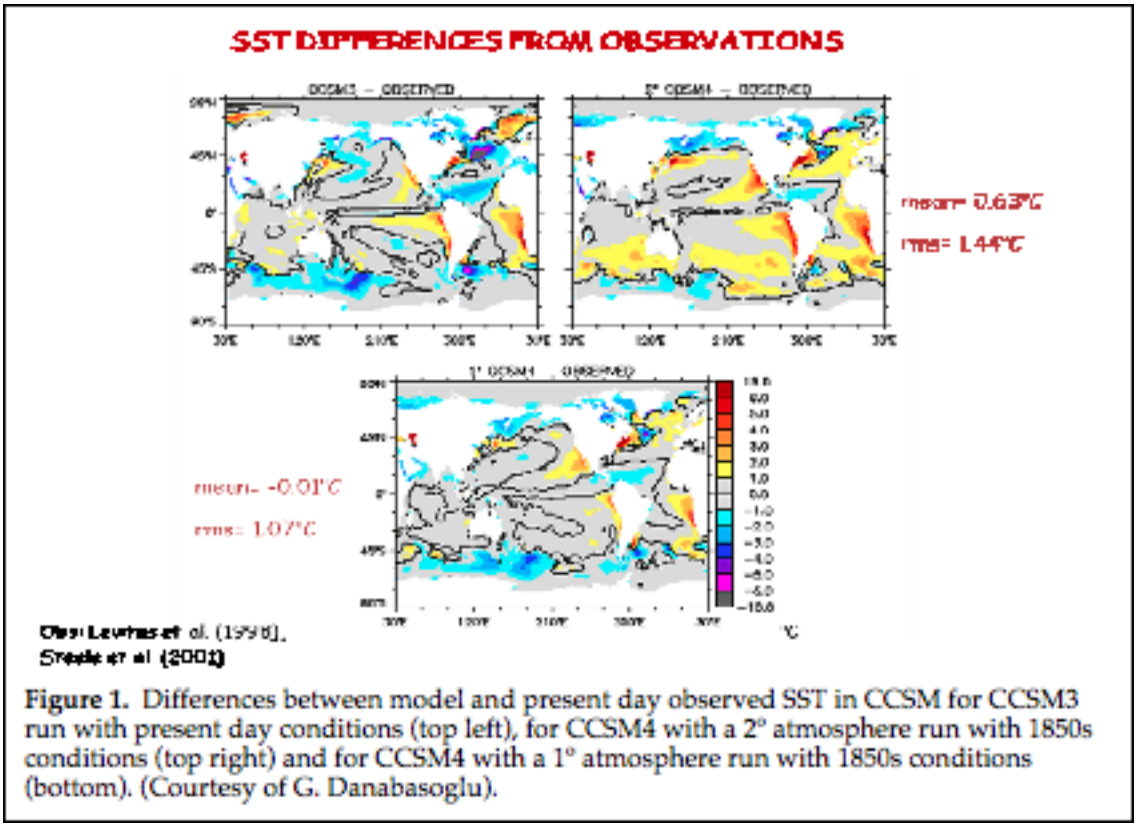

Figure 1. Differences between model and present day observed SST in CCSM for CCSM3 run with present day conditions (top left), for CCSM4 with a 2° atmosphere run with 1850s conditions (top right) and for CCSM4 with a 1° atmosphere run with 1850s conditions (bottom). (Courtesy of G. Danabasoglu).

One approach to achieve high-resolution climate-scale simulations in a given domain is the nesting of a high-resolution limited-area grid within a lower resolution large-scale numerical domain (Ito et al., 2009). With a nesting approach, information is downscaled from the coarse to a fine resolution region through an overlap in the domains. "Simple" downscaling using one-way flow of information works well when the forcing data are constrained by observations, for instance such as in the case when using atmospheric reanalysis products (e.g., Kalnay et al., 1996). The high-resolution nest can explicitly resolve features missing from the large-scale model simulation, though it is still constrained through the boundaries by the large-scale climate patterns. However, when using freely-evolving coupled models, such as those used by IPCC to study past and future climate, the mean resulting climate is unconstrained by observational data. Therefore, a given atmospheric model can be expected to respond differently to an alternative (e.g., high-resolution) ocean in the coupled system. The challenge is then to not only downscale information to the local scales, but also to understand how regional variability affects the global climate**.**

In order to address the above issues we developed a new multi-scale ocean as part of the U.S. National Center for Atmospheric Research Community Climate System Model (NCAR-CCSM). The new composite ocean consists of the global Parallel Ocean Program (POP) and the Regional Ocean Modeling System (ROMS). The new composite ocean is connected to the rest of the CCSM climate model through a modified flux coupler (See Figure 2).

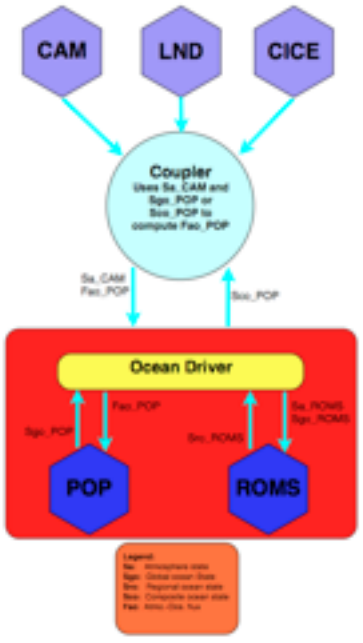

Figure 2. Schematic of the multi-scale CCSM. The original ocean module (POP) has been replaced by a composite POP/ROMS module that is controlled by a newly designed ocean driver. The Ocean driver passes fluxes and state variables to the respective oceans, controls the communications between the global and regional oceans (boundary conditions) and also assembles the output of the two oceans (e.g., SST's) that are then passed to the coupler for the computation of the fluxes to the atmosphere (CAM), Land (LND/CLM) and sea ice (CICE/CSIM) modules.

2. Results from the multi-scale coupled model

In order to test and demonstrate the capabilities of the multi-scale climate model, we have been carrying out a series of simulations where the northeast Pacific upwelling region is solved using a high- resolution (10 km) ocean within a global (1o) model. The atmosphere is on a spectral grid (~2o), sea ice is solved on the ocean grid and the land surface model on the atmospheric grid. The CCSM is initialized from a spun-up climatology and time- stepped for 150 years. This simulation is then compared to a control run without the high- resolution ocean. Figure 3 is a close-up look at the northeast Pacific showing the anomaly in the SST in a coupled climate simulation between a case with the composite ocean and the control, for all the available months of August (upwelling season). Superimposed are wind vector anomalies. What is seen is that the new multi-scale ocean is able to resolve the upwelling that is mostly missing from the global simulations, and this has a significant effect on the regional wind patterns.

Figure 4 shows the surface sea temperature and standard deviation for summer months (June-August) of the control simulation and the corresponding anomalies with the composite model for the last 140 years of simulation. The thick black lines outline regions of 95% confidence based on T- and F- tests for the mean and standard deviations, respectively. The temperature anomaly plot shows the local cooling effect that results from resolving the upwelling in the northeast Pacific and also remote effects in the Atlantic ocean. Significant, and robust, effects are also seen in other variables such as tropical precipitation and sea level pressure.

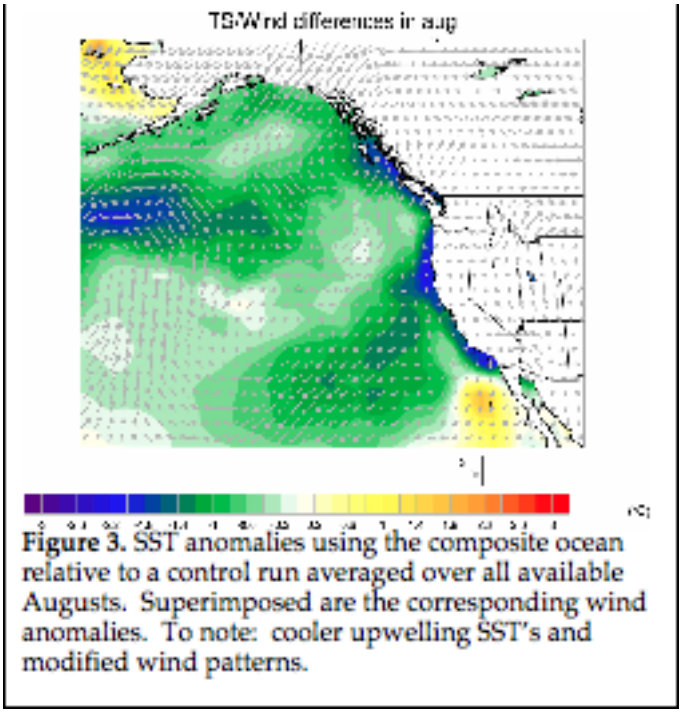

Figure 3. SST anomalies using the composite ocean relative to a control run averaged over all available Augusts. Superimposed are the corresponding wind anomalies. To note: cooler upwelling SST's and modified wind patterns.

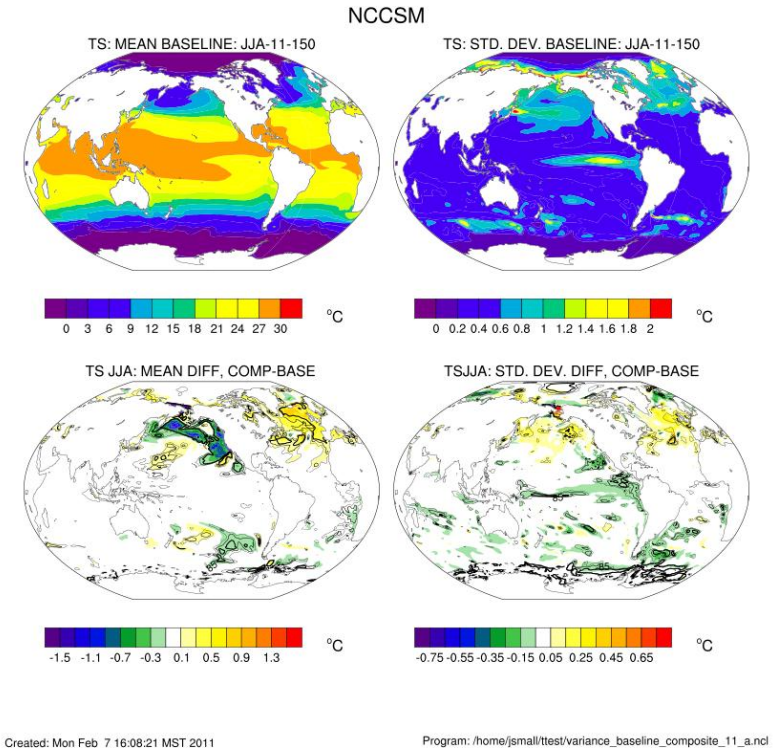

Figure 4: Mean and standard deviation for the summer months of both the control and composite simulations. Thick black lines indicate 95% confidence level using the T- and F-test for the mean and deviation, respectively. Note both the local and remote effects caused by the perturbation that results from resolving the upwelling signal in the northeast Pacific region.

3.Summary

A new multi-scale capability was developed by merging a global and a regional ocean model within a global climate model. The goal was to address some of the biases exhibited by low-resolution global models in regions with implications to marine ecosystems. Long integrations show that this configuration is able to address some of these regional biases. Furthermore, by preserving the feedbacks between the regional and global climate models we are able to study upscaling effects that arise from the regionally introduced perturbations. In the case presented here we see effect as far afield as the north Atlantic ocean. Further studies are proceeding by studying the effects of resolving other major upwelling regions as well a new study in a western boundary current region where global models also show sea surface temperature biases. Future plans include adding a biogeochemistry model to this configuration in order to study the role of upwelling regions in the global CO2 cycles.

References

Collins WD, Bitz CM, Blackmon ML, Bonan GB, Bretherton CS, et al. (2006). The Community Climate System Model version 3 (CCSM3). *J. Climate* 19: 2122-43.

Combes, V., E. Di Lorenzo and E. Curchister, (2009). Interannual and decadal variations in cross-shore mixing in the Gulf of Alaska. *J. Phys. Oce*., 39(4): 1050-1059.

Curchitser, E.N., D.B. Haidvogel, A.J. Hermann, E. Dobbins, T.M. Powell and A. Kaplan, (2005). Multi-scale modeling of the North Pacific Ocean: Assessment of simulated

basin-scale Variability (1996-2003). *J. Gophys. Res*., 110, C11021, doi:101029/2005JC002902.

Ito, S-I, K.A. Rose, A.J. Miller, K. Drinkwater, K.M. Brander, J.E. Overland, S. Sundby, E.N. Curchitser, J.W. Hurell and Y. Yamanaka, (2009). Ocean ecosystem responses to future global change scenarios: A way forward. In press.

Kalnay, E., M. Kanamitsu, R. Kistler, W. Collins, D. Deaven, L. Gandin, M. Iredell, S. Saha, G. White, J. Woollen, Y. Zhu, M. Chelliah, W. Ebisuzaki, W. Higgins, J. Janowiak, K. C. Mo, C. Ropelewski, J. Wang, A. Leetma, R. Reynolds, R. Jenne and Joseph, D., (1996). The NCEP/NCAR 40-year reanalysis project, *Bull. Am. Meteor. Soc.*, 77, 437-471.

Large, W. G., and G. Danabasoglu, (2006). Attribution and impacts of upper-ocean biases in CCSM3. *J. Climate*, **19**, 2325-2346.

Randall, D., and co-authors, (2007). Climate Models and Their Evaluation. In: Climate Change 2007: The Physical Science Basis. Contribution of Working Group I to the Fourth Assessment Report of the Intergovernmental Panel on Climate Change [Solomon, S., D. Qin, M. Manning, Z. Chen, M. Marquis, K.B. Averyt, M.Tignor and H.L. Miller (eds.)]. Cambridge University Press, Cambridge, United Kingdom and New York, NY, USA.

Veneziani, M., and C. A. Edwards, and J. D. Doyle, (2009a), A Central California coastal ocean modeling study. Part I: The forward model and the influence of realistic versus climatological forcing, J. Geophys. Res., 114, C04015, doi:10.1029/2008JC004774.

Veneziani, M., C. A. Edwards, and A. M. Moore, (2009b), A Central California coastal ocean modeling study. Part II: Adjoint sensitivities to local and remote driving mechanisms, J. Geophys. Res., 114, C04020, doi:10.1029/2008JC004775.

Development a regional ocean climate model for Northwest Pacific Marginal Seas

Yang-Ki Cho[1], Gwang-Ho Seo[1] , Byoung-Ju Choi[2]

School of Earth and Environmental Sciences, Seoul National University, Seoul, Korea[1]

(choyk@snu.ac.kr, seogwangho@gmail.com)

Department of Oceanography, Kunsan National University, Gunsan, Korea[2]

(bjchoi@kunsan.ac.kr)

1. INTRODUCTION

The temperature increase of the Northwest Pacific (NWP) and its marginal seas is significantly higher than that of the global mean (Figure 1). The temperature in the NWP marginal seas is greatly influenced by the East Asian monsoon and ocean currents like Tsushima Current (TC) and the Kuroshio. Rapid temperature change may result in great impact on the regional ecosystem.

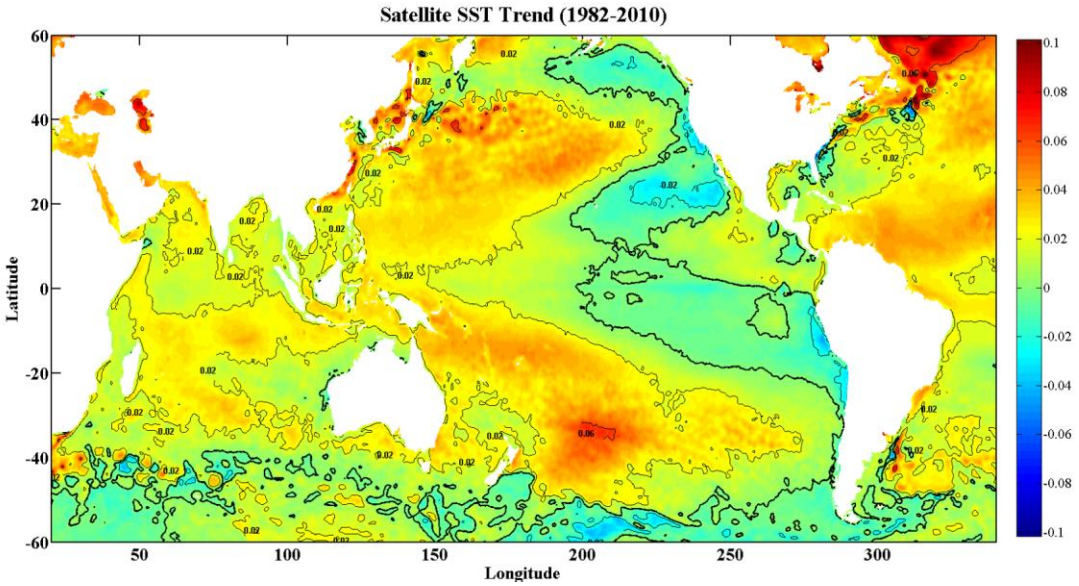

Figure 1 .Trend of sea surface temperature observed by satellite from 1982 to 2010 (http://poet.jpl.nasa.gov/).

The NWP marginal seas are characterized by complex circulation pattern and large variability, yet they are small enough for multiple simulations to be economically feasible. Great

efforts have been made to improve the understanding and predictability of the NWP circulation by using numerical models (Cho et al., 2009; Deng et al. 2010).

The relatively coarse resolution of global climate models results in isolation of the marginal seas from large open ocean basins or unreasonable large or small transport in the straits. Exchanges of water between the semi-enclosed marginal seas and the open ocean are important to simulate regional climate change and what in nature involves the straits.

We are currently in the process of downscaling global climate models using a high-resolution (10km) regional ocean model. Once this is completed, we will further refine our results with a coupled atmosphere-ocean model. This regional climate model will produce water temperature and salinity and current to 2100. This will allow us to assess climate change impacts on regional ecosystems and habitats of highly migratory pelagic species.

2. MODEL DESCRIPTION

The NWP model domain ranges from 118° N to 49° N and from 118° E to 155° E. It includes the East China Sea (ECS), the Yellow Sea (YS), the Japan/East Sea (JES) and northwestern part of the Pacific Ocean (Figure 2). The horizontal grid has a nominal resolution of 0.1° and 20 vertical sigma levels are used. Vertical mixing is calculated by the level 2.5 Mellor-Yamada turbulence closure (Mellor and Yamada, 1974). Chapman, Flather and clamped boundary conditions were used for free surface elevation, barotropic momentum, baroclinic momentum, respectively. The horizontal viscosity coefficient was set to 300 m^2/s. The bottom topography used for the model is interpolated from ETOPO1, with a minimum depth set to 5 m.

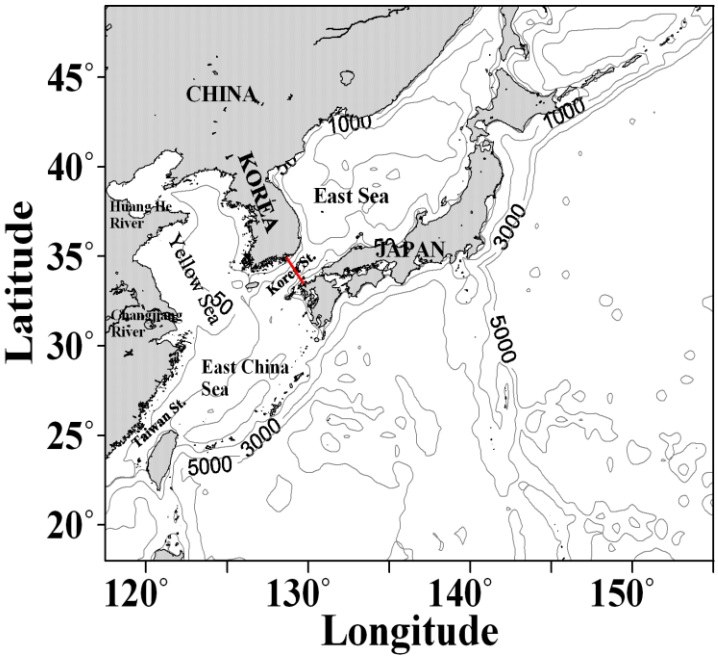

Figure 2. Bottom topography of the northwest Pacific model domain. The thick solid line represents the section monitoring transport in the Korea Strait. Contour lines are water depths

Freshwater discharges from Changjiang (Yangtze) River and Huang He (Yellow) River were included. Changjiang discharge was estimated from the precipitation using the relation equation between the precipitation and discharge by Senju et al. (2006). For the Huang He discharge, climatological data were used because its discharge is one order smaller than that of the Changjiang River. Tidal forcing was applied along the open boundaries using eight major tidal components in order to provide tidal mixing effect on the sea surface temperature (Egbert and Erofeeva, 2002). The initial values for temperature and salinity were obtained from the average of the 1979 January of SODA. Boundary conditions were obtained from a global ocean models SODA (1979-1993) and ECCO (1994-2009)

To allow the modelled ocean state to reach a quasi-steady state, the daily surface fluxes obtained from the ECMWF were applied for a spin-up period of 2 years. The surface atmospheric forcing for the hindcast simulation was provided from daily mean value of ECMWF reanalysis dataset. A bulk-flux formulation was used for calculation of the surface heat fluxes. Details on model can be found in the work of Cho et al. (2009).

3. MODEL VALIDATION

The temporal mean of the simulated SST is compared with that of the satellite SST from 2001 to 2009 (Figure 3). The satellite observations are 4 km data collected using the NOAA/AVHRR Pathfinder Version 5 distributed by Jet Propulsion Laboratory (http://poet.jpl.nasa.gov/). The paths of the Kuroshio, the TC and East Korean Warm Current (EKWC) are indicated by warm SST signatures. The Kuroshio, characterized by the warm water southwest of Japan, is clearly defined in the simulation. The TC and the EKWC in the JES are also relatively well defined by warm water in the simulation. In general, the distribution of isotherms, and the maximum and minimum of the simulated mean SST are similar to those from the observations.

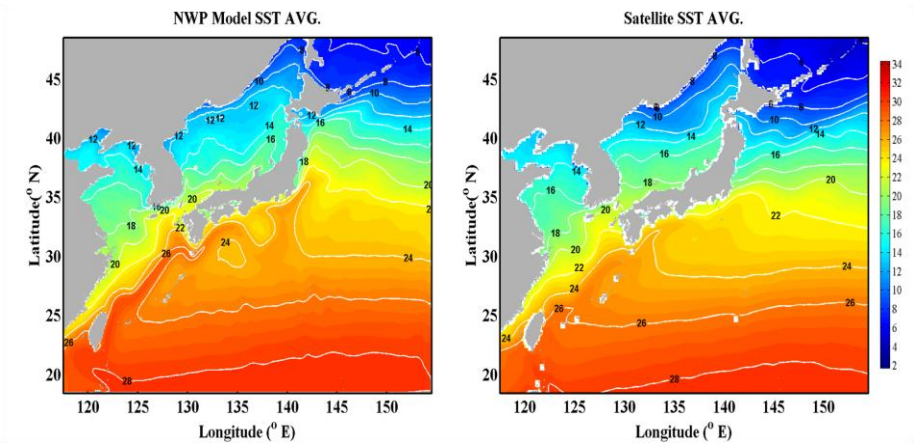

Figure 3. Mean surface temperature by model (left) and satellite (right) from January 2001 to December 2009.

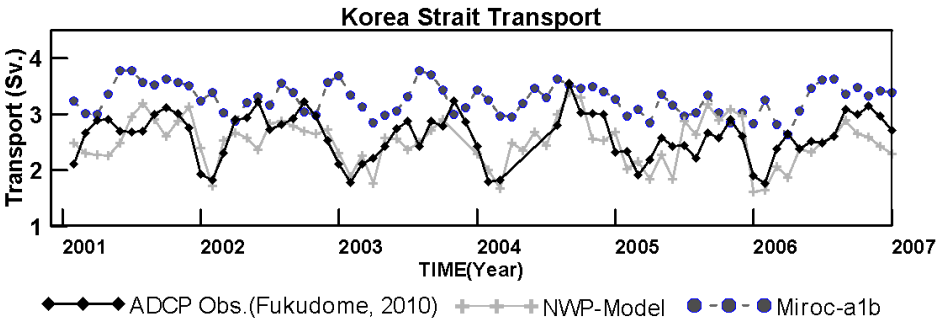

Figure 4. Monthly mean transports of ADCP observation, NWP Model and MIROC in the Korea from 2001 to 2006.

Model transports were compared with the observed transport and a global climate model MIROC in the Korea Strait (Fukudome et al., 2010). The volume transport passing the Korea Strait is important because it might determine the distribution of heat, salt and other materials not only in the JES but also in the ECS. Understanding the variation of the transport in the Korea Strait is a key factor to identify the circulation in the marginal seas of the NWP. The observed and the NWP model transports show remarkable seasonal variation (Figure 4). But it is not easy to find seasonal variation from the MIROC transport. Moreover, the MIROC transport is about

1Sv larger than the observation for the whole period, whereas the NWP model transport is similar to the observation.

5. APPLICATION TO CLIMATE PROJECTION

Accuracy of the NWP models has been limited by many uncertain model parameters and errors in the initial state estimate (Thompson, 1957; Stockdale et al., 1998). The errors might increase greatly during long term integration which is required in the study of climate change. Ocean data assimilation is a mathematical process of combining ocean observations and ocean models to extract the most important information from relatively sparse and incomplete observations of ocean. The reanalysis using assimilation are useful in our understanding on past climate change and verifying model drift by comparison with the result of the control run. The temperature data provided by the Korea Oceanographic Data Center, the Japan Oceanographic Data Center, the Global Temperature and Salinity Profile Program (GTSPP) are used. SST data from NASA and SSH data from AVISO are also assimilated.

Interannual variation of temperature simulated by NWP model using the assimilated initial was compared with the satellite observation and the MIROC temperature. Figure 5 shows the monthly mean surface temperature over the YS and the JES in February (upper) and August (lower) from 2001 to 2009. MIROC shows warm bias compared to satellite observation in both seas in winter, whereas the NWP model result is comparable to the observation. Both models show warm bias in summer. However, interannual variation of the NWP model is close to the observation despite of systematic bias, whereas that of the MIROC has little correlation with the observation.

Climate projection with the NWP model for the next 100 years will be taken. Climate components calculated from the global climate models using Cyclostationary Empirical Orthogonal Function (CSEOF) analysis (Kim et al., 1996) will be added to the surface forcing and open boundary values for the climate projection. CSEOF decomposes space-time data into cyclostationary loading vectors. Data assimilation results will be used for the initial.

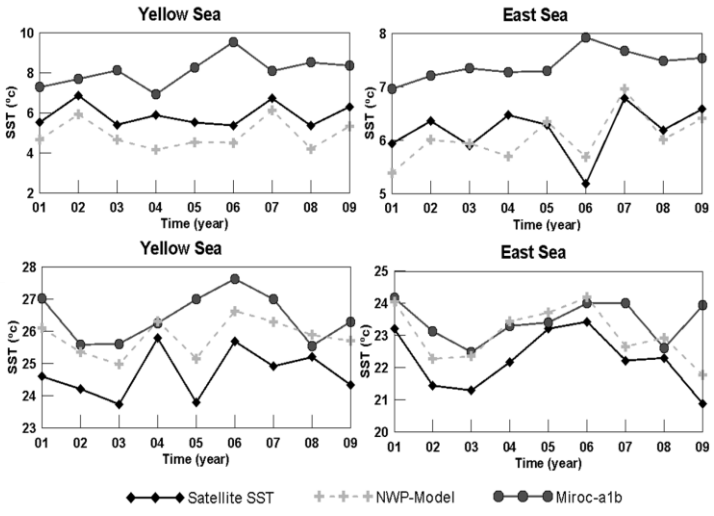

Figure 5. Monthly mean surface temperature over the YS and the JES in February (upper panels) and August (lower panels) from 2001 to 2009.

6. CONCLUSION

A regional NWP model was setup and verified. The reanalysis for the NWP is produced to understand recent climate variability and to produce initial values for climate projection. Hindcast result suggests that the NWP model has better performance than the global climate

model in regional climate projection. Especially the NWP successfully simulates the interannual variation of the observation, although it has systematic difference in summer. Warm bias of the NWP model in summer should be corrected in the future.

REFERENCES

Cho, Y.-K. G.-H. Seo, B.-J. Choi, S. Kim, Y. Kim and E.P. Dever, (2009). Connectivity among straits of the Northwest Pacific Marginal Seas. *Journal of Geophysical Research*. 114. 2008JC005218

Egbert, G.D., and S.Y. Erofeeva (2002), Efficient inverse modeling of barotropic ocean tides, J. Atmos. *Oceanic Technol*., 19(2), 183-204.

Fukudome,KI., Yoon, JH., Ostrovskii, Alexander, Takikawa, Tetsutaro, Han, IS (2010). Seasonal volume transport variation in the Tsushima Warm Current through the Tsushima Straits from 10 years of ADCP observations, *Journal of Oceanography*, Volume 66, Number 4, August 2010 , pp. 539-551(13)

Kim, K. -Y., G. R. North, J. Huang (1996), EOFs of one-dimensional cyclostationary time series: Computations, examples and stochastic modeling, *J. Atmos. Sci.*, *53*, 1007-1017.

Mellor, G., and T. Yamada, (1974). A hierarchy of turbulence closure models for planetary boundary layers. *J. Atmos. Sci*.,31, 1791–1806.

Senjyu T et al (2006). Interannual salinity variations in the Tsushima Strait and its relation to the Changjiang discharge. *J. Oceanogr*.,62, 681-692,2006.09.

Seo G.-H. S. Kim, B.-J. Choi, Y.-K. Cho, Y.-H. Kim, (2009). Implementation of the Ensemble Kalman Filter into a Northwest Pacific Ocean Circulation Model, in *Data Assimilation for Atmospheric, Oceanic and Hydrologic Applications*, edited by S.K. Park and L. Xu, pp. 341-352. Springer. Berlin.

Stockdale, T. N., A. J. Busalacchi, D. E. Harrison, and R. Seager, 1998: Ocean modeling for ENSO. *J. Geophys. Res*., 103, 14 325–14 355.

Climate change in the Northwestern Pacific seen in the CSEOF analysis of the SRES A1B simulations of the AR4 models

Inkweon Bang and Kwang-Yul Kim

School of Earth and Environmental Sciences
Seoul National University
e-mail: inkweon.bang@gmail.com

Abstract

Climate change in the Northwest Pacific during the 21st century as manifested in the SRES A1B scenario of several AR-4 models is investigated using cyclostationary EOF (CSEOF) analysis. In case of the high-resolution MIROC model, 12 atmospheric variables including t2 (2 m air temperature) and 5 oceanic variables (sea surface height and 4 ocean variables defined at 47 vertical levels) are subjected to the CSEOF analysis. Generally, CSEOF decomposition of each variable identifies two main modes—the annual cycle and the clime change signal. Then, atmospheric and oceanic variables (called the predictor variables) are regressed onto the pc time series of t2 (called the target variable) in CSEOF space to find rigorous physical relationship between the target variable and other predictor variables.

In the MIROC high-resolution dataset, climate change mode exhibits a linear trend with slight natural variability superimposed on it. The linear trend indicates that temperature increase, on average, is ~4°C over the 100 years, but is higher on land and is lower over the ocean. Oceanic variables are also highly correlated with t2. Spatially, high ocean temperatures are found to the east of Japan between 35°-45°N and are vertically barotropic in the upper 500 m. Salinity is generally oppositely correlated with temperature with warming leading to freshening of the upper ocean. Amidst general warming of the upper ocean, a sign of stronger meandering of the Kuroshio extension is seen, which alters the dynamic topography of the sea surface. This meandering is also clearly seen in the vertical section of the velocity field.

Regression analysis of the ocean temperature reveals two depth ranges of higher correlation with t2 separated by a minimum correlation layer at ~2-km depth. The upper layer may indicate that atmospheric temperature is crucially affected by the upper-ocean temperature. High correlation in the lower layer, however, cannot be due to a direct exchange of energy between the ocean and the atmosphere and thus other mechanism should be responsible for it. Salinity appears less correlated with t2 than ocean temperature, but correlation with t2 is still significant. Interestingly, salinity has two minimum correlation depths and henceforth there are three high-correlation layers.

1. Data

The family of A1 scenarios, which are characterized by rapid economic growth and focus more on economy than environment has three members. Among them is the A1B scenario,which emphasizes balances on all energy sources. In this scenario, the CO2 concentration increases continuously until 2100 when it reaches 720 ppm.Of the AR-4 (Fourth Assessment Report) models, MIROC (a Model for Interdisciplinary Research On Climate) high-resolution model data for the A1B scenario are selected to show the results in the present study. MIROC is a coupled general circulation model developed at CCSR (Center for Climate System Research, University of Tokyo) and is made up of CCSR/NIES/FRCGC AGCM 5.7 and COCO (CCSR Ocean Component Model) (Hasumi and Amori, 2004). Atmospheric variables used for the analysis are ccover (cloud cover), evap (latent heat flux), t2 (2-m temperature), prcp (precipitation), sens (sensible heat flux), ssr (surface net shortwave), ssrd (surface downward shortwave), slr (surface net longwave), slrd (surface downward longwave), q2 (2 m specific humidity), u10 (10 m zonal wind), and v10 (10 m meridional wind). Oceanic variables are sh (sea surface height), to (temperature), so (salinity), uo (zonal velocity), and vo (meridional velocity). Oceanic variables are defined at 47 vertical levels. The datasets aremonthly from Jan. 2001 to Dec. 2100. Grid spacing of the atmospheric variables is at T106 spectral truncation, which is approximately 1.125 degree in both the longitude and latitude directions. Grid spacing of the ocean variable is 0.28125 degree in the zonal direction and 0.1875 degree in the meridional direction; the original model coordinates, which are not latitude and longitude, are transformed into regular longitude-latitude grids. River runoff is defined on 0.5°×0.5°grids only on land.

2. Method of Analysis

To separate the physical processes from the datasets, the CSEOF technique was employed (Kim and North, 1997). In the CSEOF analysis, space-time data, $T(r,t)$, are written as a linear superposition:

$$T(r,t) = \sum_n LV_n(r,t)PC_n(t),$$

where $LV_n(r,t)$ and $PC_n(t)$ are cyclostationary loading vectors (LV) and principal component (PC) time series, respectively. The CSEOF representation of the data is different from the EOF representation in that the loading vectors are time dependent and periodic; that is,

$$LV_n(r,t) = LV_n(r,t+d),$$

where d is called the nested period. The nested period is set to 12 months in this study.

CSEOF analysis is conductedon each of the atmospheric and oceanic variables (on each level for oceanic variables). Then, the PC time series of a

target variable (t2 in this study) is written as a linear regression of the PC time series of a predictor variables (say, sea level height). That is,

$$PCT_i(t) = \sum_n a_n^{(i)} PC_n(t) + \epsilon(t),$$

where $PCT_i(t)$ is the target PC time series for mode i, $PC_n(t)$ is the predictor PC time series for mode n, and $\epsilon(t)$ is the regression error time series. Then, the spatio-temporal pattern of the predictor variable, $LVP_n(r,t)$, which is consistent with the loading vector of the target variable, $LVT_i(r,t)$, is obtained by

$$LVP_i(r,t) = \sum_n a_n^{(i)} LV_n(r,t).$$

This procedure is called the regression analysis in CSEOF space. Note that $LVT_i(r,t)$ and $LVP_i(r,t)$ are physically and dynamically consistent in the context of having (nearly) identical amplitude time series, not because of the identical physical evolution. For more information on the CSEOF technique, see Kim and Na (2011) and references cited therein.

3. Results and Discussion

3.1 Target variable t2

The first two modes of t2 explain 95.8% of the total variance; modes 1, 2 and 3respectively explain 95.8%, 2.7%, and 0.12%. The PC time series of mode 1 is almost constant throughout the 100 years of analysis with a value of about 7-8 (Fig. 1) and the loading vector has relatively higher values on land and lowervalues over the water (not shown). Contour lines are crowded on land, but few contour lines overthe water. The loading vector shows sign change with a period of 6 months, a typical pattern of the seasonal change.

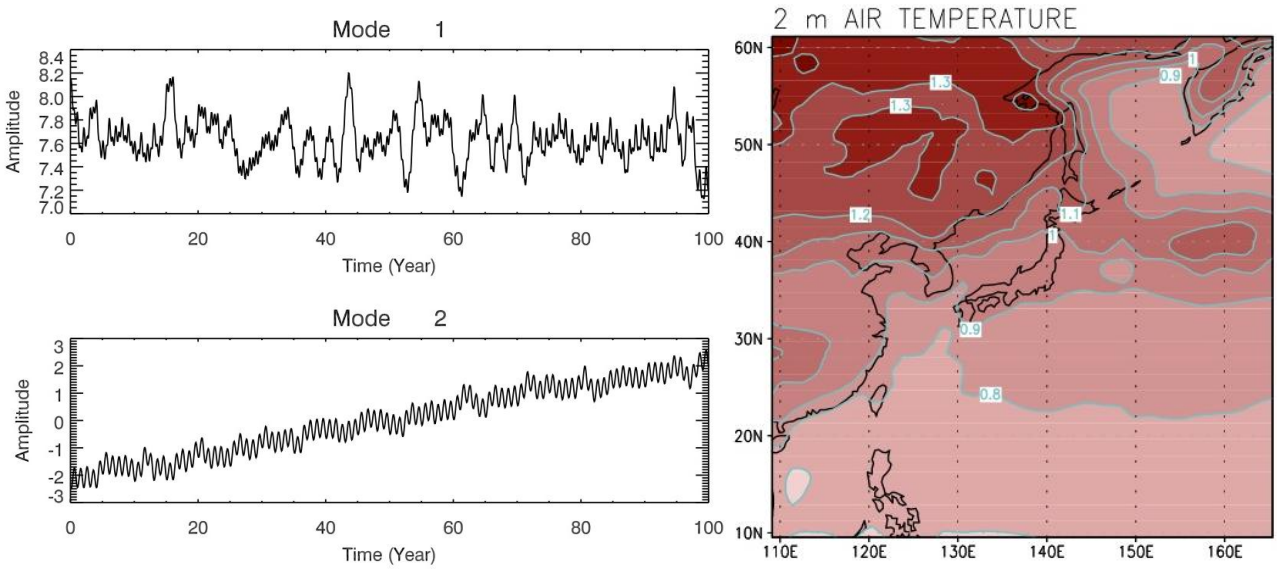

Fig. 1. The PC time series of modes 1 and 2
for variable t2 (left) and the annually averaged loading vector of mode 2 (right).

The mode 2 has an increasing linear trend from about -2 to 2. Superimposed on this linear trend are annual fluctuations with amplitude of about 0.2-0.3. Over the 12-mo nested period, loading vector of mode 2 is positive everywhere as shown in Fig. 1 meaning that t2 is increasing. As shown in Fig. 1, increasein 2 m temperature isrelatively higher on land than over theocean and a strong horizontal gradient develops along the land-sea boundary in the Okhotsk Sea. CSEOF pattern is nearly zonal in the open ocean except for the Okhotsk Sea. It is interesting to note on the ocean that larger values (about 1) are located to the east of Japan in the form of a zonal band with a center at ca. (160°E, 40°N); thus, 2 m air temperature increases by about 4°over the period of 100 years. In the East Sea and the Yellow Sea northern region exhibits larger increase than the southern region.

3.2 Patterns of ocean variables for mode 2

Regression analysis was conducted for each ocean variable at each depth using the PC time series of the first 20 modes. Prior to the regression analysis, linear trend was removed from both time series in order to remove spurious correlation because of trends. Accuracy of regression as represented by R^2 value is very high for all ocean variables. The R^2 value, and henceforth correlation, decreases gradually with depth and a minimum is reached at about 2000 m. The influence of the seasonal cycle of atmospheric forcing is typically limited to less than 100 m depth of the ocean, but the atmospheric heating of the climate change modeappears to reach much deeperpart of the ocean according to the vertical structure of correlation. The R^2 value increases with depth again with a subsurface maximum at around 4500 m. This indicates that the atmospheric influence on ocean temperatures at deeper part of the ocean is not direct but through different ocean dynamics.

Large anomalies insea level height, temperature, and current velocities are seen along the path of Kuroshio and its extension, to the south and east of Japan (Fig. 2). Most conspicuous features are an anti-cyclonic circulation with

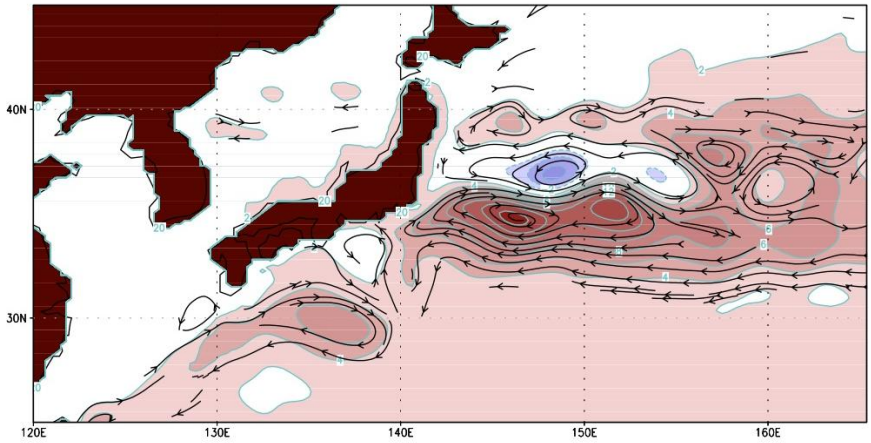

Fig. 2 Streamlines at 1.5m andsea level height (contours). Red and blue colors represent positive and negative values, respectively.

the center at (137°E, 30°N), another anti-cyclonic circulation with two centers at (146°E, 35°N) and (152°E, 36°N), and a cyclonic circulation with the center at (148°E, 38°N). These features are closely correlated with sea level changes; anti-cyclonic (cyclonic) circulationcorresponds to positive (negative) sea level height in proximity of geostrophic balance. Anti-cyclonic circulationto the south of Japan coincides with the departing portion of the meandering path of the Kuroshio and the two centers of the anti-cyclonic circulation to the east of Japan coincide with the southern flanks of the two crests of nearly stationary meander of the Kuroshio extension (Sakamoto et al., 2005).

Ocean temperature change is also closely correlated with current velocity change; anti-cyclonic (cyclonic) circulation is associated with warmer (cooler) waters. This relationship is clearly seen in the upper-ocean heat content change (Fig. 3). Figure 3 shows that ocean warming is a crucial reason for sea level height change in Fig. 2. In turn, current velocity change as a result of sea level height change is also responsible for heat content change in the upper ocean; weak heat content change along ~37.5°N appears to be due to the increased zonal current speed of the Kuroshio extension. Thus, the magnitude of current speed change does not seem to be proportional to the heat content change; heat content change is more effective in changing the current speed in a region where climatological current speed is stronger such as the Kuroshio extension region. Another peculiar characteristic in regard to the current speed change is the development of relatively strong westward current anomaly at ~32°-33°N. This westward flow seems to be associated with the increased upper-ocean heat content and sea level height to the north of ~34°N.

Figure 4 shows a comparison between climatological surface current and that under the A1B scenario. There is no significant shift in terms of the location of the Kuroshio extension but the speed of the extension has increased fairly significantly and extends more eastward before branching occurs (Figs. 4a and

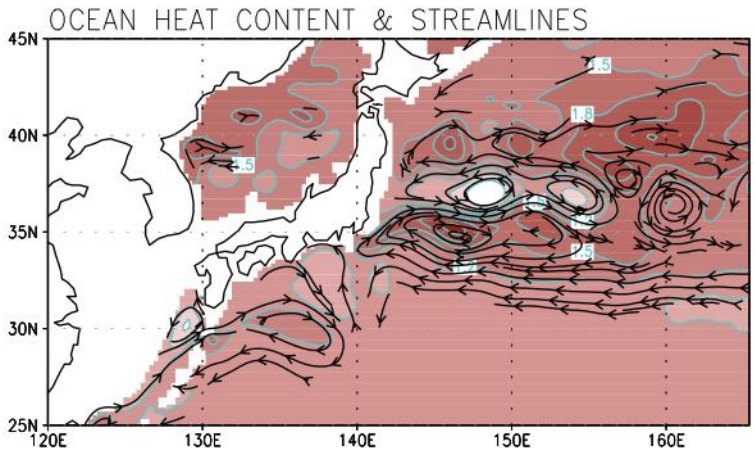

Fig. 3. Heat content change in the upper 300 m ocean and streamlines of surface currents.

4c). Another characteristic feature is well developed return flow to the south and the north of the Kuroshio extension (Fig. 4c). The increased speed of the Kuroshio extension matches well with the region of significant change in upper-ocean heat content.

In order to gain more physical insight into these changes, vertical structure of temperature is investigated in Fig. 5. Under the A1B scenario, strong

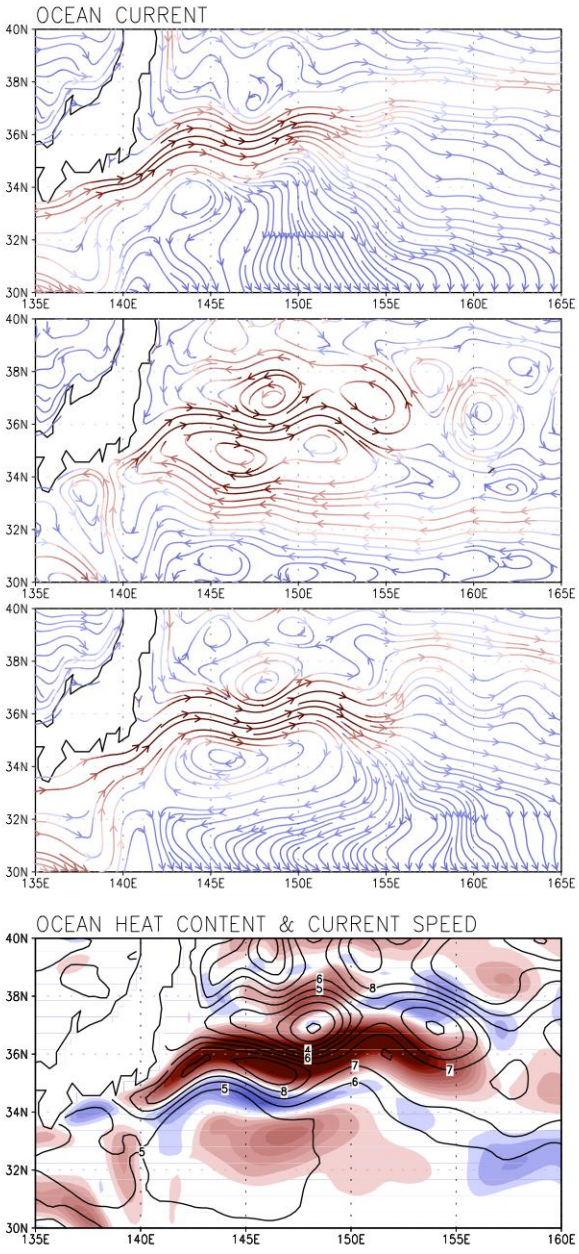

Fig. 4. Streamlines of ocean current with speed for (a) climatology, (b) climate change, and (c) A1B scenario, and (d) changes in ocean heat content in the upper 200 m (contour) and current speed (shade) under the A1B scenario.

change is seen in the Kuroshio extension, which is located between 35°-37°N at 147.5°E climatologically. Stronger north-south temperature gradient is developed under the A1B scenario as seen in the middle and lower panels of Fig. 5; isotherms become significantly deeper at the southern border of the Kuroshio extension than at the northern border. As a result, current speed of the Kuroshio extension increases. Also, westward current anomaly is clearly seen to the south and north of the Kuroshio extension in the vertical structure of isotherms in the lower panel of Fig. 8; isotherms become deeper northward at ~34°N and ~37°N in association with the westward currents to the north and the south of the Kuroshio extension. Thus, the speed of the Kuroshio extension increases while dynamically induced westward current anomalies develop to the north and south of the Kuroshio extension.

It should be pointed out that upper-ocean heat content change is well reflected in the ensuing sea level and current changes to the south of the Kuroshio extension. On the other hand, sea level and current changes are significantly weaker to the north of the Kuroshio extension even though heat content change is quite comparable to that along the Kuroshio extension. As

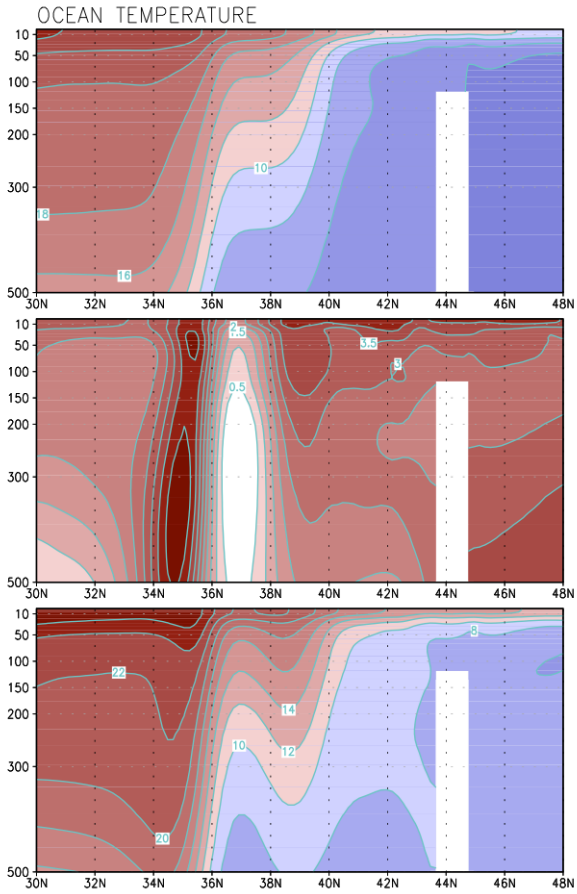

Fig. 5. Vertical section of temperature along 147.5°E: (a) climatology, (b) climate change, and (c) A1B scenario.

seen in Fig. 3, for example, heat content change at around (160°E, 40°N) is comparable to that at (147°E, 35°N). Sea level and current changes, however, at the former location is substantially lower than that at the latter location. This can be explained in terms of mild north-south gradient of isotherms. Although warming is fairly significant in the upper 200 m or so, isotherms become flatter because of the warming and a sharp gradient between warm and cold water masses is shifted further north resulting in less conspicuous warming signal at this location.

Seen on the surface of the ocean, the anti-cyclonic circulation is stronger and larger than the cyclonic circulation (Figs. 2 and 3). In the meridional section along 145°E, there are two cores of stronger temperature anomalies at 34°-36°Nand 38°-41°N (Fig. 6). These two cores extend from the seasurface down to 1500-2000m depth (the northern one is about 500 m shallower than the southern one, which reaches 2000 m). There is also a difference in the central depth of the core, where maximum temperature anomaly is found. The southern core's center is located at 350 m while the northern one is located near the surface at ~50 m. At the latitudes of two temperature cores, 35°N and 39°N, zonal velocity changes sign. Also, the latitude of the core of weaker temperature anomaly (37°N), which resides between the two positive temperature anomalies, marks the sign change of zonal velocity. Thus, there are two pairs of recirculation into the main stream of the Kuroshio along 145°E; the southern recirculation (~33°N) is stronger and reaches deeper than the northern one (~38°N) with the main Kuroshio axis exhibits increased zonal velocity down to ~1500 m.

Averaged temperature and current speed is taken from the first 10 years of simulation and also from the last 10 years and their differences (last 10 years – first 10 years) are examined in Fig. 7. At the sea surface, temperature increases by ~3-4°C and the salinity decreases by ~0.1-0.6 psu in the Pacific (larger decrease is found in the Yellow Sea and the East China Sea). The 27°C isotherm is located along 20°N in the first 10 years but moves northward to about 30°N

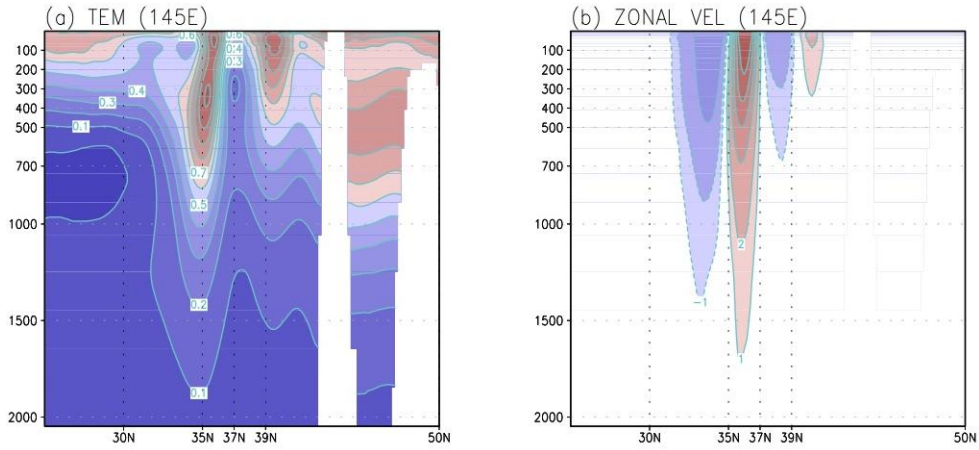

Fig. 6. Meridional section along 145°E of temperature (left) and zonal velocity (right).

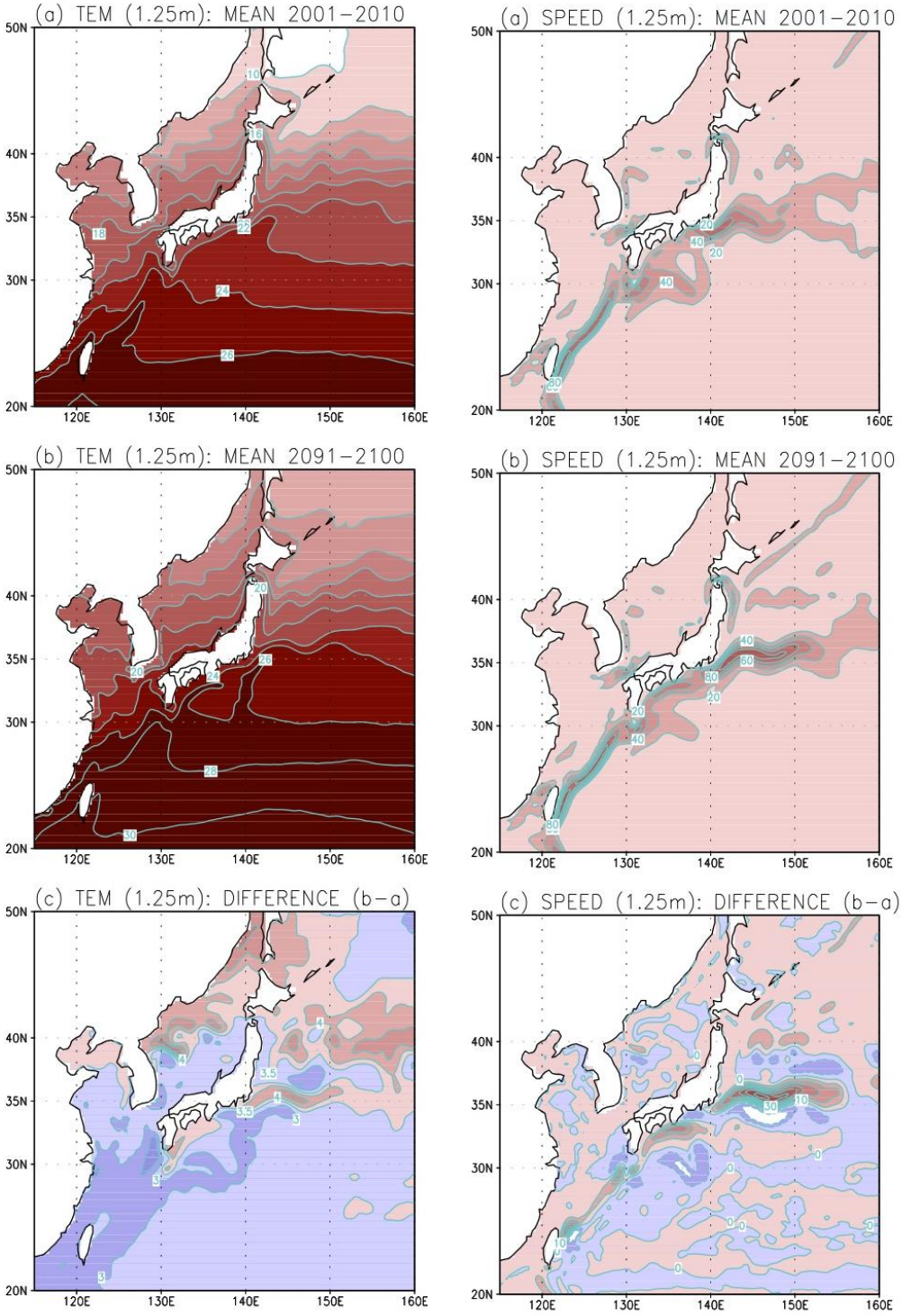

Fig. 7. 10-year averages of temperature (left) and ocean current speed (right) for 2001-2010 (top), 2091-2100 (middle), and their differences (bottom)

in the last 10 years, where 24°C isotherm was located in the first 10 years. In the Kuroshio extension region, two isotherms (18°C and 21°C in the first 10 years and 21°C and 24°C in the last 10 years) become closer to each other in the last 10

years than in the first 10 years indicating stronger current in the Kuroshio extension region. Average surface velocity shows the strengthening and a slight northward shift of the Kuroshio extension (Fig. 7).

4. Concluding Remarks

According to MIROC high-resolution model under the SRES A1B scenario, the Northwestern Pacific will undergo significant changes not only in the heat content of the upper ocean but also in the strength and location of the Kuroshio and its extension. Increased heat content is reflected, in general, in the increased sea level height and corresponding circulation change in the upper ocean of the Northwestern Pacific. Circulation change, on the other hand, induces vertical temperature redistribution, which is further reflected in the isotherm depths and upper-ocean heat content. Thus, the climate change signal in the Northwestern Pacific is not merely overall warming in the ocean but is delicate involving secondary temperature change associated with the strengthening of the Kuroshio extension. Detailed analysis is required to accurately delineate the climate change signal in the Northwestern Pacific.

References

Hasumi, H. and S. Emori, 2004:*K-1 coupled GCM (MIROC) description, K-1 Technical Report No. 1*, Center for Climate System Research, University of Tokyo; National Institute for Environmental Studies; Frontier Research Center for Global Change, pp 39.

Kim, K.-Y., and H. Na, 2011: Theoretical foundation of cyclostationary EOF analysis: concepts and examples, (to be submitted to *J. Clim*.).

Kim, K.-Y., and G. North, 1997: EOFs of harmonizable cyclostationary processes, *J. Atmos. Sci*., **54**, 2416-2427.

Sakamoto, T. T., H. Hasumi, M. Ishii, and S. Emori, 2005: Response of the Kuroshio and the Kuroshio Extension to global warming in a high-resolution climate model, *Geophy. Res. Lett.*,**32**, L14617, doi:10.1029/2005GL0233384.

Evaluation of regional ocean simulation from CMIP3 models: a case for the North Pacific Ocean mixed layer depth

Chan Joo Jang, Taewook Park, Minho Kwon, and Cheol-Ho Kim

Korea Ocean Research and Development Institute, 1270 Sa-dong, Ansan, Gyeonggi-do, Republic of Korea 426-176
(cjjang@kordi.re.kr)

1. Introduction

Ocean mixed layer defines a vertically quasi-homogeneous surface region of temperature, salinity or density, which directly interacts with the overlying atmosphere. Atmosphere-ocean interaction, therefore, can be modulated by the ocean mixed layer whose depth is determined by wind mechanical stirring, surface buoyancy forcing such as heat flux or freshwater flux, or ocean circulation changes. Changes in the mixed layer depth (hereafter MLD), for example, influence variability of the sea surface temperature, oceanic uptake of atmospheric CO2 (Kraus and Businger, 1994). In addition to air-sea interaction, MLD also affects phytoplankton dynamics through controlling the availability of nutrients and light and thus biological productivity in the ocean (Sverdrup, 1953; Yentsch, 1990).

On the other hand, significant changes in the circulation of ocean or atmosphere have been projected by coupled climate models under global warming (e.g. Lu et al., 2007; Vecchi and Soden, 2007; Xie et al., 2010). Therefore, MLD would change in response to the circulation changes under global warming. For example, the deep mixed layers in the Southern Ocean are projected to shoal and shift southward in response to intensified surface warming and poleward shift of wind field (Sen Gupta et al., 2009). The winter MLD is also projected to decrease (Jang et al, 2011; Merryfield and Kwon, 2007; Luo et al, 2009) in most of the North Pacific Ocean including the Kuroshio Extension, resulting in a reduction in formation of mode waters in response to global warming (Luo et al., 2009). The projected decrease in the Kuroshio Extension is estimated to reduce the new primary production by 10.7 ~ 40.3 % (ranges of medians from 11 models) through decreased amount of nitrate available for primary production and to cause earlier spring bloom by 0 ~ 13 days (ranges of medians from 11 models) (Jang et al., 2011). Although most of the CMIP3 (coupled model intercomparison projects phase 3) models projects the MLD decrease in the North Pacific Ocean, the magnitude and distribution of the changes varies significantly across the models. Furthermore, Jang et al. (2011) find that the CMIP3 models suffer from a systematic bias in reproducing the present climate MLD, compared with observational estimate: a deep bias in the KE and a shallow bias in the Oyashio region. However, the detailed systematic bias pattern and its possible causes from individual models have not been well understood. This study investigates the systematic bias in the North Pacific Ocean and its possible causes in present climate by comparing outputs from 11 CMIP3 models

with MLD climatology based on observational data.

2. Data and Methods

This study examined the model outputs from CMIP3, as used in the Intergovernmental Panel on Climate Change (IPCC) Fourth Assessment Report (AR4). The outputs from all the CMIP3 models are available from the Program for Climate Model Diagnosis and Intercomparison (PCMDI, archived at http://www-pcmdi.llnl.gov/about/index.php) at the Lawrence Livermore National Laboratory. For present climate, we used data from the 20th climate simulation (20th Century Climate in Coupled Models, 20C3M) driven by both anthropogenic and natural forcing. For the analysis, outputs from the last two decades were used: 20-year period is believed to be sufficient to account for interannual variability, giving a robust climate (Sen Gupta *et al.*, 2009). This study analyzes as many models as possible to calculate MLD because we aim to examine individual model simulations, as well as ensemble means, focusing on difference and similarity of model simulations. Table 1 lists 11 of total 25 models used in this study, based on the following criteria. First, we removed six models because MLD estimation was not possible: two models (BCC-CM1, INMCM3.0) were removed simply because of unavailability of temperature and salinity data in the archives. Four models (CCCMA-CGCMT47, CCCMA-CGCMT63, NCAR-PCM1, and UKMO-HadGEM1) were additionally excluded because their 1st vertical levels start below 10 m depth that is the reference depth used for MLD estimation in this study. Second, we excluded four models (GISS-AOM, GISS-EH, GISS-ER, and IAP-FGOALS-g1.0) because they have unrealistic 20th century MLD spatial patterns: three GISS models show a big deep bias exceeding 400 m in the northwestern Pacific, and IAP-FGOALS-g1.0 have nearly an unrealistic uniform spatial pattern at high latitudes. Third, we further eliminated four models (BCCR-BCM2.0, CSIRO-MK3.0, GFDL-CM2.1, and INGV-ECHAM4) whose data were not available from the PCMDI archive for estimation of net heat flux or for wind stress. In total, 14 of 25 models were excluded for our analysis. Although ensemble runs initialized with slightly different conditions are available for some models, just one realization (mostly 'run 1') for each model was used, focusing on multi-model simulation. All the models were interpolated to a common 2.5˚ longitude x 2.5˚ latitude grid for multi-model ensemble means and standard deviations. To assess model performance in 20th century climate, the simulated MLD in each model was compared with an observational estimate by de Boyer Montégut *et al.* (2004) (available from http://www.locean-ipsl.upmc.fr/~cdblod/mld.html) that uses the same MLD definition, providing direct comparison between model MLDs and the observation. This study uses a paired t-test (also called "repeated-measures" t-test) (Storch and Zwiers, 1999) to check whether the multi-model ensemble difference from the observational estimate is significant or not.

Among various methods for MLD estimation, this study utilizes the variable density threshold method (Sprintall and Tomczak, 1992) that considers, in addition to temperature effect on density, salinity stratification that are not negligible at high latitudes where we are also interested in. This method defines MLD as the depth where the density increase compared to density at 10 m depth equals an increase of density equivalent to a temperature decrease of 0.2℃. This MLD estimation method has been

widely used for various studies, including observational estimation (e.g. de Boyer Montégut *et al.*, 2004) and verification of simulated upper ocean density structure (e.g. Jang and Kang, 2009).

3. Results

Figure 1 shows simulated MLD in February averaged over 20 years, together with the observational MLD. The observed MLD shows three local maxima where mode waters form (Thompson and Cheng, 2008): deep mixed layers in the subtropical mode water (STMW) south of the KE (~ 200 m), central mode water (CMW) (~ 200 m) north of the KE, and eastern subtropical mode water (ESTMW) (~ 180 m) around 140°W & 30°N. The models simulate relatively well the deep mixed layer associated with the ESTMW, but its location and depth significantly differs from the observation. For instance, GFDL-CM2.0 has a deep bias with excessive southwestward extent, while MRI-CGCM2.3.2a shows a shallow bias. Meanwhile, the MLD associated with CMW and STMW has only one core in the GFDL-CM2.0 and MIROC3.2 (MEDRES). In contrast, the other 9 models separate the CMW and STMW although the locations differ from the observation.

All 11 models tend to have a deep bias in the MLD that is related with CMW and STMW. In contrast, they produce a shallow bias in the Oyashio region north of KE (40°N) (Fig. 2). To investigate this systematic bias that commonly occurs in the models, the ensemble average of MLD is compared with observed MLD (Fig. 3a). The systematic bias of simulated MLD shows a dipole pattern. That is, the ensemble mean MLD in the KE (30°N ~ 40°N) is about 50% (120 m) deeper than the observed one, whereas the MLD in the Oyashio region north of KE is about 30% (80 m) shallower than the observation. The deep bias in the KE is partly attributable to the strong wind biases in the mid-latitude in the models (Fig. 3b). Another possible cause is the weak surface currents in the Kuroshio Extension in the models compared with observation (Fig. 4): the weaker currents carry less heat in the region and thus less stratification, giving the deep mixed layer bias there (Thompson and Cheng, 2008). On the other hand, the shallow bias in the Oyashio region north of the KE seems to be related with a strong bias in the upper ocean stratification associated with surface salinity bias in the CMIP3 models. The MLD south of the KE (20°N ~ 25°N) is about 20% (40 m) deeper than observed MLD, which is attributable to excessive surface cooling in the models.

To check overall similarity of the North Pacific Ocean MLD between the models and observation, we estimate pattern correlation using 20-year mean winter (February) MLDs from individual models and the observational estimate. The pattern correlation for the North Pacific Ocean ranges 0.2 ~ 0.7, indicating poor performance of CMIP3 MLD simulation, compared with the sea surface temperature and salinity whose pattern correlations are up to 0.9.

4. Summary and conclusion

This study investigates how well the coupled model intercomparison projects phase 3 (CMIP3) models simulate the mixed layer depth (MLD) in the North Pacific Ocean in

present climate by comparing outputs from 11 CMIP3 models with MLD climatology based on observational data. The most common biases in winter MLD are a deep bias (about 50 % (120 m) deeper than the observation) in the Kuroshio Extension region (KE) and a shallow bias (about 30 % (80 m) shallower than the observation) in the Oyashio region. The deep bias in the KE is mainly driven by the fact that the simulated KE is too broad and goes too far north. The deep bias is also attributable to the too strong (30 % or greater than observation) midlatitude westeries in CMIP3 models. The shallow bias in the Oyashio region is related with stratification bias in the upper ocean. The pattern correlation between simulated MLDs and observed climatology for the North Pacific Ocean ranges 0.2 ~ 0.7, indicating poor performance of CMIP3 MLD simulation, compared with sea surface temperature and salinity whose pattern correlations are up to 0.9. Our analysis suggests that the CMIP3 climate models suffer from a substantial MLD bias and need significant improvement.

Table 1. The CMIP3 models used in this study.

No.	Model ID	Ocean model	Oceanic resolution (latitude x longitude, vertical levels)	References
1	CNRM-CM3	OPA8.1	0.5° - 2° × 2°, L31	Salas Melia (2002)
2	CSIRO-MK3.5	MOM2.2	0.84° × 1.875°, L31	Gordon et al. (2002)
3	GFDL-CM2.0	OM3P4	1/3° - 1° × 1°, L50	Delworth et al. (2006)
4	IPSL-CM4	OPA	1° - 2° × 2°, L31	Marti et al. (2006)
5	MIROC3.2 (HIRES)	COCO3.3	0.19° × 0.28°, L47	K-1 model Developers (2004)
6	MIROC3.2 (MEDRES)	COCO3.3	0.5° - 1.4° × 1.4°, L43	K-1 model Developers (2004)
7	MIUB-ECHO-G	HOPE-G	0.5° - 2.8° × 2.8°, L20	Min et al. (2005)
8	MPI-ECHAM5	MPI-OM	1.5° × 1.5°, L40	Jungclaus et al. (2006)
9	MRI-CGCM2.3.2A	Bryan-Cox	0.5° - 2.0° × 2.5°, L23	Yukimoto et al. (2001)
10	NCAR-CCSM3	POP	0.27° - 1.1° × 1.1°, L40	Collins et al. (2006)
11	UKMO-HadCM3	Bryan-Cox	1.25° × 1.25°, L20	Gordon et al. (2000); Johns et al. (2003)

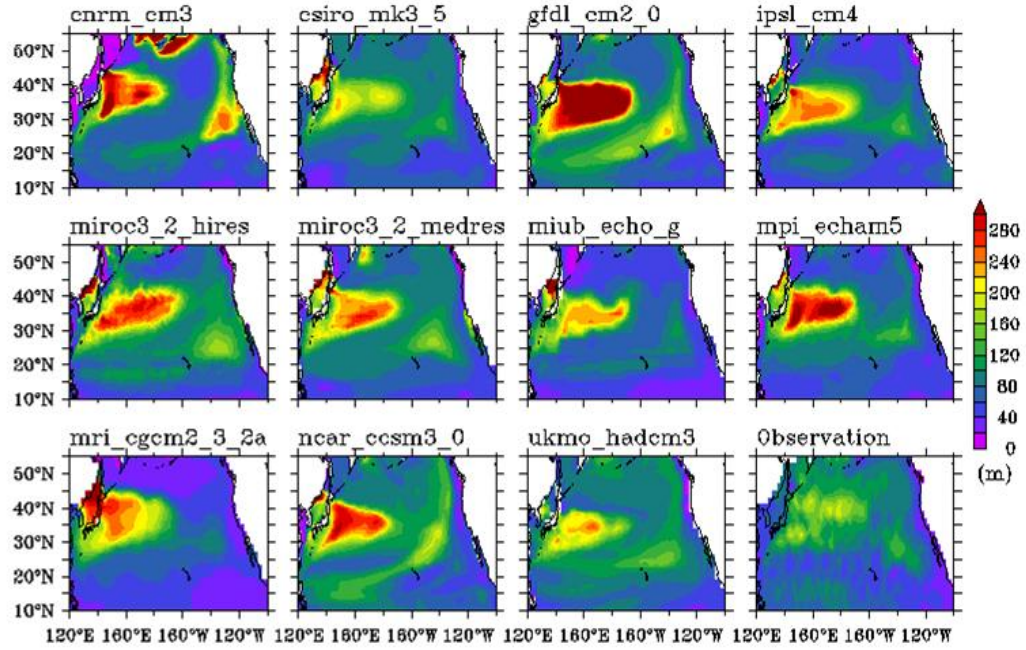

Fig. 1. Winter (February) mixed layer depth simulated from CMIP3 models and observational estimate (last panel). The observational estimate is from de Boyer Montégut et al. (2004) and is downloaded from the web site (http://www.lodyc.jussieu.fr/~cdblod/mld.html).

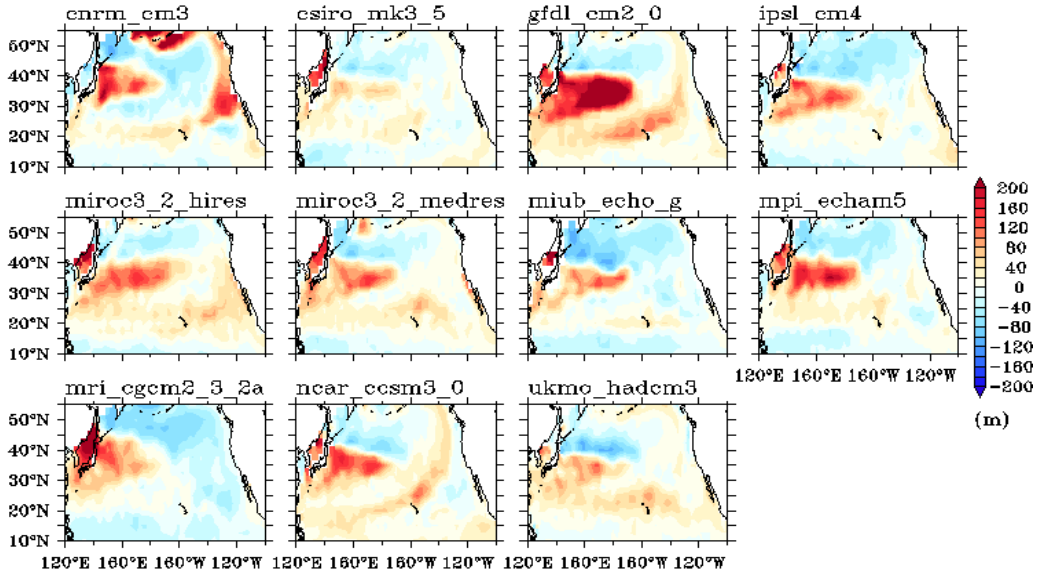

Fig. 2. Horizontal distribution of the difference (model minus observation) of winter (February) mixed layer depth.

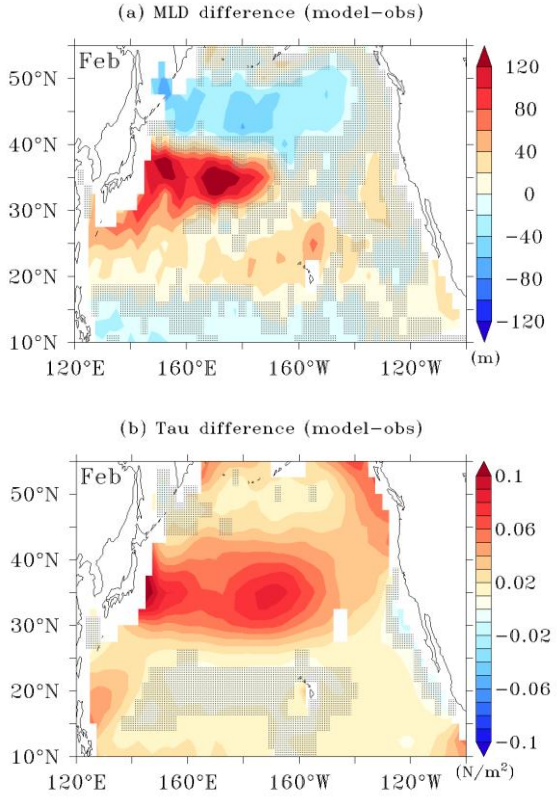

Fig. 3. Horizontal distributions of the difference (model minus observation) in (a) the mixed layer depth (m), and (b) the wind stress (Pa) in winter (February). The stippled region indicates that the difference is not statistically significant at 95 % confidence level.

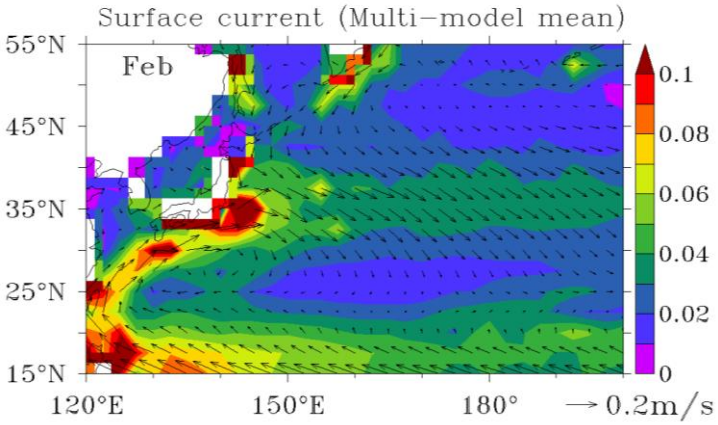

Fig. 4. Horizontal distribution of the multi-model mean surface current (m/s) (arrows) and multi-model standard deviation (m/s) (color shading) in winter (February).

References

Collins, W. D., and Coauthors, 2006. The Community Climate System Model Version 3

(CCSM3). Journal of Climate, 19, 2122–2143.
de Boyer Montégut, C., Madec, G., Fischer, A. S., Lazar, A., and Iudicone, D. 2004. Mixed layer depth over the global ocean: an examination of profile data and a profile-based climatology. Journal of Geophysical Research, 109, C12003, doi:10.1029/2004JC002378.
Delworth, T. L., and Coauthors, 2006. GFDL's CM2 global coupled climate models. Part I: Formulation and simulation characteristics. Journal of Climate, 19, 643–674.
Gordon, C., C. Cooper, C. A. Senior, H. Banks, J. M. Gregory, T. C. Johns, J. F. B. Mitchell, and R. A. Wood, 2000. The simulation of SST, sea ice extents and ocean heat transports in a version of the Hadley Centre coupled model without flux adjustments. Climate Dynamics, 16, 147–168.
Gordon, H. L., and Coauthors, 2002. The CSIRO Mk3 Climate System Model. CSIRO Atmospheric Research Technology Paper 60, 134 pp.
Jang, C. J., and Kang, H. -W. 2009. Effects of vertical mixing parameterization on the mixed layer depth over the North Pacific in a global OGCM. Ocean Science Journal, 44(4), 205-214, 10.1007/s12601-009-0019-y.
Jang, C. J., Park, J., Park, T., and Yoo, S. 2011. Response of the ocean mixed layer depth to global warming and its impact on primary production: a case for the North Pacific Ocean. ICES Journal of Marine Science, 68, 996–1007.
Johns, T. C., and Coauthors, 2003. Anthropogenic climate change for 1860 to 2100 simulated with the HadCM3 model under updated emissions scenarios. Climate Dynamics, 20, 583–612.
Jungclaus, J. H., and Coauthors, 2006. Ocean circulation and tropical variability in the coupled model ECHAM5/MPIOM. Journal of Climate, 19, 3952–3972.
K-1 model developers, 2004. K-1 coupled model (MIROC) description. K-1 Tech. Rep. 1, H. Hasumi and S. Emori, Eds., Center for Climate System Research, University of Tokyo, 34 pp.
Kraus, E. B., and Businger, J. A. 1995. Atmosphere-ocean interaction. 2nd edition. Oxford University Press, 362 pp.
Lu, J., Vecchi, G. A., and Reichler, T. 2007. Expansion of the Hadley cell under global warming. Geophysical Research Letters, 34, L06805, doi:10.1029/2006GL028443.
Luo, Y., Liu, Q., and Rothstein, L. M. 2009. Simulated responses of North Pacific mode waters to global warming. Geophysical Research Letters. 36, L2360910.1029/2009GL040906.
Marti, O., and Coauthors, 2006. The new IPSL climate system model: IPSL-CM4. Institut Pierre-Simon Laplace Note du Pole de Modélisation 26, 84 pp.
Merryfield, B., and Kwon S. 2007. Changes in North Pacific mixed layer depth in the 20th and 21st centuries as simulated by coupled climate models. PICES 16th Annual Meeting, Oct. 26- Nov. 5, Victoria, BC, Canada.
Min, S.-K., S. Legutke, A. Hense, and W.-T. Kwon, 2005. Internal variability in a 1000-yr control simulation with the coupled climate model ECHO-G-II. El Niño Southern Oscillation and North Atlantic Oscillation. Tellus, 57A, 622–640.
Salas Melia, D., 2002. A global coupled sea ice-ocean model. Ocean Modelling, 4, 137–172.
Sen Gupta, A., Santoso, A., Taschetto, A. S., Ummenhofer, C. C., England, M. H., and Trevena, J. 2009. Projected changes to the Southern Hemisphere ocean and sea-ice in the IPCC AR4 climate models. Journal of Climate, doi: 10.1175/2008JCLI2827.1.

Sprintall, J., and Meyers, G. 1991. An optimal XBT sampling network for the eastern Pacific Ocean. Journal of Geophysical Research, 96, 10539-10552.

Storch, H. von, and Zwiers, F. W. 1999. Statistical analysis in climate research, Cambridge University Press, Cambridge.

Sverdrup, H. U. 1953. On conditions for the vernal blooming of phytoplankton. J. Cons. Perm. Int. Explor. Mer., 18, 287-295.

Thompson, L., and Cheng, W. 2008. Water Masses in the Pacific in CCSM3. Journal of Climate, 21, 4514–4528.

Vecchi, G. A., and Soden, B. J. 2007. Global warming and the weakening of the tropical circulation. Journal of Climate, 20, 4316-4340.

Xie, S. -P., Deser, C., Vecchi, G. A., Ma, J., Teng, H., and Wittenberg, A. T. 2010. Global warming pattern formation: Sea surface temperature and rainfall. Journal of Climate, 23, 966-986.

Yentsch, C. S. 1990. Estimates of 'new production' in the Mid-North Atlantic. Journal of Plankton Research, 12,717-734.

Yukimoto, S., and Coauthors, 2001. The new Meteorological Research Institute coupled GCM(MRICGCM 2). Model climate and variability. Pap. Meteor. Geophys., 51, 47–88.

Indonesian Throughflow Transport Change in a Warming Climate

Hyoun-Woo Kang, Chan Joo Jang and Ok Hee Seo

Climate Change and Coastal Disaster Research Department ,
Korea Ocean Research and Development Institute, 787 Haean-Ro,
Sangrok-Gu, Ansan, Gyeonggi-do, 426-744, Republic of Korea

ABSTRACT

Indonesian Throughflow (ITF) transport change under the global warming scenario has been investigated using a coarse resolution global ocean circulation model based on the HYCOM (Hybrid Coordinate Ocean Model). Two cases of atmospheric forcing have been applied to compare the ITF transport change, one is adopted from the daily surface heat and momentum fluxes of ERA-interim data from 1989 to 2010 for the 20th century and the other is the monthly forcing from MIROC 3.2 hi-resolution results for the A1B scenario during 21st century. For the surface flux correction, the sea surface salinity has been relaxed to the climatological data with a time scale of 30 days and the long wave correction has been applied to the surface thermal radiation flux. Comparison shows that the ITF transport is decreased in a warming climate. The reasons of this decrease of ITF transport and its impact have been discussed.

1. Introduction

The Indonesian Throughflow (ITF) contributes to both regional (Indo-Pacific region) and global climate by transporting heat and freshwater from the tropical Pacific to the Indian Ocean [3, 5]. The ITF is also closely associated with climate phenomena such as the El Nino-Southern Oscillation (ENSO), the Asian Monsoon, the Indian Ocean Dipole (IOD). Most of the ITF transport change can be explained by the Island rule which is related with the wind stresses around an Island [1,2]. Because global warming has been known to change the associated climate phenomena including wind stresses given latitude, ITF is likely to be changed in its transport and physical properties.

This study investigates the responses of ITF to global warming by doing comparisons of the model solutions obtained from different atmospheric forcing. We find that the ITF transport is decreased due to global warming, which is also supported by the Island rule [1, 2].

2. GLOBAL OCEAN CIRCULATION MODEL

A global ocean circulation model based on the HYbrid Coordinate Ocean Model (HYCOM) has been developed. The longitudinal grid spacing of the ocean model is 1.5 degree and the latitudinal grid spacing is 1/3 ~ 1 degree in the south of 65°N with finer resolution near the equatorial region. By applying the arctic bipolar patch grid, north of 65°N have variable resolution finer than 0.5 degree in general. The model has 30 vertical layers with maximum depth of 4500 m. The intrinsic energy loan sea ice module of HYCOM is also switched on. Before we apply the interannual forcing, the model had spun up for 50 years with COADS climatology forcing. And the atmospheric forcing is adopted from the monthly surface heat and momentum fluxes of ECMWF 40 year Reanalysis (ERA-40) data for 1958 to 1988. After then, the ERA-interim data derived atmospheric forcing applied from 1989 up to 2010. For the surface flux correction, the sea surface salinity has been relaxed to the climatological data with a time scale of 30 days and the long wave correction has been applied to the surface thermal radiation flux. To simulate the global warming scenario, we derived and applied a future forcing from the solution of MIRCO 3.2 hi-resolution for the case of IPCC A1B scenario from 2001 to 2100.

3. RESULTS

3.1 ITF transport change in a model solution

Figure 1 shows temporal evolution of ITF transport from year 1991 to year 2100. The ITF transport in Fig. 1 is a year running mean value to filter out the seasonal cycle and those high frequency fluctuations. In this case, the first 20 year (1991 to 2010) result is the response of the ERA-interim data daily forcing and the rest (2011 to 2100) of them is the response of the IPCC A1B solution of the MIROC 3.2 hi-resolution version. It is noteworthy that the ITF transport is decreased during the 21st century which is related with the global warming signal. The decreasing rate of the transport is about 0.07 Sv/year. The large interannual fluctuations during the 1991 to 2010 seem to be caused by the daily forcing and it has clear ENSO related signal. The ITF transport in general is larger during the La Nina period while it is smaller during the El Nino period. Similar fluctuation in the 21st century solution may be related with this ENSO phenomenon.

To investigate the seasonal cycle change of the ITF transport in a warming climate, comparisons of the seasonal climatology calculated during the 20 year period are shown in Figure 2. In both cases, the seasonal maximum transport occurs in summer while the seasonal minimum occurs during the winter, which suggests that the global warming does not affect the ITF transport seasonal cycle itself. Table 1 shows the statistics of the seasonal cycle of the ITF transport. Global warming by A1B scenario from MIROC data decrease the mean ITF transport by 6.5Sv and it is much more decreased during the winter to spring compared to the other seasons. It is noteworthy that the seasonal fluctuation of the ITF transport in the warming climate is larger than the present situation.

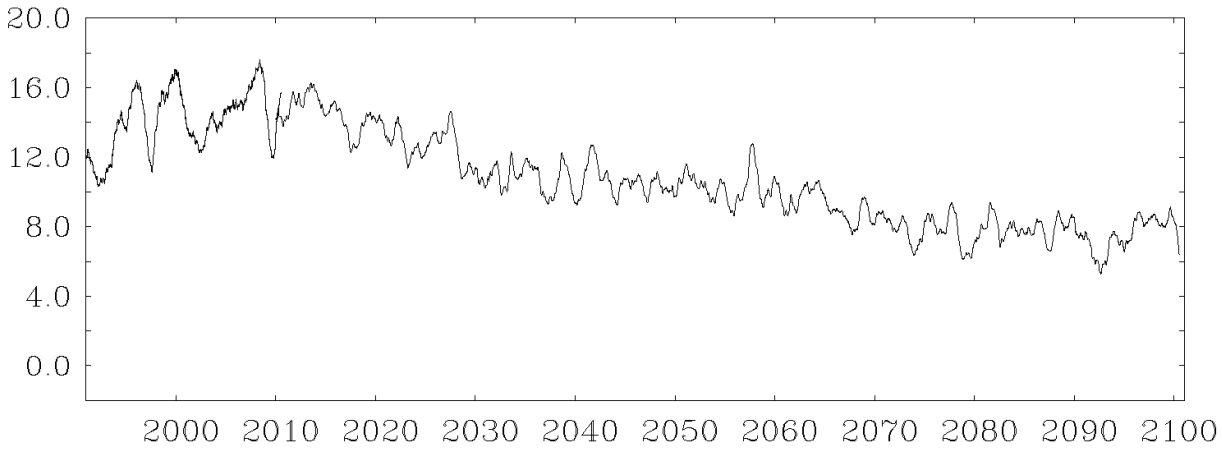

Fig. .1 Indonesian Throughflow (ITF) transport (a year running mean value in Sv) change during the 1991 to 2100.

Table 1. Statistics of the seasonal transport cycle of the Indonesian Throughflow

Period	Mean	Min.	Max.	STD
1991~2010	14	9.4	18.5	2.9
2081~2100	8.5	2.1	14.8	4.5
difference	6.5	7.3	3.7	-1.6

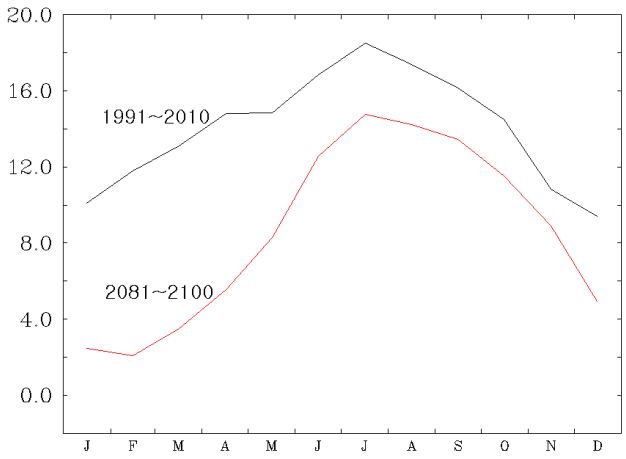

Fig. 2. Comparison of the seasonal cycle of the ITF transport (Sv) derived from the 20 year period climatology.

3.2 Solutions by the Island rule

It is known that the major forcing for the long-term mean ITF transport is the line integral of wind stress along the closed path surrounding the southern Pacific Ocean and the

Australia-Irian Jaya continent as suggested by Godfrey's Island rule [1,2]. Assuming a line integral path as in Fig.3, the Island rule in a steady state can be reduced to the following equation in case that we ignore the dissipation and the nonlinearity.

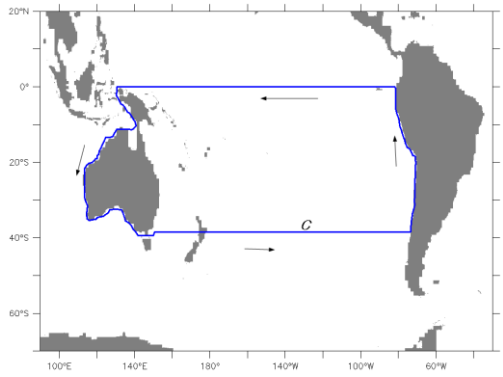

Fig. 3. Contour for the Godfrey's island rule.

$$\beta(y_n - y_s)\Psi_l = -\frac{1}{\rho_0}\oint_C \vec{\tau} \bullet \hat{t}\, ds$$

Thus we can calculate the ITF transport simply from the wind stress field. We applied this simple rule to the global warming (A1B) scenario produced wind stresses and compared them to their ITF transports. Fig. 4 shows the Island rule generated the ITF transport variability for the miroc_3.2 hi-resolution solutions. It is noteworthy that all the ITF transports calculated by the Island rule is larger than the model solution itself and it also decreases consistently in the 21st century under A1B scenario, which means that the line integral of the wind stresses following the contour decreases in the global warming environment. Fig. 5 shows the climatological ITF transport cycle calculated by the Island rule from the 20th century run during 1981 ~ 2000 and from the 21st century run during 2081 ~ 2100. It is consistent that the ITF transport change obtained by the model simulation in Fig. 2 except for the smaller magnitude change. The average transport change is about 3.6Sv.

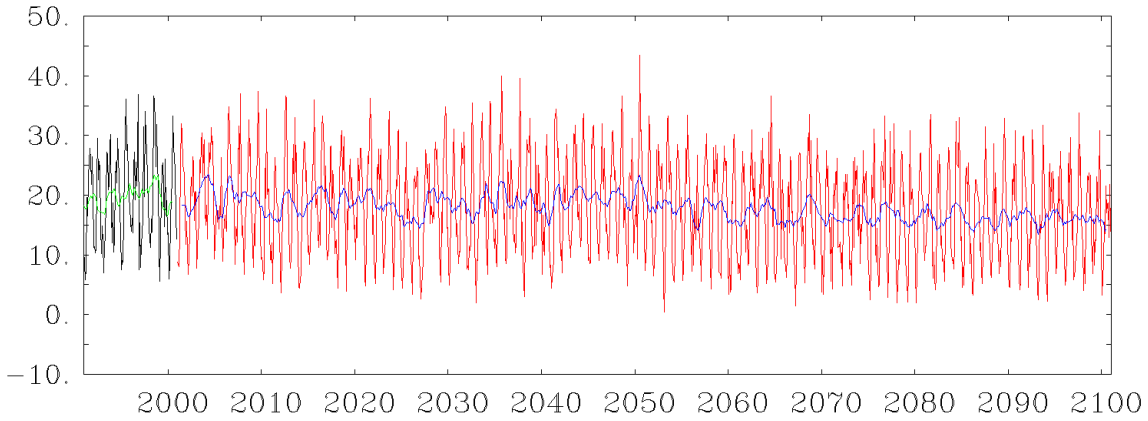

Fig. 4. ITF transports variability calculated by the line integral of the wind stresses using the Godfrey's island rule. Green (blue) lines denote 13-month moving average in the 20th (21st) century.

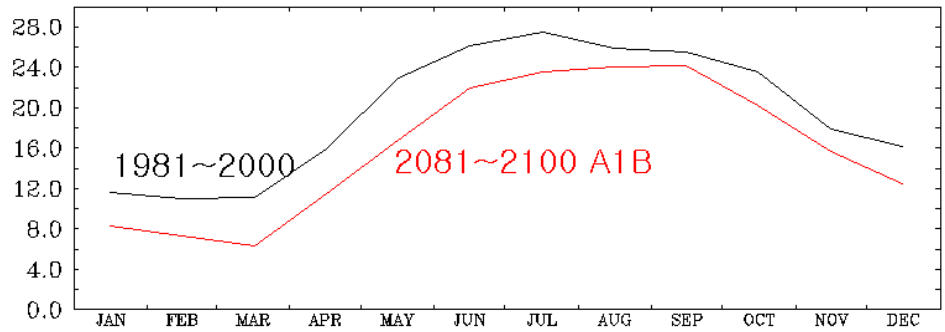

Fig. 5. Seasonal cycle difference of the ITF transport derived from the Island rule (The black curve is for the period of 1981 to 2000 and the red curve is for the period of 2081 to 2100 under the A1B scenario)

4. SUMMARY

We have developed a coarse resolution global ocean circulation model based on the HYCOM and applied it to the investigation of the ITF transport change due to the global warming. To find a solution that is consistent with the developed global ocean model, we choose one of the IPCC AR4 CGCM result (MIROC 3.2 hi-resolution case) for the future atmospheric forcing. Comparisons between the solutions show that the ITF transport may be decreased in the warming ocean considerably. This ITF transport decrease is also supported by Godfrey's Island rule, indicating that wind stress change surrounding the southern Pacific Ocean contributes to the reduction of the ITF transport.

The decrease of the ITF transport in the warming climate is related with the decrease of both thermal and freshwater contrast between the Pacific and the Indian Ocean. There has been a debate on whether the tropical Pacific response to the warming would be El Nino-

like or La Nina-like warming pattern [4]. ITF decrease found in this study favours the El Nino-like warming pattern because the pattern elevates the thermocline and diminishes the sea level of the western Pacific, driving a weak ITF flow into the Indian Ocean. The ITF transport change is likely to be associated with changes in the global thermohaline circulation, which needs further study.

Acknowledgements

This study is supported by the KORDI projects of PM56290, PE98651 and PN64983

References

Godfrey, J.S. (1989). A Svedrup model of the depth-integrated flow from the world ocean allowing for island circulations, *Geophysics. Astrophys. Fluid Dyn*., 45, 89-112.

Godfrey, J.S. (1996), The effect of the Indonesian throughflow on ocean circulation and heat exchange with the atmosphere: A review, *J. Geophys. Res*. 101(C3), 12,217-12,237.

Gordon, A.L., R.D. Suasanto, and K. Vranes (2003), Cool Indonesian throughflow as a consequence of restricted surface layer flow. *Nature*, 425, 824-828.

Kug, J.-S, K.P. Sooraj, F.-F. Jin, Y.-G. Ham, and D. Kim (2010), A possible mechanism for El Nino-like warming in response to the future greenhouse warming. *Int. J. Climatol*. DOI: 10.1002/joc.2163.

Oppo, D.W. and Y. Rosenthal (2010), The great Indo-Pacific communicator. *Science*, 328, 1492.

New ICES Working Group on Integrative Physical, Biological and Ecosystem Modelling: An Overview and an Invitation

Myron A. Peck, Miguel Bernal, et al.

1) Myron A. Peck, Institute of Hydrobiology and Fisheries Science, Center for Marine and Climate Research, University of Hamburg, Germany
2) Miguel Bernal, Spanish National Research Council (CSIC) and Instituto de Ciencias Marinas de Andalucia. Country (ICMAN), Spain

Extended Abstract

The coupling of biological and physical models in the 1980s has significantly enhanced our understanding of the dynamics of marine species and the ecosystems in which they live (Werner et al., 2001). For example, 3-d biophysical individual-based models (IBMs) are increasingly employed to explore population connectivity (Pineda et al., 2007) and/or the processes affecting rates of survival and growth of early life stages (ELS) of marine fishes and invertebrates (Peck and Hufnagl, 2011). For IBMs applied to ELS of commercially important fish and invertebrate species, a "best practices" guide has recently been published (North et al., 2009) and the usefulness of IBMs for marine management has been reviewed (Hinrichsen et al., 2010). Thus, these models are becoming well established.

In parallel to the development of IBMs, spatially-explicit food web (Christensen and Walters, 2004; Christiansen et al., 2005) and fishing fleet models (e.g., Venables et al., 2009) have been coupled (e.g., Fulton et al., 2003; Brand et al., 2007). These more complex "end-to-end" models (e.g., Atlantis) specifically include management evaluation frameworks for scenario testing (Fulton et al., 2010). This new generation of integrated modelling has recently attracted the interest of not only the scientific community but also of science programs and marine resources managers (Plagányi et al., 2011; Rose et al., 2011). One appealing aspect of these coupled models is that they integrate across various parts of the ecosystem and have the potential to incorporate human and environmental drivers in a single framework (Fulton et al., 2010; Plaganyi, 2010) and act as a risk assessment tool for management measures of marine ecosystems (Fulton, 2011). These models are well-suited for use in regional climate modelling activities.

Although more "simple" 3-d IBMs have been applied for some time, their use in management (e.g., marine spatial planning) is not widespread. For the more "complex" end-to-end models, continued development is needed and requires a large international and multidisciplinary effort. A wide range of key issues include spatial and temporal scaling (e.g., the use of "forcing functions" affecting larger (often global) scales than those studied) and best ways of incorporate human behaviour (van Putten et al., 2011). These models often contain parameter-rich physical, geological, chemical and biological sub-models, requiring the interaction of specialist in earth systems, climate and human systems. The complexity, data and knowledge requirements, and variety of

statiotemporal scales and objectives of these models require adequate fora to foster development and critical discussions.

This presentation discusses a new ICES Working Group that can attract the required expertise to promote both management applications of existing bio-physical models and that can further develop integrated end-to-end models. For successful implementation of all modelling activities, the group would also construct and/or maintain the required oceanographic, environmental, fisheries and other data products including operational real or near real-time data. This Working Group is initially promoted within the ICES community, although a future objective is to expand to attract experts (and co-sponsorship) from PICES and other scientific organizations / communities.

The expertise of working group members should encompass a range of disciplines required to construct and apply biological-physical models in marine systems including: 1) hydrodynamics, 2) numerical methods, 3) ecophysiology, 4) food-web dynamics, 5) socio-economics, and 6) Earth System dynamics. It is envisioned that this group will be composed of both modelers and experimentalists, fostering inter-disciplinary discussions with the end goal of advancing coupled modelling in marine systems. The involvement of leading researchers with active links to ongoing, large-scale European and North American research programs will help build bridges beyond the ICES community, particularly to recruit new working group members.

The presentation is an invitation for PICES involvement in this working group. The presentation briefly review ongoing modelling activities in the Atlantic that can take advantage of regional climate modelling. The review briefly discusses various EU research programs charged with 1) building model couplers (MEECE), 2) utilizing biophysical IBMs for single fish species (FACTS), and 3) constructing and utilizing End-to-end models in various European seas (VECTORS).

References

Brand, E.J., Kaplan, I. C., Harvey, C. J., Levin, P. S., Fulton, E. A., Hermann, A. J., and Field, J. C., 2007. A spatially explicit ecosystem model of the California Current's food web and oceanography. U.S. Dept. Commer., NOAA Tech. Memo. NMFS-NWFSC-84, 145 p.

Christensen, V., and Walters, C. J., 2004. Ecopath with Ecosim: Methods, capabilities, and limitations. Ecological Modelling, 172:109–139.

Christensen, V, Walters, C. J., and D. Pauly, D., 2005. Ecopath with Ecosim: a User's Guide. Fisheries Centre, University of British Columbia, Vancouver. November 2005 edition, 154 p. (available online at www.ecopath.org)

Fulton, E. A., Smith, A. D. M., Smith, D. C., and Van Putten, I. E., 2010. Human behaviour: the key source of uncertainty in fisheries management. Fish and Fisheries, 12: 2–17.

Fulton, E. A., Smith, T., and Punt, A.E., 2003. Indicators of the ecosystem effects of fishing: Case-study 1: Temperate bay ecosystem. CSIRO Report-No-MR-C-96/12.

Hinrichsen, H. - H., Dickey-Collas, M., Huret, M., Peck, M. A., Vikebø, F., 2011. Evaluating the suitability of coupled biophysical models for fishery management. ICES Journal of Marine Science, 68(7):1478–1487.

Hollowed, A. B., Bond, N. A., Wilderbuer, T. K., Stockhausen, W. T., A'mar, Z. T., Beamish, R. J., Overland, J. E., et al. 2009. A framework for modelling fish and

shellfish responses to future climate change. ICES Journal of Marine Science, 66: 1584–1594.

North, E.W., Gallego, A., Petitgas, P., 2009. Manual of recommended practices for modelling physical – biological interactions during fish early life. ICES Cooperative Research Report No. 295, 112, pp.

Peck, M.A., Hufnagl, M., In Press. Can IBMs explain why most larvae die in the sea? Model scenarios and sensitivity analyses reveal research needs. Journal of Marine Systems doi:10.1016/j.jmarsys.2011.08.005

Plagányi, E. E., and Butterworth, D. S., 2004. A critical look at the potential of ECOPATH with ECOSIM to assist in practical fisheries management. African Journal of Marine Science, 26: 261–287.

Plagányi, É. E., Weeks, J. S., Skewes, T. D., Gibbs, M. T., Poloczanska, E. S., Norman-López, A., Blamey, L. K., Soares, M., and Robinson, W. M. L., 2011. Assessing the adequacy of current fisheries management under changing climate: a southern synopsis. – ICES Journal of Marine Science, doi:10.1093/icesjms/fsr049

Pineda, J., Hare, J. A., and Sponaugle, S., 2007. Transport and dispersal in the coastal ocean and consequences for population connectivity. Oceanography, 20(3): 22–39.

Pörtner, H.O., Peck, M.A., 2010. Climate change impacts on fish and fisheries: towards a cause and effect understanding. Journal of Fish Biology 77: 1745–1779.

Rose, K. A., and 24 co-authors, 2010. End-to-end models for the analysis of marine ecosystems: Challenges, issues, and next steps. Marine and Coastal Fisheries: Dynamics, Management, and Ecosystem Science, 2: 115–130.

van Putten, I. E., Kulmala, S., Thébaud, O, Dowling, N., Hamon, K. G., Hutton, T., and Pascoe, S., 2011. Theories and behavioural drivers underlying fleet dynamics models. Fish and Fisheries, DOI: 10.1111/j.1467-2979.2011.00430.x

Venables, W. N., Ellis, N., Punt, A. E., Dichmont, C. M., and Deng, R. A., 2009. A simulation strategy for fleet dynamics in Australia's northern prawn fishery: effort allocation at two scales. ICES Journal of Marine Science, 66: 631–645.

Werner, F., Quinlan, J., Lough, R., and Lynch, D., 2001. Spatially-explicit individual based modeling of marine populations: a review of the advances in the 1990s. Sarsia 86, 411–421.

Regionally downscaled climate modelling: physics to fisheries

J Icarus Allen

Climate change is already affecting marine ecosystems and their services as indicated by both ocean observations and models. The biological responses to these effects are visible but uncertain as to the consequences for man. Our ability to understand, predict and mitigate the effects of global change on marine ecosystems and their services is at present heavily dependent upon the application of coupled atmosphere ocean ecosystem models. In this presentation I will discuss with examples some key issues in the quantification of direct climate impacts on marine ecosystems in coastal seas, including regional downscaling of climate forcing, coupling plankton models to those of higher trophic levels, model skill assessment and anthropogenic scenario definition drawing on the experience gained in the MEECE project (www.meece.eu) for the northwest European continental shelf and the QUEST_FISH project (www.quest-fish.org.uk) for multiple shelf sea regions around the world. The complexity of the multiply coupled system suggests a process oriented approach is most appropriate, to establish the envelope of potential future responses to global change scenarios.

Development of a regional plankton ecosystem model for the Pacific coast of Canada

Angelica Peña

Fisheries and Oceans Canada, Institute of Ocean Sciences,
P.O. Box 6000, Sidney, BC, V8L 4B2, Canada.
(Angelica.Pena@dfo-mpo.gc.ca)

1.Introduction

The development of coupled regional climate-ecosystem models is critical for assessing the likely responses of the marine ecosystem to climate change. This is particularly important in the coastal region where the coarse spatial scale of global models is not able to capture mesoscale patterns such as eddies, river plumes, coastal jets, and associated upwelling fronts. Ecosystem models are important tools to study biogeochemical cycles that are driven by complex interactions among physical, chemical and biological processes. Given the high temporal and spatial variability of coastal regions it is often indispensable to couple ecosystem models to high-resolution circulation models to simulate realistic conditions. Ecosystem models also have the potential to help us understand and quantify the interactions between marine ecosystems and climate changes and to predict plausible ecosystem responses.

A first step to address the impacts of climate variability on marine ecosystem is to develop coupled circulation-ecosystem models that simulate the present ecosystem state in relation to the climate record and can be use to examine the influence of different forcing acting, at different scales, on ecological processes. This allows us to evaluate the role of specific mechanisms in governing the observed and future variability of the physical-chemical environment, marine populations, and biogeochemical fluxes in a region. Models that aim to improve understanding of how phytoplankton respond to environmental conditions are crucial to assessing the effects of climate change on marine ecosystems. However, because these models currently lack the complexity (species or functional groups, parameters that 'adapt/change' in response to changing ocean conditions/forcing, etc.) to evolve to new states that could not be envisaged from their formulation, they can not properly predict ecosystem changes under changing environmental forcing. Much work is necessary to improve confidence in climate-change prediction based on this type of ecosystem model.

This study presents results from coupled plankton / circulation (ROMS) models developed to study factors determining regional-scale patterns of lower trophic levels in the Pacific coast of Canada. The Pacific coast of Canada is at the northern end of the California

Current Systems and is influenced by summer coastal upwelling. It is also influenced by mesoscale eddies, strong tidal currents, and freshwater inputs producing an estuarine circulation. All these processes contribute to the dynamics of nutrient supply and phytoplankton productivity.

2. Model Description

Three implementations of ROMS (Regional Ocean Modeling System) circulation model (Fig. 1) have been developed in the Pacific coast of Canada: British Columbia shelf (BC) model, Southwest coast of Vancouver Island (SWCVI) model, and the Salish Sea model. (The Salish Sea includes Puget Sound, Juan de Fuca Strait, Strait of Georgia and adjacent inlets.) An NPZD-type model has been coupled to the SWCVI model to study the effect of Juan de Fuca eddy on summer bloom dynamics. Similarly, and NPZD-type model was embedded on the Salish Sea model to study the annual cycle of phytoplankton dynamics in this region. Work is in progress to couple a biogeochemical-plankton model to the BC shelf model to study the effect of circulation on plankton production and oxygen concentration.

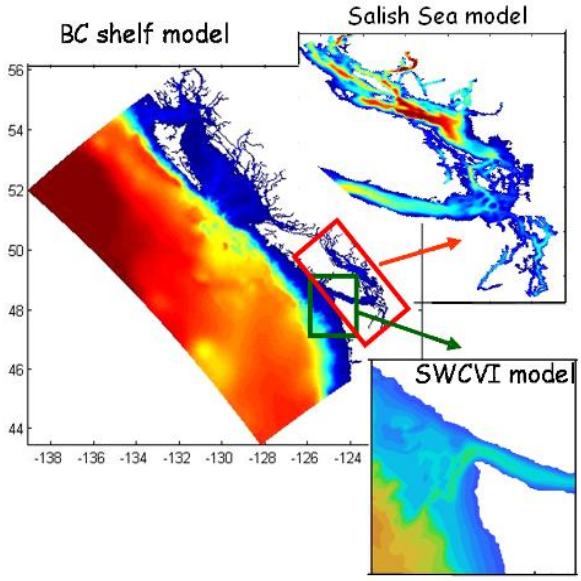

Figure 1. Domain and bathymetry of the British Columbia shelf, Salish Sea and Southwest coast of Vancouver Island models in the Pacific coast of Canada.

2.1 Ocean circulation model (ROMS)

The Southwest coast of Vancouver Island circulation model developed by Forman et al. (2008) is bounded by approximately 45.5°N to 50.0°N and 123.5°W to 128.5°W, with 30 non-uniform vertical layers, with increased resolution near the surface and bottom boundary layers. A stretched coordinate rectangular grid, with horizontal resolution as coarse as 5 km adjacent to the western boundary and as fine as 1 km near the entrance of Juan de Fuca Strait, is employed to obtain an accurate representation of topographic and coastal features of the region. The model is forced with tides, average summer upwelling-favorable winds, temperature and salinity monthly climatologies, and buoyancy boundary conditions that maintain an estuarine flow in Juan de Fuca Strait.

The Salish Sea model developed by Masson (2010) includes the Strait of Georgia, Puget Sound, Juan de Fuca Strait and adjacent inlets. It has a horizontal resolution of 1 km, 31 non-uniform vertical levels, with clustering near the surface. The model is forced by tides, freshwater daily discharge from 20 rivers, hourly wind forcing from observations, monthly atmospheric forcing (heat flux) from observations, and seasonal temperature and salinity profiles along open boundaries.

2.2 Biological Model

The NPZD type model (Fig. 2) has nine compartments: 3 nutrients (ammonium, nitrate and silicate), 2 groups of phytoplankton (diatoms, flagellates), 2 groups of zooplankton (microzooplankton and mesozooplankton) and 2 types of detritus (nitrogen and silicon detritus). All model compartments are expressed in terms of their nitrogen concentration (mmol-N m^{-3}). The main processes incorporated in the model include growth of small phytoplankton and diatoms controlled by light, NO_3 and NH_4, and for diatoms also by $Si(OH)_4$. Grazing by microzooplankton on small and large phytoplankton and nitrogen detritus and grazing by mesozooplankton on diatoms and microzooplankton are modeled by the Holling type-III formulation. Natural loss processes (i.e., mortality and excretion) for both phytoplankton and zooplankton are linear. Temperature affects all physiological parameters in the model according to Q_{10} factors referenced to10℃

The initial and boundary conditions for nitrate and silicate in both models are derived from 3D summer climatology generated from a combination of data from the Institute of Ocean Sciences and the World Ocean Database 2001. For lack of better information, all other compartments are initialized with a constant value.

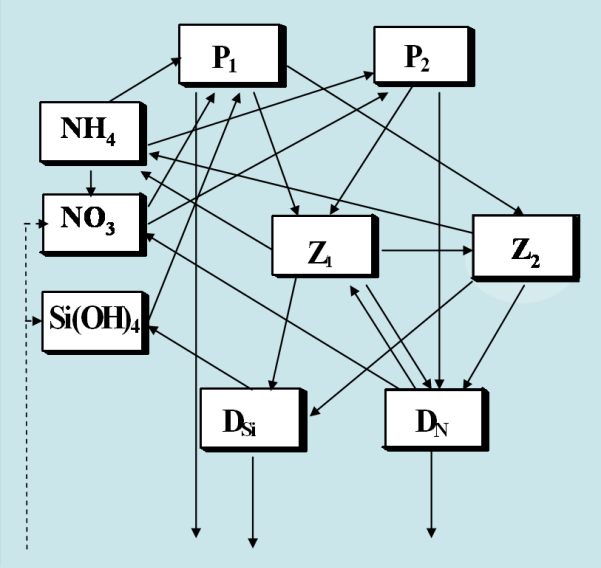

Figure 2. Diagram of the NPZD-type model: fluxes are shown with solid lines, external input of nutrients by dashed lines. Nine model compartments are represented in the model: P_1 diatoms, P_2 flagellates, Z_1 microzooplankton, Z_2 mesozooplankton, D_N nitrogen detritus and D_{Si} silicon detritus, NH_4, NO_3 and $Si(OH)_4$.

3. Models Application

3.1 Southwest coast of Vancouver Island

The southwest coast of Vancouver Island is influenced by summer coastal upwelling, by freshwater inputs from the Fraser River and many smaller rivers, and by strong tidal currents, producing an estuarine circulation. All these processes contribute to the dynamics of nutrient supply and ultimately to the high primary productivity observed in this region. In addition to reproducing realistic circulation features and water properties, simulating a realistic near surface stratification is a primary concern, since the model is used to force the lower trophic model. As shown in Figure 3, the model output is sensitive to the algorithm used for vertical mixing and thus care must be taken in its selection.

In the summer, phytoplankton blooms are often found in this region associated with the Juan de Fuca Eddy, a seasonal cyclonic cold eddy located west of the entrance to Juan de Fuca Strait. Results from the coupled circulation-NPZD model (Figure 4) show the influence of the Juan de Fuca eddy on the growth and retention of phytoplankton. Phytoplankton concentration and primary production at surface are higher around the circumference of the eddy and along the Washington upwelling coast, in agreement with remotely-sensed observations of ocean color during the summer.

This eddy is formed during periods of upwelling favourable winds, which in combination with the estuarine flow and tides, produce enhanced upwelling off Cape

Flattery (Foreman et al., 2008). The model also shows the importance of different sources of nutrients (i.e., wind-driven upwelling, topographically controlled upwelling, and the outflow from Juan de Fuca Strait) on primary production and biogeochemical cycles.

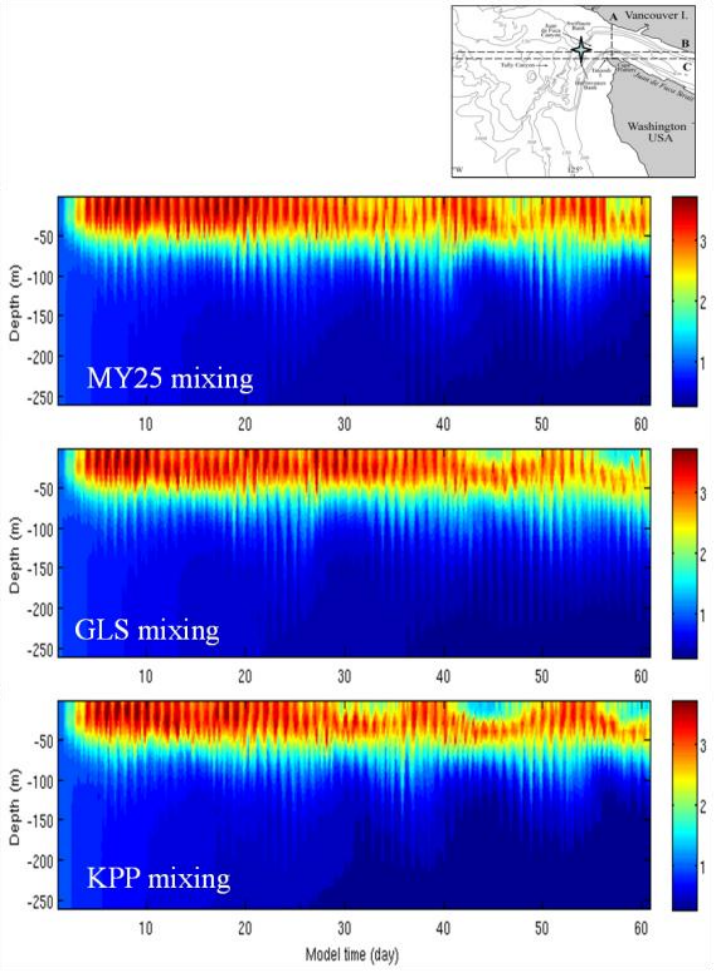

Figure 3. Simulated time-series of phytoplankton biomass (mmol-N m^{-3}) at a station in the SWCVI showing the influence of vertical mixing algorithm on model output. Mellor-Yamada 2.5 (top), GLS (center), and KPP (bottom) algorithms.

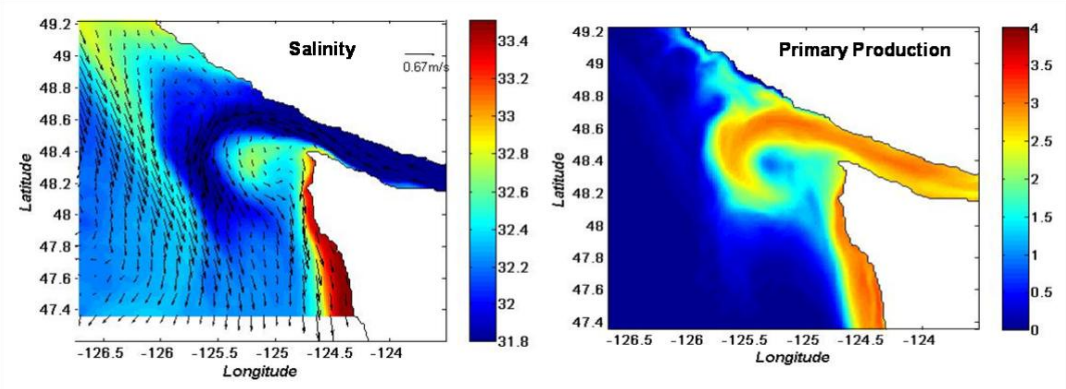

Figure 4. Model surface salinity and currents (left panel) and primary production (right panel) averaged over days 46-60 of the 60-day simulation.

3.2 Salish Sea

The Strait of Georgia is a highly productive, semi-enclosed sea with strong estuarine circulation connected to the North Pacific by the Juan de Fuca Strait. At both ends of the Strait of Georgia, strong tidal currents mix the water column and reduce local stratification. The model is able to reproduce the main horizontal features of the region (Figure 5) and simulates the annual cycle reasonably well. Model and observations indicate maxima phytoplankton biomass in April, when the increase in solar radiation and abundance of nutrients provides optimal growing conditions. In summer, the model chlorophyll has low levels in the central basins, but substantial values occur near the river outlets due to nutrient discharge. Model results show the importance of physical variability, driven by freshwater inflow and tidal mixing, in maintaining the high spatio- temporal variability of phytoplankton and zooplankton. In particular, the influence of spring-neap tidal mixing on phytoplankton production and biogeochemical cycles dominate summer variability.

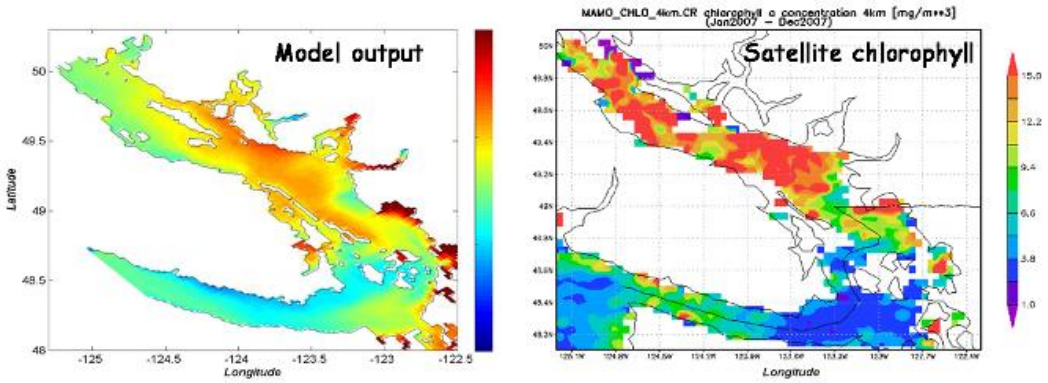

Figure 5. Annual mean surface chlorophyll concentration simulated by the model (left panel) and derived from satellite observations (right panel).

In summary, our results indicate that phytoplankton production is influenced by nutrient fluxes, stratification, and temperature, all of which are likely to be affected by climate change. Impacts on phytoplankton will lead to cascading effects throughout the marine ecosystem. Thus, the development of biophysical models that capture the main processes responsible for temporal-spatial variability in a region are important tools to predict plausible future conditions.

References

Foreman, M. G. G., Callendar, W., MacFadyen, A., Hickey, B. M., Thomson, R. E. and Di Lorenzo, E. (2008) Modeling the generation of the Juan de Fuca Eddy. *Journal of Geophysical Research* **113,** doi:10.1029/2006JC004082.

Masson, D. (2010). Development of the Strait of Georgia ROMS model. Project status report. http://www.pac.dfo-mpo.gc.ca/science/oceans/detroit-Georgia-strait/documents/ERI_0809_reports/Masson_statusreport_0809.pdf

The East/Japan Sea circulation in the MIROC-hires climate model

Gyun-Do Pak and Kyung-Il Chang

Seoul National University, Korea

1. Introduction

The East/Japan Sea (EJS, hereafter), which has experienced dramatic climatic changes including the warming and declining of dissolved oxygen contents of deep water, is a semi-closed, deep marginal sea in the northwestern Pacific (Figure 1a). Since the EJS contains large-scale ocean-like processes with smaller time and space scales, many nowcasting and climatological numerical experiments have been tried. However, only a few studies about long term variations of the EJS and future climate projections have been available. In this study, oceanic features such as temperature profiles and surface/subsurface currents based on forecasting results of Model for Interdisciplinary Research on Climate version 3.2-high resolution (MIROC-hi) in EJS are evaluated by comparing them with climatological dataset and data assimilative ocean model product of the EJS. Also, projected results of warming and temporal variations of volume transports of the major currents in the EJS, the Tsushima Warm Current (TWC) and Liman Cold Current (LCC), are presented using the MIROC-hi product.

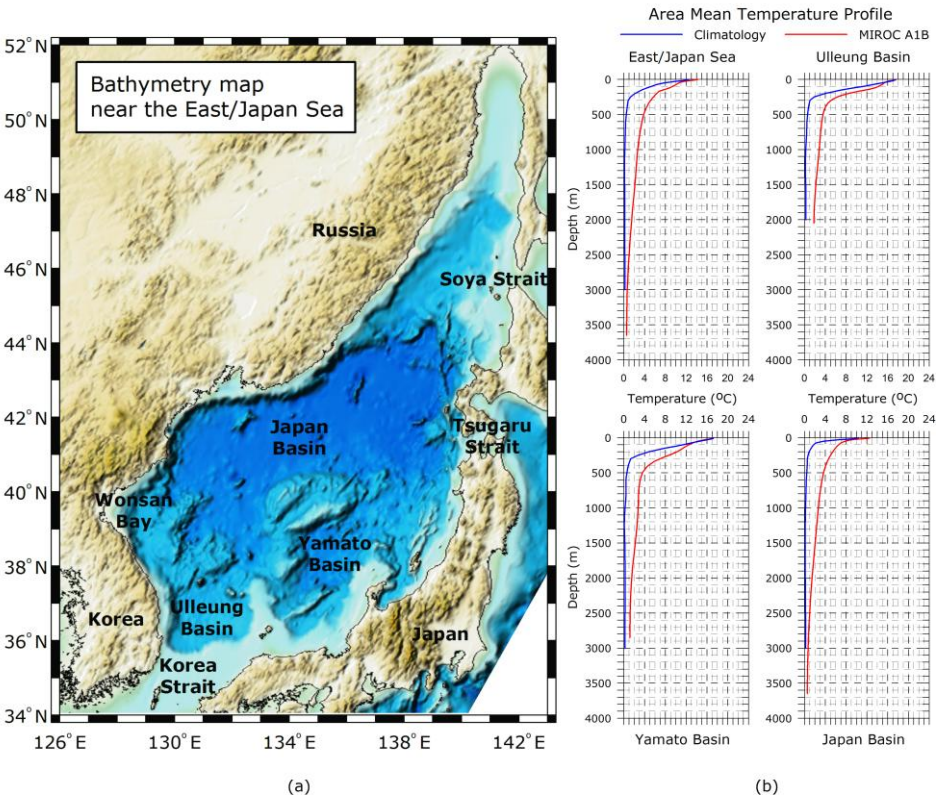

Figure 1. (a) Bathymetry of the EJS, and (b) basin-averaged time-mean vertical temperature profiles from MIROC-hi (red) and GDEM (blue).

2. MIROC-hi Model

MIROC-hi, which is one of very fine resolution Atmosphere-Ocean General Circulation Model, is developed cooperatively by Center for Climate System Research, University of Tokyo, National Institute for Environmental Studies, and Frontier Research Center for Global Change of Japan. The model consists of five component models: atmosphere, land, river, sea ice, and ocean parts.

MIROC-hi was integrated using Earth Simulator in Japan from 1901 to 2100 after 100 years of spin-up. Only the experiment case named A1B-run is selected to evaluate and analyze the model results. The A1B-run based on Intergovernmental Panel on Climate Change's A1B scenario from 2001 to 2100 is integrated after the 20C-run forced by historical data. More detailed descriptions of MIROC-hi can be found on K-1 Model Developers (2004).

3. Evaluation of the present status (2001 – 2010)

1) Area Mean Temperature Profile

We have used the climatological monthly mean temperature data from U.S. Navy's unclassified Generalized Digital Environmental Model (GDEM, Chu et al., 2001) based

on observational dataset for the comparison with the MIROC-hi product. Figure 1b shows basin-averaged, time-mean vertical profiles of temperature from MIROC-hi (red line) in period from 2001 to 2010 and GDEM (blue line). MIROC-hi and GDEM look similar in surface temperature for each basin and whole area of the EJS. Temperature gradients in the thermocline are relatively weak in MIROC-hi so that temperature below surface is much higher in MIROC-hi than that of GDEM. Also, the profiles of MIROC-hi are gradually decreasing and show very high temperature below thermocline, while the profiles below thermocline of GDEM show uniform temperature less than 1℃.

2) Comparison with Data-Assimilative Model Product

We have prepared Hirose et al. (2007)'s product (RIAMOM, hereafter), which assimilates sea surface height data to ocean model, to compare the circulation patterns of EJS with MIROC-hi. Both of MIROC-hi and RIAMOM reproduce realistic surface current system: branches of TWC, meso-scale eddies, separating and meandering of East Korean Warm Current (EKWC), southwestward flow along the Russian coast, and so on. However, an overshooting of the EKWC occurs in MIROC-hi while the separation latitude of the EKWC is realistic in RIAMOM probably due to the resolution of ocean model (0.28° x 0.19° for MIROC-hi, 1/12° x 1/12° for RIAMOM). Also, both the MIROC-hi and RIAMOM simulate similar current patterns near the depth of 400 m, except for the path of coastal jet along the Russian coast. Coastal jets along the Russian coast exist in both models, but the coastal jet from MIROC-hi separates from the coast before reaching to Wonsan Bay (see Fig. 1) while the coastal jet from RIAMOM flows southward continuously along the coast (Figure 2).

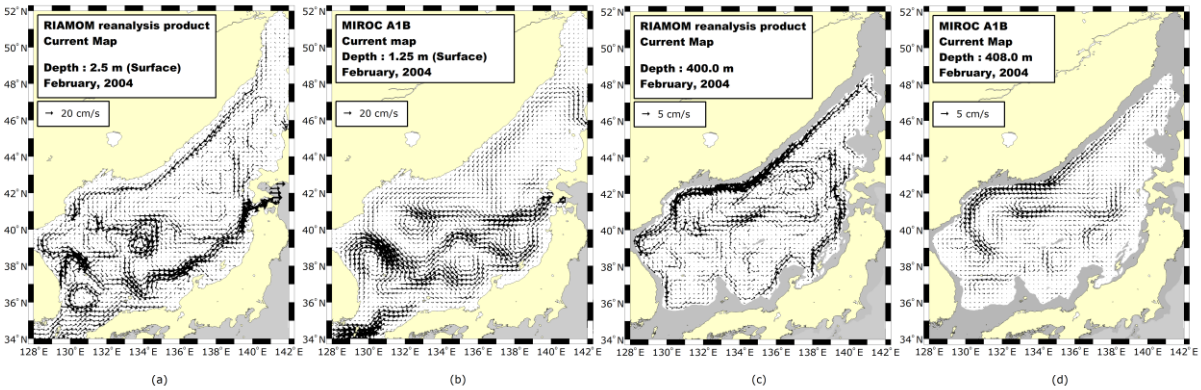

Figure 2. Horizontal circulation of (a) RIAMOM at surface and (c) at depth of 400 m, (b) MIROC-hi at surface and (d) at depth of 408 m.

4. Some projected results

1) Warming Trend

A clear warming trend for each basin and the entire EJS is calculated in MIROC-hi product between 2001 and 2100 (Figure 3). Only positive warming trends are found over all the depth. The maximum warming of about 4.0℃/100years (4.0℃/100years in Japan Basin) and the minimum warming about 0.5℃/100years are projected at surface and depth of 1600 m, respectively, for every basin. Temperature trends of locally minimum about 2.5℃/100years and locally maximum about 3.0℃/100years are found at the depth of 200 m and 400 m, respectively in Ulleung Basin. Similarly, locally maximum and minimum of the warming trends can be found on subsurface in Yamato Basin, while the locally maximum and minimum does not exist in Japan basin.

2) Variations of Volume Transports of major Currents

Volume transports of TWC, LCC, and North Korean Cold Current (NKCC) are calculated using MIROC-hi results. TWC is the only inflow of the EJS so that the volume transport of TWC has an important effect on the circulation of the EJS. LCC and NKCC are southward flowing cold currents, the transport variation of which has been little studied. Unfortunately, the NKCC could not be resolved with Kim et al. (2009)'s definition of NKCC section (37°N, 129.4°E - 130.4°E, 100 m - 700 m) using MIROC-hi due to the separation of the coastal jet along the Russian coasts shown in Figure 2. Figure 4 shows monthly mean transport of (a) TWC and (b) LCC in MIROC-hi data. TWC shows almost zero-trend while LCC shows an increasing trend.

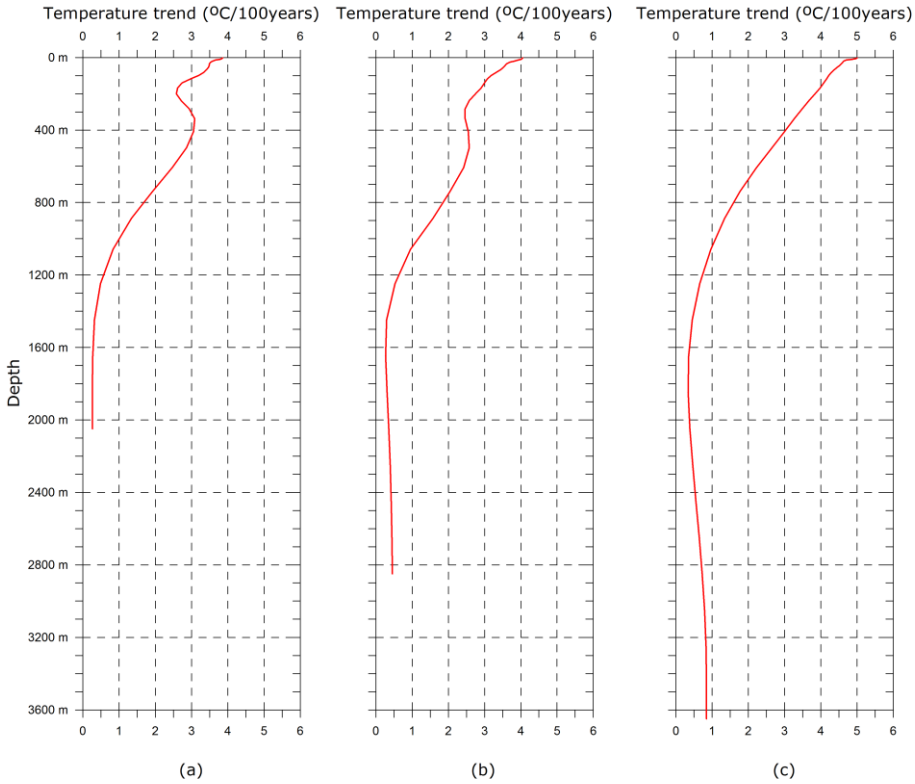

Figure 3. Calculated basin-averaged temperature trends in (a) Ulleung Basin, (b) Yamato Basin, and (c) Japan Basin using MIROC-hi product.

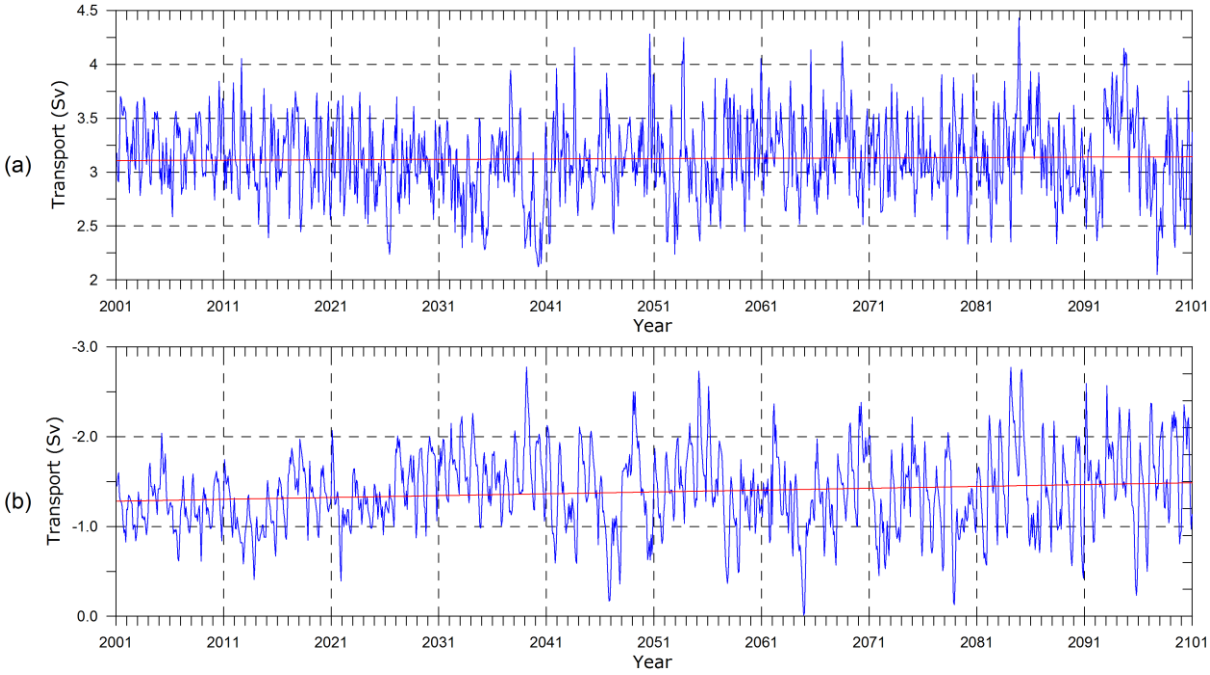

Figure 4. Monthly mean transports of (a) TWC and (b) LCC. Linear trends are indicated by red lines.

5. References

Chu, P.C., Lan, J., Fan. C. 2001. Japan Sea Thermohaline Structure and Circulation. Part I: Climatology. *J. Phys.Oceanogr.*,**31**, 244-271.

Hirose,N.,H.Kawamura,H.J.Lee, and J.-H. Yoon. 2007. Sequential Forecasting of the Surface and Subsurface Conditions in the Japan Sea. *J. Oceanogr.*, **63**, 467-481.

K-1 Model Developers 2004.K-1 Coupled Model (MIROC) Description, eds. Hasumi, H. &Emori, S. (Center for Climate System Research, Univ. of Tokyo, Tokyo), K-1 Tech. Rep. 1.

Kim, Y.H., K.-I.Chang, J.J. Park, S.K. Park, S.-H.Lee, Y.-G.Kim, K.T. Jung, and K. Kim. 2009. Comparison between a reanalyzed product by 3-dimensional variational assimilation technique and observations in the Ulleung Basin of the East/Japan Sea. *J. Mar. Syst.*, **78**, 249-264

Interannual surface salinity variability in the Yellow and East China Seas in response to ENSO

Taewook Park[1], Chan Joo Jang[1], Minho Kwon[1], Hanna Na[2] and Kwang-Yul Kim[2]

[1]Korea Ocean Research and Development Institute,
1270 Sadong, Ansan 426-744, Korea.
[2]School of Earth and Environmental Sciences, Seoul National University,
Seoul 151-742, Korea

Abstract

This study investigates interannual variability of sea surface salinity (SSS) in the Yellow and East China Seas (YECS) using a global ocean general circulation model with regional focus on the YECS. An interannual variability of the SSS in the YECS is linked to ENSO-related precipitation over east China. When El Niño event occurs in winter, more rainfall is observed over central China in the rainy season of the following years. The heavy precipitation leads to a large amount of CRD, which results in decreasing SSS in the YECS. This suggests that summer SSS variability in the YECS is closely linked to ENSO via the summer precipitation system over east China.

1. Introduction

In efforts to understand year-to-year variability of sea surface salinity (SSS) in the Yellow and East China Seas (YECS), Ichikawa et al. (2001) analyzed observed SSS data from 1972-1988 and showed that the path of Changjiang freshwater has a large interannual variation depending on the magnitude of Changjiang river discharge (CRD). Chang and Isobe (2003) showed that interannual variations in the movement of Changjiang water are derived from a dominant periodicity of CRD based on a numerical study. Senjyu et al. (2006) investigated interannual variability of salinity in the Korea Strait utilizing 30-year historical hydrographic data and showed that the first EOF mode of salinity variability at the Korea Strait is almost consistent with that of CRD.

Interannual variation of SSS in the YECS could be influenced by El Niño–Southern Oscillation (ENSO) because CRD in summer increases following El Niño events (e.g., 1973, 1983, and 1998), which is linked to the rainfall system in the central China (Shankman et al., 2006; Lau and Weng, 2001). Bueh et al. (2003) revealed that Changjiang discharge is closely related to monsoon precipitation, with CRD showing a tendency toward more frequent and greater flooding since the 1990s. Investigating relationship between ENSO and monsoon-related CRD may help clarify interannual SSS variation in the YECS.

Nevertheless, observations or numerical simulations of the SSS distributions in the YECS are not yet sufficient to investigate the interannual variability because those observational data are scarce. In this sense, global ocean models that represent the YECS properly are very useful for studying interannual variations. This study investigates the linkage of summer SSS in the YECS with ENSO through CRD variability.

2. Model and Methods

A global OGCM, Max Planck Institute Ocean Model (MPI-OM) with regional focus on the YECS, was used (Fig. 1). The model was initialized with the annual mean temperature and salinity from the Levitus et al. (1998) monthly climatology. Initially, the model was spun up for 400 years using the OMIP forcing. Then, additional 40-year integrations were carried out with 1960 atmospheric forcing from ERA-40 and the observed CRD in 1960. Experiment was performed by taking year-to-year variations over 42 years into account for both surface forcing and CRD.

Spatio-temporal variability of surface salinity was investigated using cyclostationary EOF (CSEOF) analysis (Kim et al., 1996; Kim and North, 1997). The CSEOF method can be applied to a single time series, hence CRD for 42 years is analyzed using the CSEOF method and compared with PC time series of SSS. Both observed CRD and the ERA-40 precipitation data over east China were compared with ENSO index to investigate relationship between El Niño and rainfall that is responsible for CRD fluctuation. SST anomalies over Niño3.4 (120-170°W, 5°S-5°N) were used as an ENSO index.

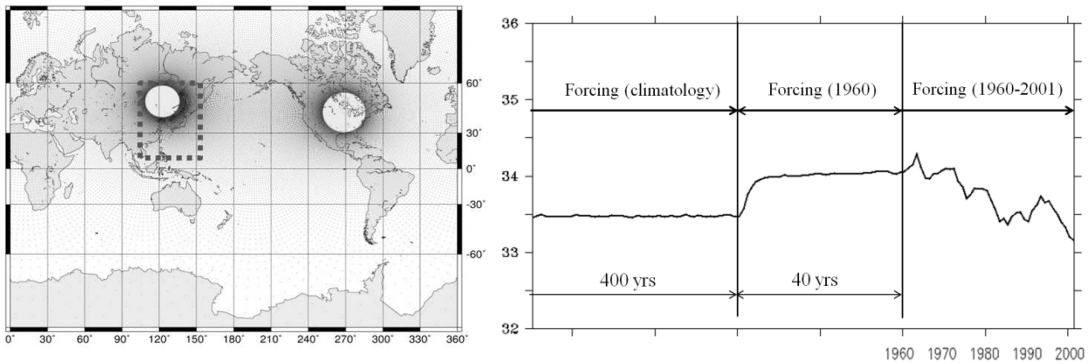

Fig. 1. (left) Model grid points denoted by dots. No salinity restoring is applied in the dashed box. (right) Design of spin-up and experiment. Time evolutions of salinity averaged in the area of the Yellow and East China Seas.

3. Results

Interannual variability of SSS in the YECS in response to CRD

To investigate year-to-year variation of SSS in the YECS in connection with CRD variation, both SSS and CRD for 42 years are analyzed using the CSEOF method. The third CSEOF mode of SSS (Fig. 2a), which explains 25% of the total variance aside

from both the seasonal cycle and the long-term trend, shows large negative anomalies in summer near the Changjiang river mouth. The corresponding PC time series significantly resembles the first PC time series of CRD (Fig. 2b). The CRD PC time series is positively correlated with the SSS PC time series with a correlation coefficient of 0.67, which suggests that larger CRD corresponds to freshening over the areas of negative SSS anomalies in the CSEOF patterns.

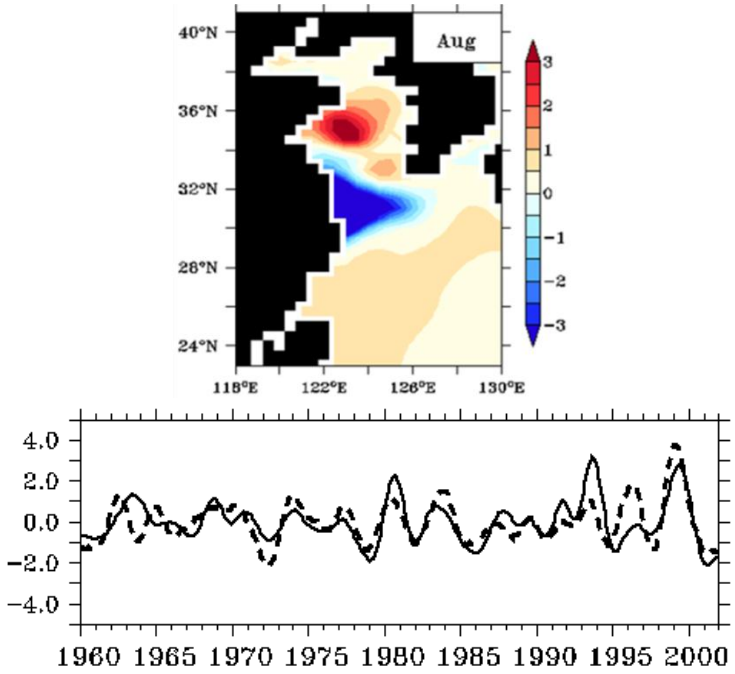

Fig. 2. (left) The third cyclostationary EOF of SSS and (right) the corresponding PC time series (solid line) in comparison with the first PC time series of CRD (dashed line).

Variabilities of CRD and precipitation over east China in relation to ENSO

SST anomalies over Niño3.4 are used as an ENSO index, which is plotted together with the CRD time series (Fig. 3). Note that both time series are standardized with respect to their standard deviations. Large CRD, such as in 1973, 1983, and 1998, occurs following huge El Niño events. Figure 4 shows a time series of precipitation averaged over the Yangtze River valley and CRD, and demonstrates that heavy precipitation occurs and CRD increases as a result after El Niño events except for the 1992 El Niño.

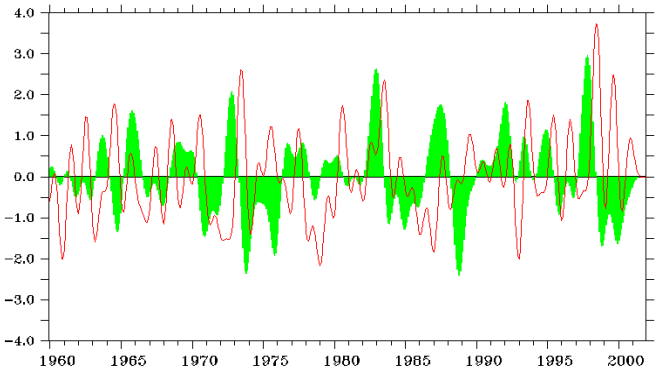

Fig. 3. Niño3.4 index (shaded curve) superimposed on the year-to-year variation of CRD (red line). All variables are normalized after annual cycles are removed from 1-year moving average.

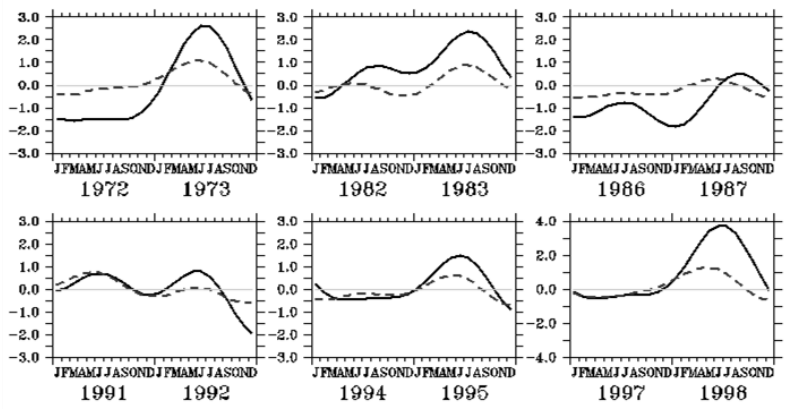

Fig. 4. Anomalies of precipitation (dotted lines) averaged over the Yangtze River valley (29°-32°N, 105°-122°E) and CRD (solid lines). All variables are normalized by their standard deviations. El Niño occurred in 1973, 1983, 1987, 1992, 1995, and 1998.

ENSO effect on SSS variability via precipitation over east China

In order to explore SSS variability that is linked to ENSO-related precipitation, composite precipitation patterns in El Niño and La Niña years are produced. Composite map for precipitation averaged from May to July (Fig. 5) is then constructed during the peak rainfall over the central-east China. The difference map shows that when El Niño events occur in winter, more rainfall is observed over the central China in rainy season of the following years. The heavy precipitation over the central-east China following El Niño events causes surface salinity to decrease in the YECS through CRD (Fig. 6). This suggests that summer SSS variability in the YECS is closely linked to ENSO variability via CRD; when El Niño occurs, heavy precipitation in the east China decreases SSS in the YECS through increased CRD.

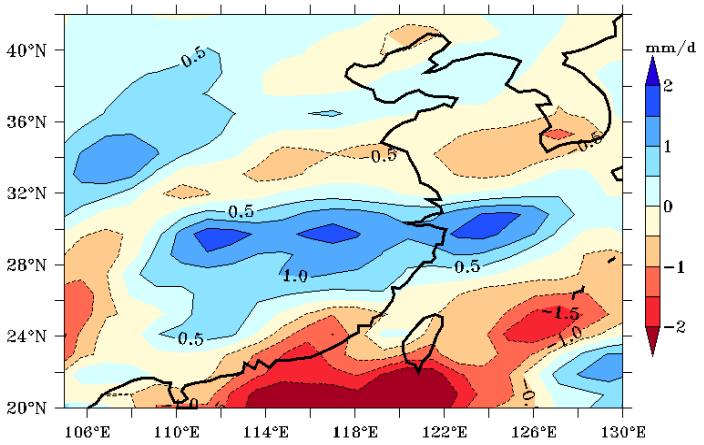

Fig. 5. Map of difference between El Niño and La Niña composites of precipitation averaged for May-July. On the basis of the Nino3.4 SST index for December-February, 8 El Niño events (1979, 1978, 1983, 1984, 1988, 1992, 1993, 1999) and 7 La Niña events (1972, 1975, 1976, 1985, 1990, 2000, 2001) exceeding one standard deviation of the Nino3.4 time series are selected.

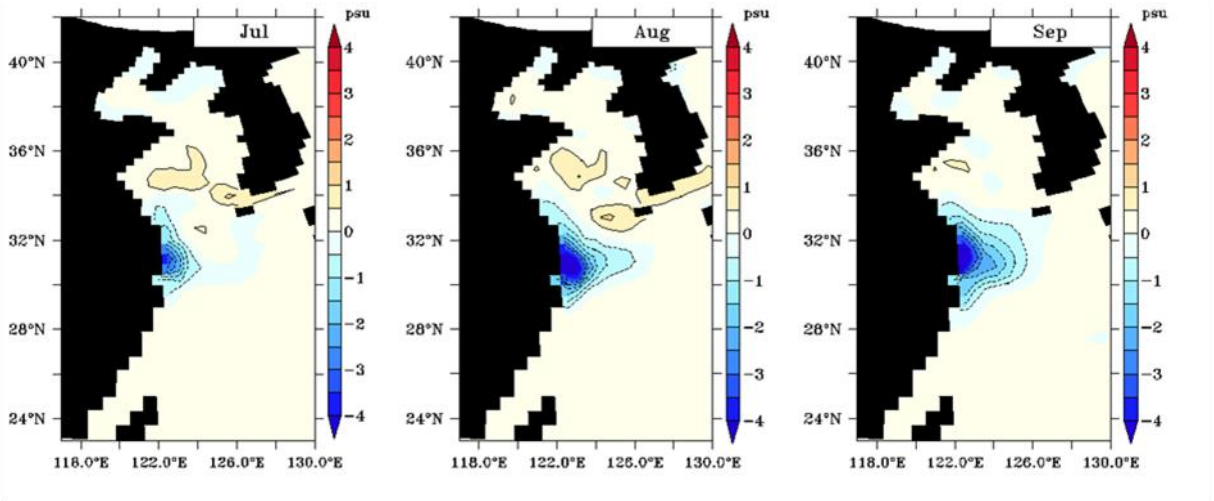

Fig. 6. Maps of difference between the El Niño and La Niña composites of sea surface salinity in July, August, and September.

4. Conclusions and Discussion

A cyclostationary EOF analysis finds that the interannual variability of the SSS in the YECS is mainly attributable to a CRD variability. The CRD variability is linked to ENSO-related precipitation over east China. Composite precipitation patterns in El Niño and La Niña years show that when El Niño events occur in winter, more rainfall is observed over central China in the rainy season of the following years. The heavy precipitation leads to a large amount of CRD, which results in decreasing SSS in the YECS. This suggests that summer SSS variability in the YECS is closely linked to ENSO via the summer precipitation system over east China.

References

Bueh, C., U. Cubasch, S. Hagemann (2003), Impacts of global warming on changes in the East Asian monsoon and the related river discharge in a global time-slice experiment, Climate Research, 24, 47–57.

Chang, P.H., Isobe, A. (2003), A numerical study on the Changjiang diluted water in the Yellow and East China Seas. Journal of Geophysical Research 108, 3299, doi: 10.1029/2002jc001749.

Ichikawa, H., H. Sakajiri, H. Nakamura, A. Nishina (2001), Year to year variation of sea surface salinity in the East China Sea, Proc. Extended Abstract Volume, The 11th PAMS/JECSS Workshop, April 11–13, 2001, Cheju, Korea, 73–76.

Kim, K. -Y., G. R. North, J. Huang (1996), EOFs of one-dimensional cyclostationary time series: Computations, examples, and stochastic modeling, *Journal of Atmospheric Sciences*, *53*, 1007–1017.

Kim, K. -Y., G. R. North (1997), EOFs of harmonizable cyclostationary processes, *Journal of Atmospheric Sciences*, *54*, 2416–2427.

Lau, K.-M., H. Weng (2001), Coherent modes of global SST and summer rainfall over China: An assessment of the regional impacts of the 1997–98 El Niño, *Journal of Climate*, *14*, 1294–1308.

Levitus, S., T. P. Boyer, M. E. Conkright, T. O'Brien, J. Antonov, C. Stephens, L. Stathoplos, D. Johnson, R. Gelfeld (1998), World Ocean Database 1998 vol. 1, U. S. Government Printing Office, Washington, D.C.

Shankman, D., B. D. Keim, J. Song (2006), Flood frequency in China's Poyang Lake region: Trends and teleconnections, *International Journal of Climatology*, *26*(9), 1255–1266.

Senjyu, T., H. Enomoto, T. Matsuno, S. Matsui (2006), Interannual salinity variations in the Tsushima Strait and its relation to the Changjiang discharge, *Journal of Oceanography*, *62*, 681–692.

A numerical experiment on the typhoon intensity change on a warmed ocean using a coupled typhoon-ocean model

Ok-Hee Seo, Hyoun-Woo Kang, Chan Joo Jang, Sok Kuh Kang, Jae-Gwi So and Kyung Tae Jung

Climate Change and Coastal Disaster Research Department ,
Korea Ocean Research and Development Institute, 787 Haean-Ro, Sangrok-Gu, Ansan, Gyeonggi-do, 426-744, Republic of Korea

ABSTRACT

Tropical cyclone intensity change in a warmed ocean has been investigated using a coupled ocean and tropical cyclone model named STORM (Synchronized Typhoon-Ocean Research Model). It has been developed for the Northwestern Pacific area by coupling the GFDL (Geophysical Fluid Dynamics Laboratory) tropical cyclone model and the HYCOM (HYbrid Coordinate Ocean Model). We have reproduced comparatively well the typhoon USAGI in 2007 using the STORM and applied it for the state of warmed ocean assuming that the atmospheric condition is same to 2007 Usagi case. In the state of warmed ocean, The SST (Sea Surface Temperature) has been increased about 3~5 ℃ around typhoon path and the MLD (Mixed Layer Depth) deepens about 20m compared with the state of present ocean. The future USAGI in warmed ocean by the A1B scenario from the MIROC_3.2 hi-resolution model shows its intensity is increased very much compared to the USAGI 2007 case. It also cooled down the sea surface much larger because of the intensified typhoon strength. It is found that the typhoon-ocean feedback process also be intensified due to the global warming.

1. INTRODUCTION

The interaction between the tropical cyclone and the ocean is known to be a strong negative feedback process (Price 1981). As the typhoon strengthens, the evaporation rate grows due to the increase in the surface wind speed. The enhancement of the moisture supply from the ocean leads to an increase in the latent heat energy that drives the circulation of the tropical cyclone. As the typhoon continues to intensify, the increasing surface wind stress generates strong turbulent mixing that deepens the ocean mixed layer. The associated Sea Surface Temperature (SST) decrease can then result in a reduction of the total heat flux (latent plus sensible) into the atmosphere and this can lead to a decrease in typhoon intensity (Ginis 2002). Interaction between the tropical cyclone and the

underlying ocean has been studied much in the Atlantic Ocean. Observed records of hurricane activity in Atlantic Ocean show a strong correlation, on multi-year time-scales, between local tropical Atlantic SST and the Power Dissipation Index (PDI). PDI is an aggregate measure of Atlantic hurricane activity, combining frequency, intensity, and duration of hurricanes in a single index (Emanuel 2007). He also concluded that both Atlantic SST and PDI have risen sharply since the 1970s, and there is some evidence that PDI levels in recent years are higher than in the previous active Atlantic hurricane era in the 1950s and 60s.

What changes in typhoon activity such as frequency and intensity are expected on a warmed ocean? Knutson (2011) explains that climate warming will cause typhoons in the coming century to be more intense globally and to have higher rainfall rates than present-day typhoons. He also suggested that the numbers of very intense (category 4 and 5) typhoons will increase by a substantial fraction in some basins, while it is likely that the annual number of tropical storms globally will either decrease or remain essentially unchanged.

In this study, we developed a coupled ocean and tropical cyclone model in the Northwestern Pacific in order to investigate the changes in typhoon intensity on a future projected ocean by the global warming scenario. To incorporate a warmed ocean status, we integrated the Northwestern Pacific nested global ocean circulation model using the IPCC A1B scenario generated atmospheric forcing based on the MIROC_3.2 hi-resolution model results. Section 2 describes the coupled typhoon-ocean model and the comparisons of the typhoon simulation with the different ocean state are presented in section 3. Summary with some discussions and suggestions is followed in section 4.

2. MODEL EXPERIMENTS

2.1 STORM (Synchronized Typhoon and Ocean Research Model)

An ocean-atmosphere coupled modeling system for the typhoon simulation, STORM (Synchronized Typhoon and Ocean Research Model), has been developed based on the Hybrid Coordinate Ocean Model (HYCOM) and the GFDL (Geophysical Fluid Dynamics Laboratory) Tropical cyclone model (GFDLTM).

The GFDLTM is a northwestern pacific version of coupled GFDL hurricane model which is operated in the United States. It uses a triple nested movable mesh system to depict the interior structure of tropical cyclones. The model initial condition is defined through a method of vortex replacement. Time integration of the model is carried out by a two-step iterative method that has a characteristic of frequency selective damping (Kurihara et al., 1998). The STORM follows the same framework of coupled GFDL hurricane model replacing the originally coupled Princeton Ocean Model in the Atlantic by the HYCOM implemented for the Northwest Pacific.

As shown in Fig. 1, the outer domain of the GFDLTM covers 75°x75° with 1/2° spacing, the intermediate domain covers 11°x11° with 1/6° spacing and the finest and innermost domain covers 5°x5° with 1/12° horizontal grid resolution. The intermediate and

innermost grids are movable following the typhoon. The Northwest Pacific HYCOM including East Asian Marginal Seas (HYCOM-EAMS) covers 10°N ~ 63°N and 105°E ~ 171°E with the horizontal grid spacing of 1/4° and 30 hybrid vertical layers. The boundary and initial conditions of HYCOM-EAMS are provided by the global HYCOM (HYCOM-G) with longitudinal spacing of 1.5° and tropical region enhanced latitudinal spacing of 1/3 ~ 1° in the south of 65°N. In the north of 65°N, the arctic bipolar patch grid applies to resolve the North Pole singularity and to represent energy loan sea ice model more precisely.

The coupling of the GFDLTM and HYCOM-EAMS has been established directly using the Message Passing Interface (MPI) library. The GFDLTM get its sea surface temperature as a surface boundary condition from the HYCOM-EAMS and put those momentum and heat fluxes to the ocean model with the coupling interval of 30 minutes.

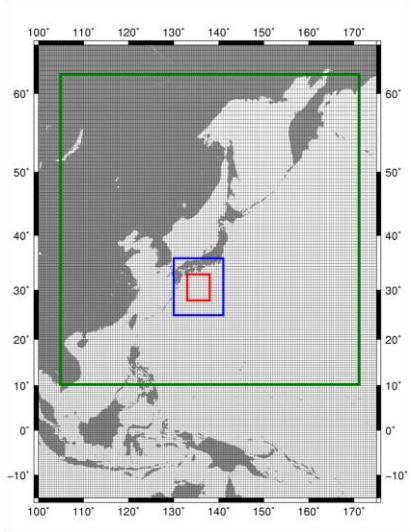

Fig. 1. STROM domain : outer is ocean model (HYCOM).
Green-blue-red box is typhoon model GFDLTM)

2.2 Experiment Design

To carry out typhoon development experiment under the different ocean status, typhoon USAGI 2007 has been selected as a reference typhoon. Since the STORM needs initial and boundary conditions, the GFDLTM has been initialized with the realistic typhoon USAGI 2007 vortex and the boundary conditions are provided by the NOAA Global Forecasting System data in the real calendar. The HYCOM_EAMS has been spun-up in two ways to make different initial conditions as well as the boundary conditions. The present state of ocean (USAGI-P, 30-JUL-2007) has been reproduced by the external force using ECMWF Re-Analysis interim data which have been applied to the HYCOM-G. The state of warmed ocean (USAGI-F, 30-JUL-2100) has been derived by external force using MIROC_3.2 high resolution model data projected for the 21st century by IPCC AR4 A1B scenario. To save the integration time for the HYCOM-EAMS we initialized the ocean state of Jul 30, 2100 by integrating the HYCOM-EAMS from Jan 1 2100 of HYCOM-G.

3. RESULTS

SST in the state of warmed ocean is increased 3~5℃ around the typhoon path compared with the present state. In this case, Mixed Layer Depth (MLD) is calculated based on the assumption that it is located at certain depth where the temperature is 0.5℃ lower than that of 10m depth. It is shown that the MLD in the state of warmed ocean is deeper about 20m than the present state. The transport of Kuroshio in the east of Taiwan is increased about 10 Sv especially in summer.

Fig. 5 compares the paths and intensities of typhoon USAGI in the present and the future states. Typhoon paths are similar in two cases before they arrived in the East Sea, the paths, however, are quite different after they passed the Japan Islands, which is not expected. This could be happened due to the different of the East Sea state as well as the different typhoon intensity after they are fully developed. It is notable that the typhoon intensity in the warmed ocean is much stronger than in the present state. The difference of the minimum pressure is 44 hPa (USAGI-P is 948 hPa vs USAGI-F is 904 hPa). The difference of the maximum wind speed is 21 kt (USAGI-P is 108 kt vs USAGI-F is 129 kt). The strong typhoon drives the cooler SST covering the wider area (Fig. 6).

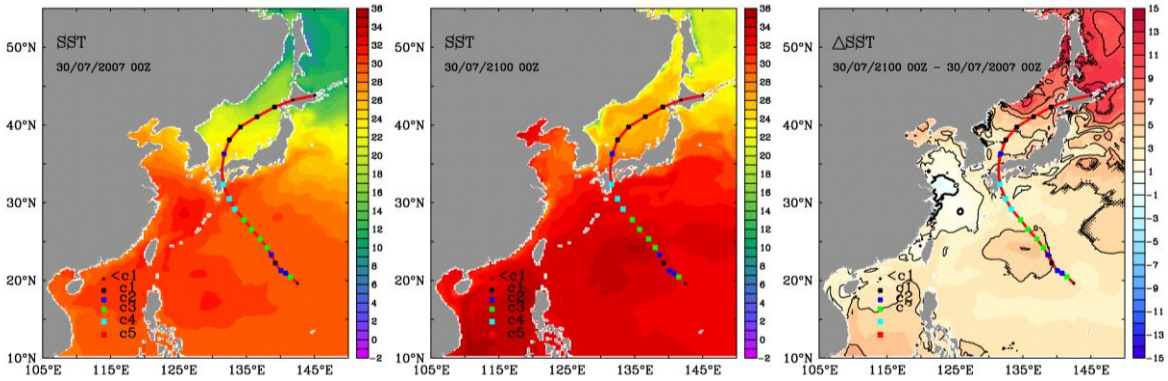

Fig. 2. Sea surface temperature in the present state of ocean (left, 2007), the future state of warmed ocean (middle, 2100) and their difference (2100-2007). The line and marking indicates the typhoon path and its intensity at that point, respectively.

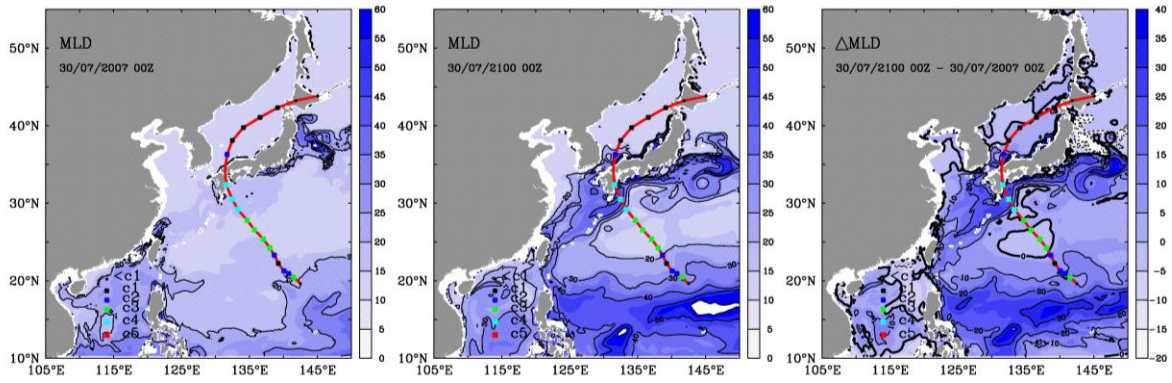

Fig. 3. Mixed layer depth in the present state of ocean (left, 2007), the future state of warmed ocean (middle, 2100) and their difference (2100-2007). The line and marking indicates the typhoon path and its intensity at that point, respectively.

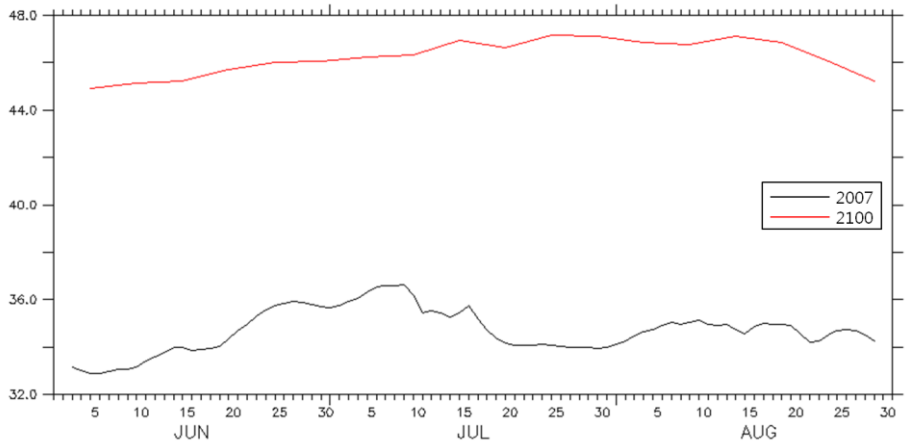

Fig. 4. Volume transport of Kuroshio in the east of Taiwan during summer (Black is the present state and the red is the future warmed state)

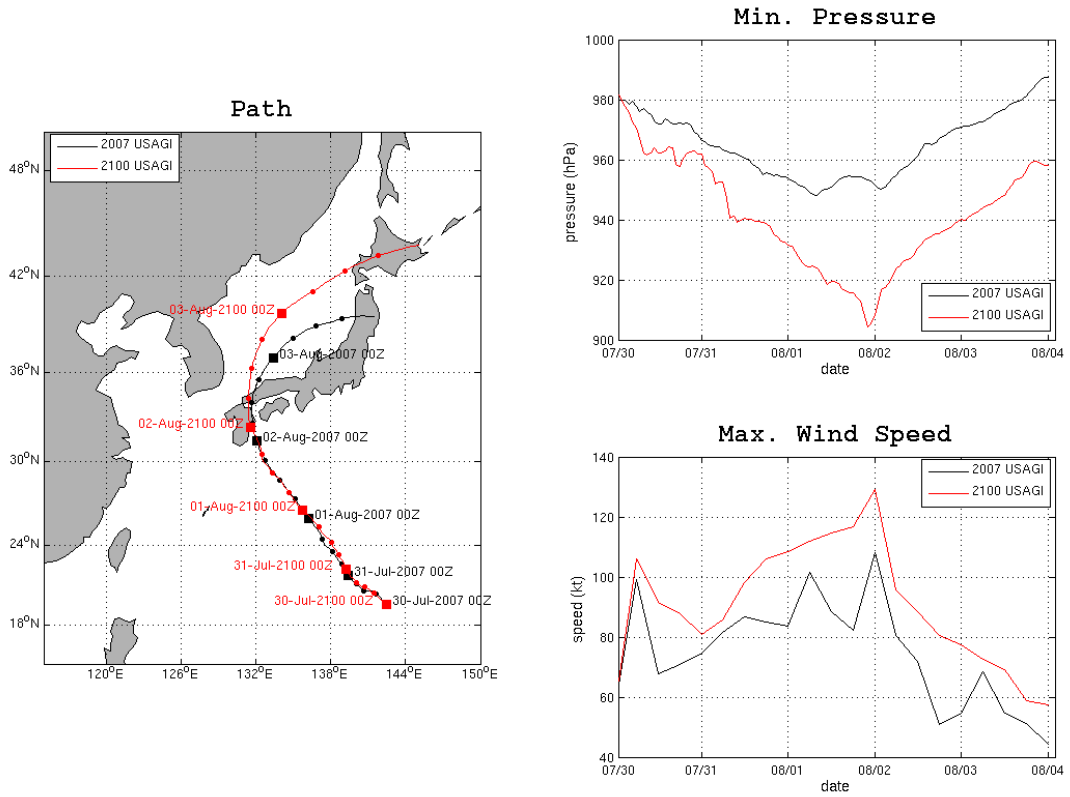

Fig. 5. Comparisons of the typhoon paths and intensity changes of the USAGI on the present state of ocean (black, USAGI-P) and on the state of warmed ocean (red, USAGI-F)

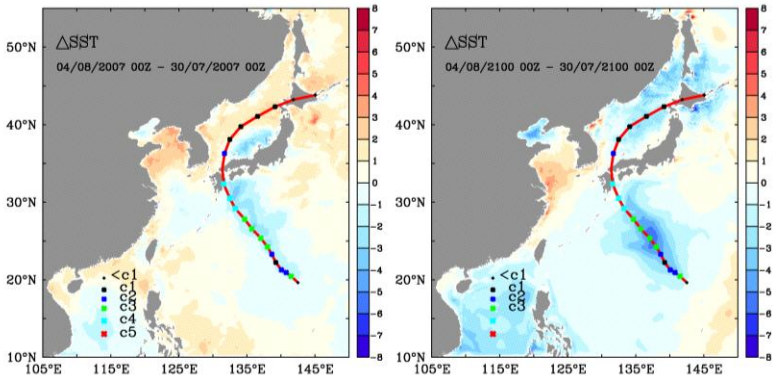

Fig. 6. SST differences (℃) after the typhoon passed through the Northwestern Pacific Ocean (Left is USAGI-P on the present state of ocean and right is the USAGI-F on the state of warmed ocean).

4. SUMMARY

Tropical cyclone intensity change in a warmed ocean has been investigated using a coupled ocean and tropical cyclone model named STORM (Synchronized Typhoon-Ocean Research Model). We have reproduced comparatively well the typhoon USAGI in 2007 using the STORM and applied it for the state of warmed ocean assuming that the atmospheric condition is same to 2007 USAGI case. In the state of warmed ocean, The SST has been increased about 3 to 5℃ around typhoon path and the MLD deepens about 20m compared to the present state of ocean. The future USAGI in warmed ocean by the A1B scenario from the MIROC_3.2 hi-resolution model shows its intensity is increased very much compared to the USAGI 2007 case. It also cooled down the sea surface much larger because of the intensified typhoon strength. It is found that the typhoon-ocean feedback process also be much intensified due to the global warming.

Since this study assumes that the atmospheric condition in the future is same to the present state when the typhoon USAGI generated, it has some weak point of its conclusion, but our aim is to find out the ocean's role on the typhoon development especially in the global warming scenario. Another caveat of this experiment is the simulation of the future state of the Northwestern Pacific by simply applying the last year solution of the global ocean circulation model. It should be further integrated using the whole time span of global solution on the East Asian Marginal Seas circulation model. Despite of its weakness, however, it is worthwhile to note that the global warming could accelerates the typhoon-ocean interaction and would give a chance to so called super typhoon generation in the Northwestern Pacific area which could be a big threat to the people's lives and properties.

Acknowledgements

This study is supported by KORDI grant PM56290, PE98652 and PG47570.

REFERENCES

Emanuel, K. A., 2007: Environmental Factors Affecting Tropical Cyclone Power Dissipation. Journal of Climate, Vol. 20, 5497-5509

Ginis, I., 2002: Tropical Cyclone-Ocean Interactions. Atmosphere-Ocean Interaction, Advances in Fluid Mechanics Series, MO. 33, WIT Press, 83-114

Knutson, T. R., 2011: Global Warming and Hurricanes. An Overview of Current Research Results. Geophysical Fluid Dynamics Laboratory/NOAA, Sept. 3, 2008; Last Revised August 26. 2011

Lin, I. I., IAM-FEI PUN, and CHUN-CHIEH WU, 2009: Upper-Ocean Thermal Structure and the Western North Pacific Category 5 Typhoons. Part Ⅱ: Dependence on Translation Speed. Monthly Weather Review, 137, 3744-3757

Price, I. F., 1981: Upper ocean response to a hurricane. J. Phys. Oceanogr., 11, 153-175.

Mixed layer depth variability and its associated chlorophyll-a concentration changes in the East Sea

Jihyeon So, Chan Joo Jang, Taewook Park, Hera Kim

Climate Change & Coastal Disaster Research Department ,
Korea Ocean Research and Development Institute, 1270 Sa-dong, Ansan, Gyeonggi-do,
Republic of Korea 426-170

Abstract

This study investigates year-to-year variability of mixed layer depth (MLD) and its associated chlorophyll-a concentration changes in the East Sea. Comparison between winter MLD and wind from 2004 to 2010 finds that MLD decreases (increases) in the years of weak (strong) wind. Distinct deepening of MLD in 2008 is associated with increase of chlorophyll-a concentration in some areas of the East Sea, while such an increase of chlorophyll-a concentration does not appear in some areas of the East Sea showing that surface heat flux or oceanic advection dominates chlorophyll-a concentration.

Keywords: Mixed layer depth, East Sea, Wind, Chlorophyll-a,

1.INTRODUCTION

Seasonal variation of mixed layer depth (MLD) in the East Sea is apparent showing maximum value in winter and minimum value in summer (Yoo et al., 2008). This study, based on model-simulated MLD data, wind speed data, and remote-sensed chlorophyll-a (CHL) concentration data from 2004 to 2010, investigates year-to-year variation of winter MLD in the East Sea in relation to wind variability, and explores its effect on chlorophyll-a concentration change.

2.DATA AND METHOD

This study calculates MLD using temperature and salinity datasets from 1/12° Global HYbrid Coordinate Ocean Model (HYCOM) for 2004~2010. Among various methods for MLD estimation, this study utilizes the variable density threshold method (Sprintall and Tomczak, 1992), which considers salinity stratification as well as the temperature effect on stratification. Wind stress data were from NCEP Reanalysis data (Kalnay, et al., 1996). Surface CHL concentrations were obtained from Sea-viewing Wide Field-of-view Sensor (SeaWiFS) data and Moderate-Resolution Imaging Spectroradiometer (MODIS) Aqua data for 2004~2010. To examine the variability of

MLD, wind, and CHL in the East Sea, six areas were selected (Fig. 1).

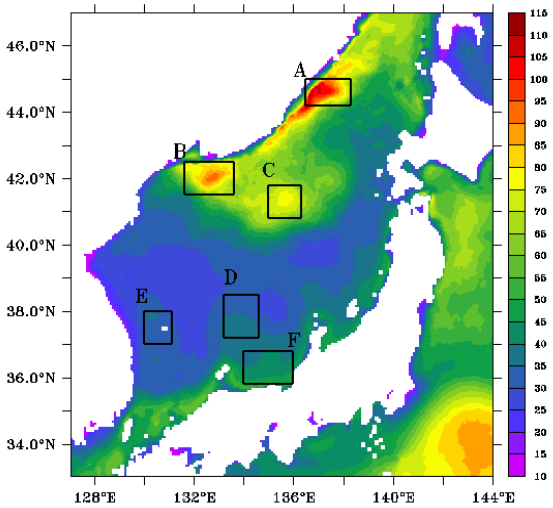

Fig. 1. Distribution of mixed layer depth averaged from 2004 to 2010. Six areas (A~F) were chosen for comparisons among MLD, wind, and chlorophyll-a concentration.

3.RESULTS

Figure 2 that compares MLD with wind speed shows that winter (February) MLD variation in the East Sea agrees well with wind variation in winter. For example, the MLD decreases from 2005 to 2006 when wind is weakened, and the MLD increases in 2008 in accordance with strong wind. The relationship between MLD and wind strength similarly appears in long-term trend of MLD and wind (Figs. 3, 4). MLDs in the most regions except area E show decreasing trends, which is consistent with decreasing trend in wind. Figure 5 that compares MLD in February with CHL concentration in April shows that an increase of MLD in 2008 is accordance with strong CHL concentration in areas of B, C, and E.

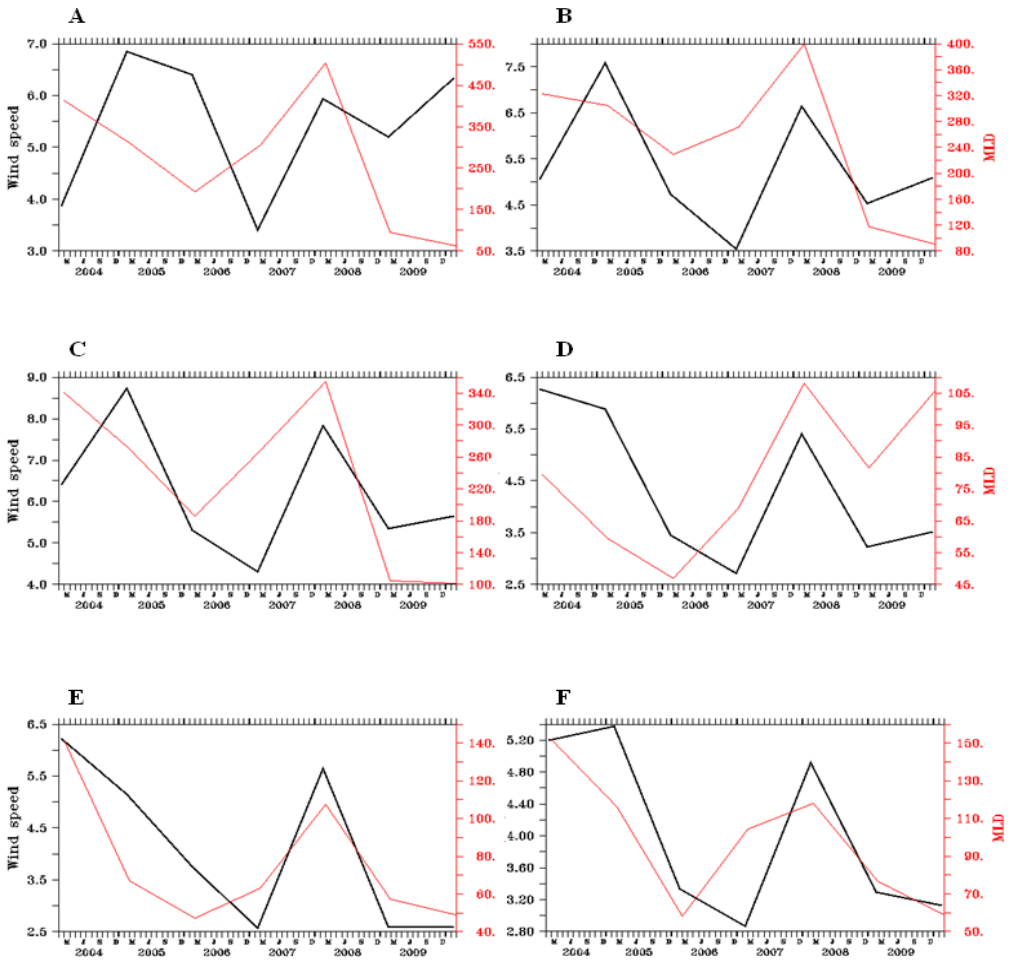

Fig. 2. Year-to-year variations of MLD in February (red line) and wind speed in February (black line) from 2004 to 2010 in the areas of A~F.

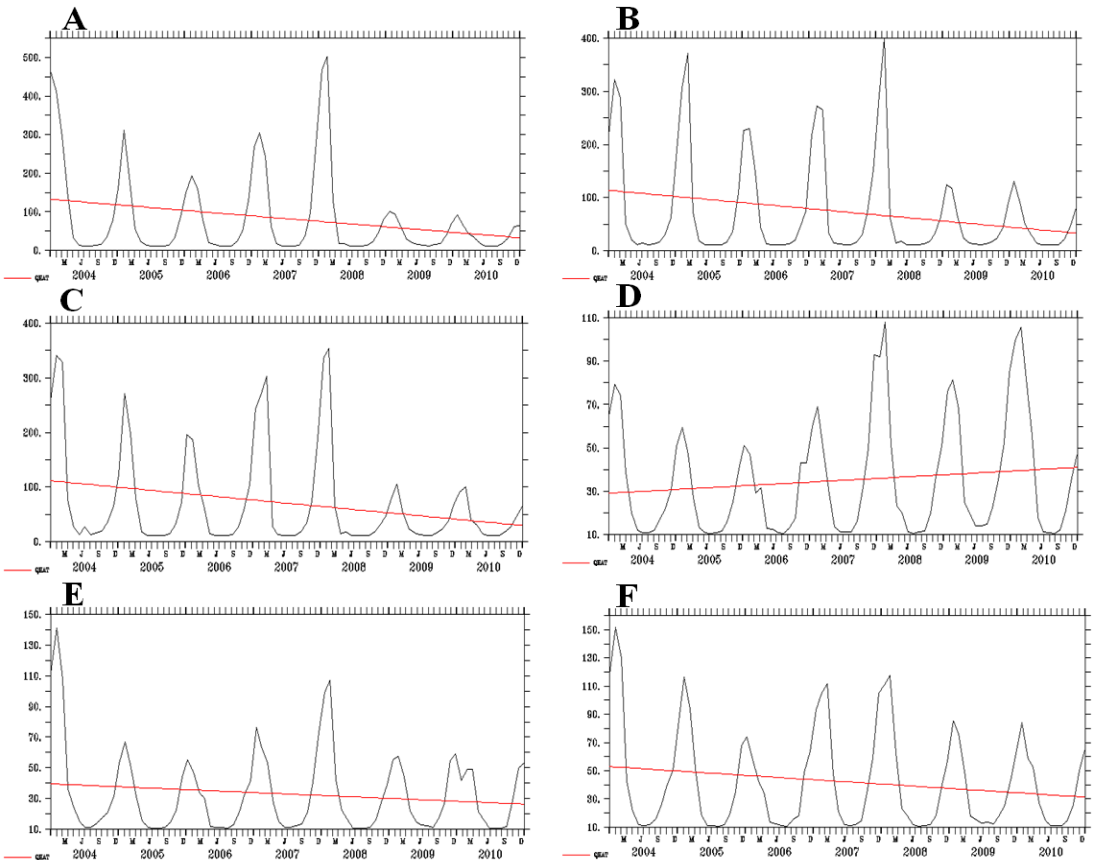

Fig. 3. Year-to-year variations of monthly-averaged MLD (black line) superimposed by long-term trend of MLD (red line) in the areas of A~F.

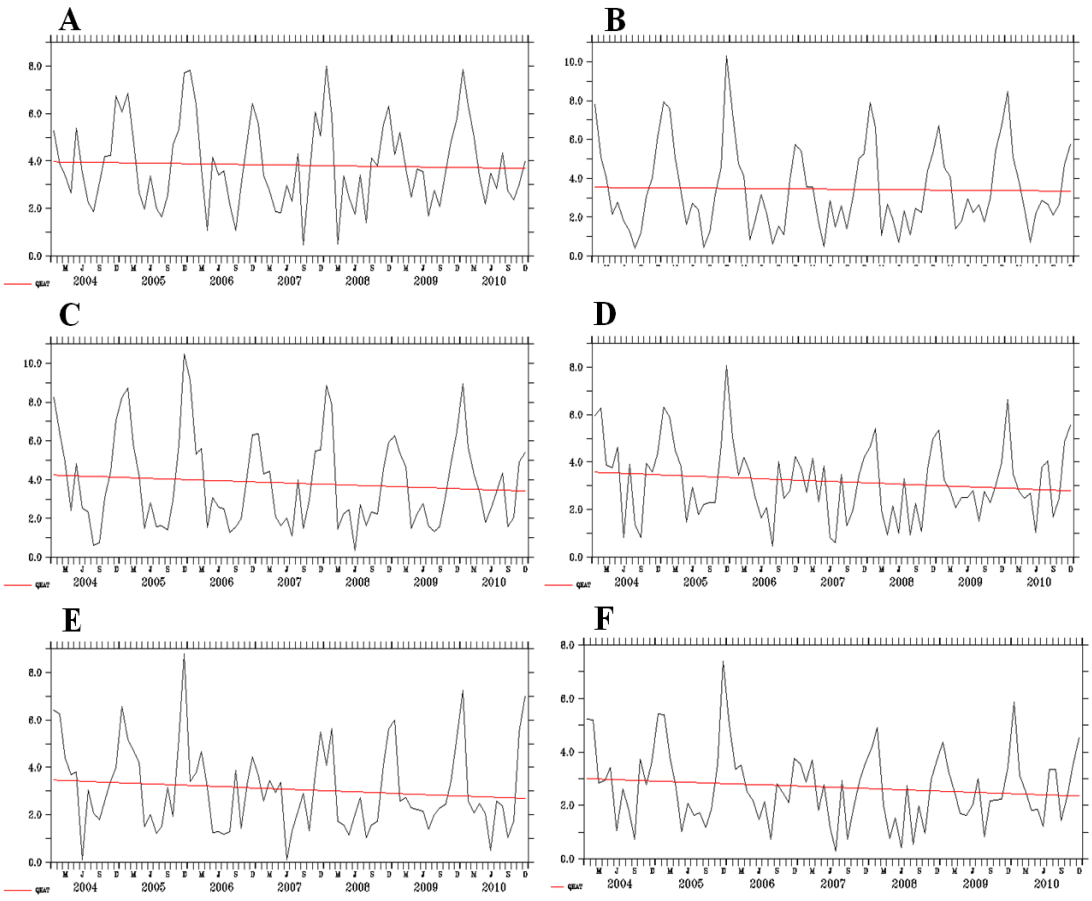

Fig. 4. Year-to-year variations of monthly-averaged wind (black line) superimposed by long-term trend of wind (red line) in the areas of A~F.

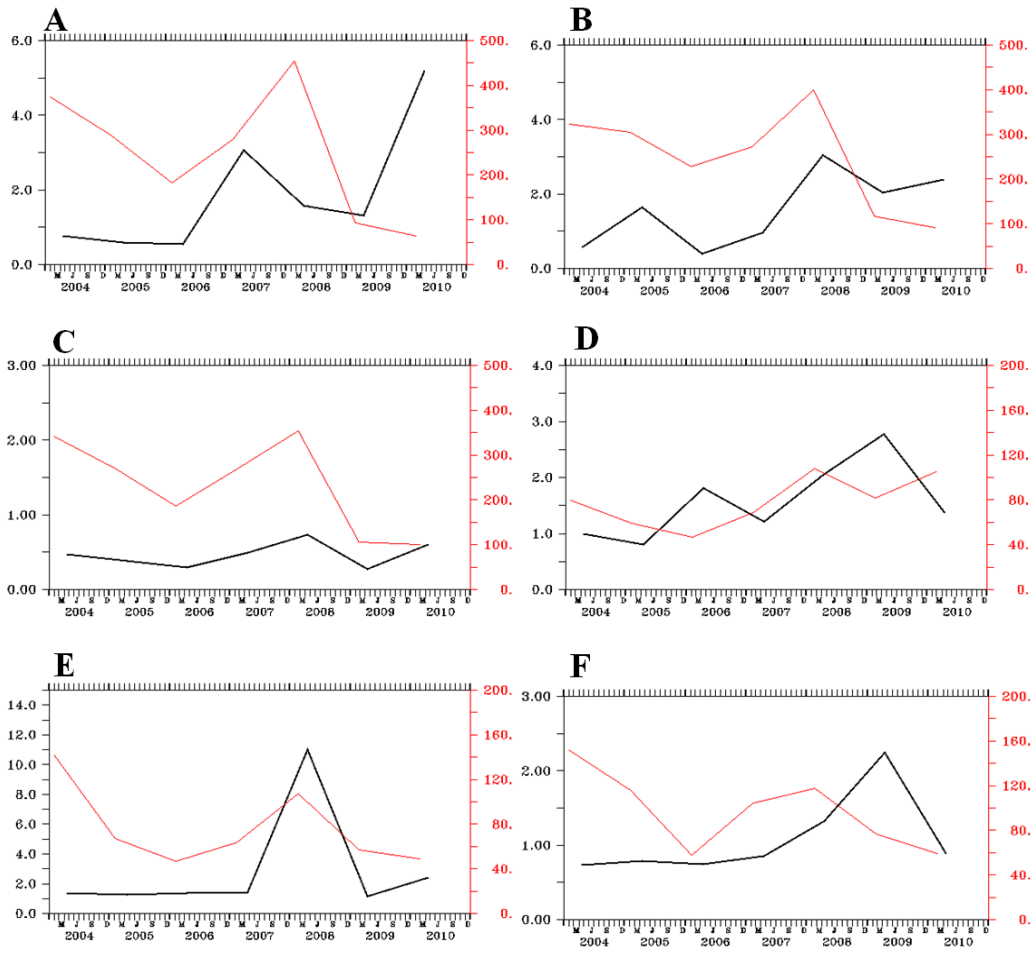

Fig. 5. Year-to-year variations of MLD in February (red line) and Chlorophyll-a concentration in April (black line) from 2004 to 2010 in the areas of A~F.

4.CONCLUSIONS & DISCUSSION

This study represents that winter MLD in the East Sea is associated with wind strength, based on comparing MLD and wind data from 2004 to 2010. When wind speed is strong (weak), enhanced (reduced) vertical mixing results in MLD increase (decrease). Long-term decrease of MLD in the most regions in the East Sea is consistent with decreasing trend in wind. The long-term decreasing trend of wind is suggested to result from weakening of the Siberian anticyclone (Seong et al., 2010).

MLD deepening causes nutrients to be entrained into upper ocean, which increases chlorophyll-a concentration. For example, distinct deepening of MLD in the areas near Ulleung Island and southern Prymorie coast in 2008 is associated with increase of chlorophyll-a concentration. On the other hand, the relationship between MLD deepening and chlorophyll-a concentration increase could be neglected when surface heat flux or oceanic advection dominate chlorophyll-a concentration.

REFERENCE

Kalnay et al., 1996. The NCEP/NCAR 40-year reanalysis project, Bull. Amer. Meteor. Soc., 77: 437-470

Kim, H.C., S.J. Yoo, I.S Oh, 2007. Relationship between phytoplankton bloom and wind stress in the subpolar frontal area of the Japan/East Sea.. Journal of Marine Systems, 67: 205-216

Park, J.S., M.S. Suk, S. Yoon, S.J Yoo, 2008. Variability of Surface Chlorophyll Concentration in the Northwest Pacific Ocean. Ocean and Polar Research, 30(3):277-287

Sprintall, J., and Tomczak, M., 1992. Evidence of the barrier layer in the surface layer of the tropics. Journal of Geophysical Research, 97: 7305–7316

Seong, K.T., J.D. Hwang, I.S. Han, W.J. Go, Y.S. Suh, J.Y Lee, 2010. Characteristic for Long-term Trends of Temperature in Korean Waters. Journal of the Korean Society of Marine Environment & Safety, pp.252-360

Development and Evaluation of a Regional Ocean-Atmosphere Coupled Model with Focus on the Western North Pacific Summer Monsoon Simulation: Impacts of Different Atmospheric Components

Liwei Zou[1, 2] and Tianjun Zhou[1]

1 LASG, Institute of Atmospheric Physics, Chinese Academy of Sciences, Beijing, China

2 Graduate University of Chinese Academy of Sciences, Beijing, China

(zoulw@mail.iap.ac.cn)

A regional ocean atmosphere coupled model (ROAM) is developed through coupler OASIS3, and is composed of regional climate model RegCM3 and CREM (Climate version of egional Eta Model) as its atmospheric component and of a revised Princeton ocean model (POM2000) as its oceanic component (Fig.1). The performance of the ROAM over the western North Pacific summer monsoon region is assessed by the case simulation of warm season in 1998. Impacts of different atmospheric model components on the performance of ROAM are investigated. Compared with stand-alone simulation, CREM (RegCM3) produces more (or less) rainfall over ocean area with inclusion of the air-sea coupling. Different biases of rainfall are caused by the different biases of SST derived from the coupled simulation. Warm (or cold) SST bias simulated by CREM_CPL (RegCM3_CPL) increases (or decreases) the evaporation at sea surface, then increases (or decreases) the rainfall over ocean. The analyses suggest that the biases of vertical profile of temperature and specific humidity in stand-alone simulations may be responsible for the SST biases in regional coupled simulations. Compared with reanalysis data, the warmer (or colder) and moister (or dryer) lower troposphere simulated in CREM (RegCM3) produces less (or more) sea surface latent heat flux. Meanwhile, the more unstable (or stable) lower troposphere produces less (or more) cloudiness at low-level, which increases (or decreases) the solar radiation reaching on the sea surface. CREM (RegCM3) forced by observed SST overestimates (or underestimates) the sea surface net heat flux, implying a potential warm (or cold) heat source. After coupling with POM2000, the warm (or cold) heat source would further increase (or decrease) the SST. The biases of vertical profile of temperature and

specific humidity may be ascribed to the different representation of cumulus convection in atmospheric models.

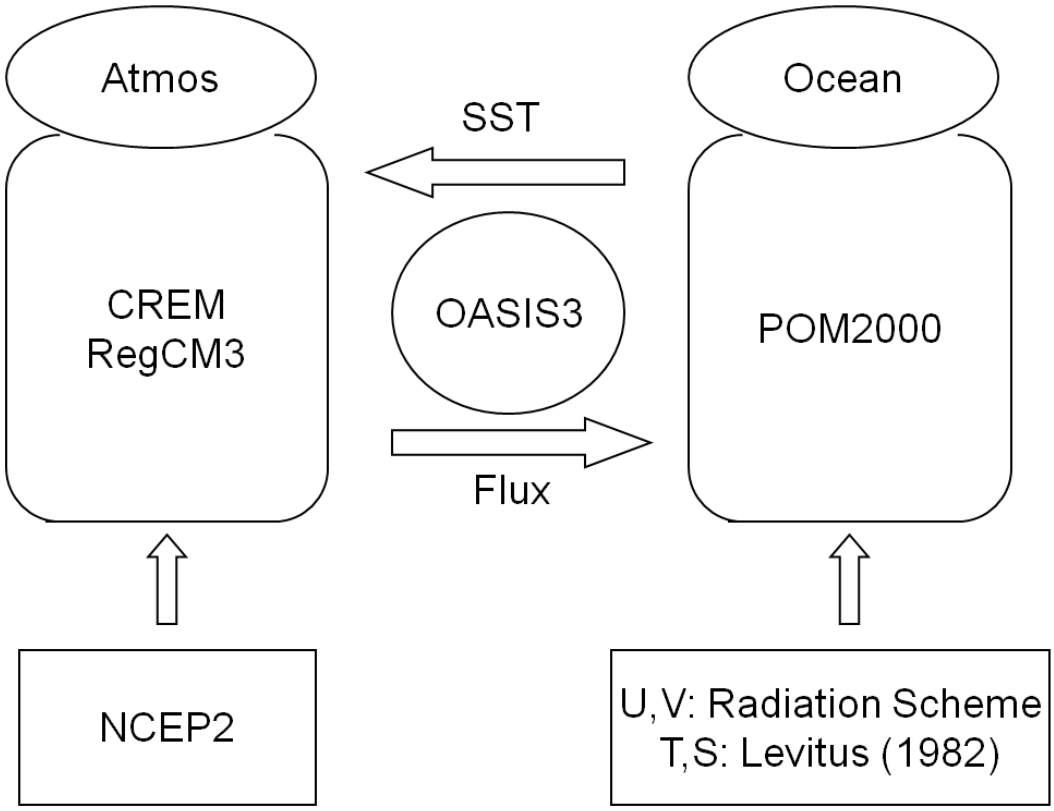

Figure 1. The framework of Regional ocean-atmosphere coupled model. The regional atmospheric models (RegCM3 and CREM) and POM2000 are coupled through the Ocean Atmosphere Sea Ice Soil 3.0 (OASIS3.0) coupler. During the process of coupling, the atmospheric model provides sea surface heat flux, wind stress to POM2000, while the POM2000 supplies the SST field to atmospheric model as the surface condition. The initial and lateral boundary conditions of the atmosphere are derived from NCEP/DOE reanalysis 2. The lateral temperature and salinity boundary conditions of POM2000 were derived from the Levitus climatological monthly mean data. A non-gradient extrapolation method is adopted to treat the open boundary condition.

Reference

Zou, L., and T. Zhou. 2011, Development and Evaluation of a Regional Ocean-Atmosphere Coupled Model with Focus on the Western North Pacific Summer Monsoon Simulation: Impacts of Different Atmospheric Components. *Science China (D): Earth Science*, Accepted and In Press

The extreme summer precipitation over East China during 1982-2007 simulated by LASG/IAP Regional Climate Model

LIU Jingwei, ZHOU Tianjun, LI Bo, ZENG Xianfeng, and FENG Lei

Abstract

The extreme summer precipitation over East China during 1982-2007 was simulated using LASG/IAP regional climate model CREM. The results show that the probability density functions (PDFs) of precipitation intensity are reasonably simulated, except that the PDFs of light and moderate rain are underestimated, while the PDF of heavy rain is overestimated. The extreme precipitation amount (R95p) and the percentage contribution of extreme precipitation to the total precipitation (R95pt) are also reasonably reproduced by CREM. However, the R95p and R95pt over most parts of East China are generally overestimated, while the R95p along the coastal area of South China (SC) is underestimated. The bias of R95pt is consistent with the bias of precipitation intensity on wet days (SDII). The inter-annual variation for R95p anomalies (PC1) is well simulated, but that of R95pt anomalies (PC2) is poorly simulated. The skill of the model in simulating PC1 (PC2) increases (decreases) from north to south. The bias of water vapor transport associated with the 95th percentile summer daily precipitation (WVTr95) well explains the bias of the simulated extreme precipitation.

Keywords: regional climate simulation, extreme precipitation, East China, CREM

Comparisons of experiments

for a nested grid regional forecast model

Sung-Tae Jang, Soo-Yong Nam, Yuri Oh, Ho Sik Eum

GeoSystem Research Corporation, #306 Hanlim Human Tower, 1-40 Geumjeong-Dong,

Gunpo-Si, Gyeongi-do, Korea,

(stjang@geosr.com)

The experiments were performed with result of two different models. RIAMOM(Research Institute of Applied Mechanics' Ocean Model) was shown to be applicable to the simulation of the East Sea circulation and uses Arakawa-B grid system horizontally and the z-coordinate vertically. The grid interval is 1/12° in the longitudinal and latitudinal direction. The other is ROMS(Regional Ocean Modeling System) which widely used by the scientific community and uses stretched, terrain-following coordinates in the vertical and Arakawa-C grid system in the horizontal and the interval is 1/10°(Fig.1). Main goal of the ocean models is to calculate the real time situation and to predict the oceanographic processes.

The purpose of a nested grid ocean model is to increase grid resolution in a subregion without having a computational expense of high resolution over the whole domain. Nesting method is generally recommended for regional models. The regional forecast model was conducted on a nested grid from 9-10 km to 0.33km horizontal resolution with RIAMOM and ROMS(Fig.2).

To measure the misfit between the observations and the computed currents in the Jung-ja(AA04 in Fig.3) shown in Fig.4, we use a value of γ^2 defined below.

$$\gamma^2 = \frac{\sum_k^N [(u_k^o - u_k^s)^2 + (v_k^o - v_k^s)^2]}{\sum_k^N [(u_k^o)^2 + (v_k^o)^2]}$$

Where (u_k^o, v_k^o) are the horizontal components of the observed data and (u_k^s, v_k^s) are the simulated currents produced by the nested model.

The γ^2 value for the 1st nested grid model results 0.55 which is about 40% larger than the γ^2 value of the 3th nested grid model results. Therefore the nesting technique performs better than the result of RIAMOM and ROMS.

The nested grid system has been tested with real data and the nesting technique is computationally stable and suitable for regional prediction model.

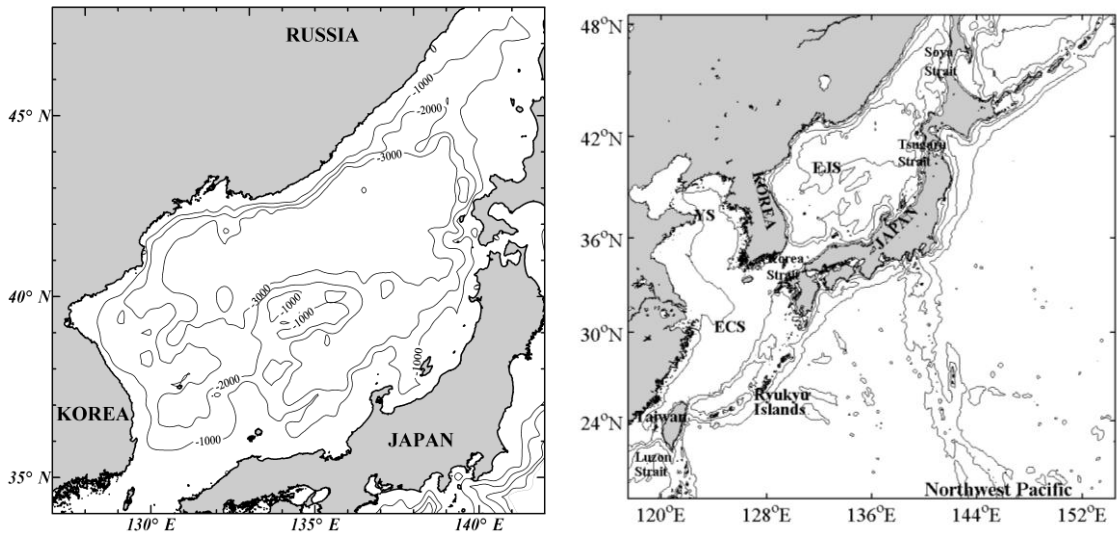

(a) RIAMOM (b) ROMS

Fig.1. The domains of the RIAMOM and ROMS model. Grid sizes of the domains are (a) 9 km and (b) 10 km, respectively.

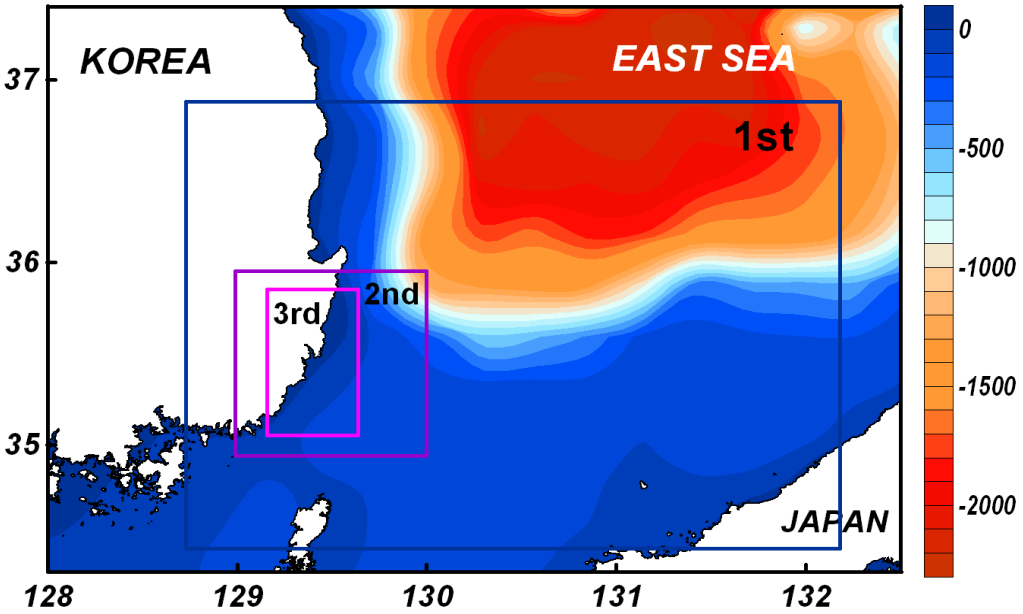

Fig.2. Configuration of the three -way-nested domains of the RIAMOM and ROMS model. Grid sizes of the domains are 3, 1, 0.33 km. Topography of the model domain is shaded.

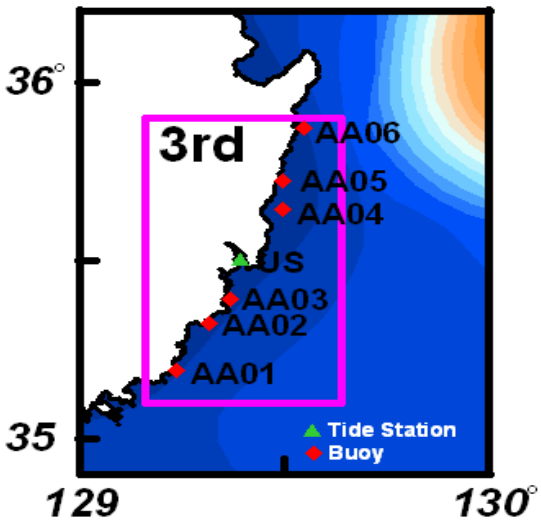

Fig.3. The domain of 3th nested model and the location of monitoring buoys.

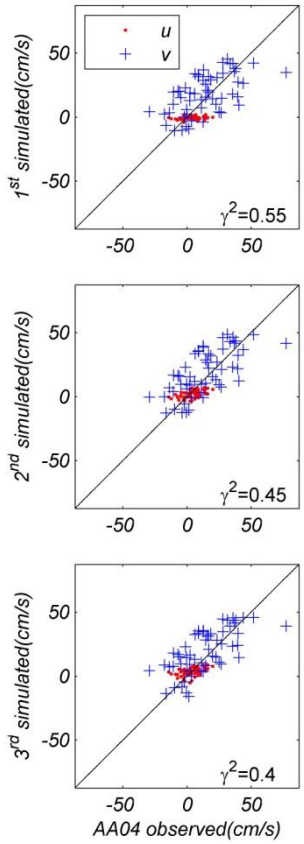

Fig.4. Scatterplots of observed and model-computed near-surface currents in Jung-ja(AA04). The top, middle and bottom are 1st, 2nd and 3rd nested model currents respectively.

Registrants

Dr. Bjørn Ådlandsvik
Institute of Marine Research
P.O. Box 1870, Nordnes, Bergen, N-5817, Norway
Phone: +47-55-23-84-52
E-mail: bjorn@imr.no

Dr. Icarus Allen
Plymouth Marine Laboratory
Prospect Place, Plymouth, PL13DH, UK
Phone: +44-1752-633441; Fax: +44-1752-633101
E-mail: jia@pml.ac.uk

Dr. Inkweon Bang
School of Earth & Environmental Sciences, Seoul National University
Sillimdong, Gwanak-gu, Seoul 151-747, Korea
Phone: +82-2-876-3719
E-mail: Inkweon.bang@gmail.com

Ms. Qiongqiong Cai
LASG, Institute of Atmospheric Physics (IAP)
Hua YanLi No.40, QiJiaHuoZi, Chaoyang District, P.O. Box 9804
Beijing 100029, China
Phone: +8610-82995334
E-mail: qiongqiongcai@mail.iap.ac.cn

Prof. Yang-Ki Cho
School of Earth & Environmental Sciences, Seoul National University
Sillimdong, Gwanak-gu, Seoul 151-747, Korea
Phone: +82-2-880-6749
E-mail: choyk@sun.ac.kr

Dr. Enrique Curchitser
Institute of Marine and Coastal Sciences, Rutgers University
71 Dudley Rd. New Brunswick, NJ 08901, USA
Phone: +1(732)932-7889; Fax: +1(732)932-8578
E-mail: enrique@marine.rutgers.edu

Dr. Mike Foreman
Fisheries and Oceans Canada, Institute of Ocean Sciences
P.O. Box 6000, Sidney B.C., V8L 4B2, Canada
Phone: +1-250-363-6306; Fax: +1-250-363-6746
E-mail: mike.foreman@dfo-mpo.gc.ca

Prof. Hiroyasu Hasumi
Center for Climate System Research, The University of Tokyo
5-1-5 Kashiwanoha, Kashiwa 277-8568, Japan
Phone: +81-4-7136-4407; Fax: +81-4-7136-4375
E-mail: hasumi@ccsr.u-tokyo.ac.jp

Dr. Chan Joo Jang
Climate Change & Costal Disaster Research Laboratory
Korea Ocean Research & Development Institute
787 Haeanro Sangrok-ku, Ansan 426-744, Korea
Phone: +82-31-400-6317; Fax: +82-31-408-5829
E-mail: cjjang@kordi.re.kr

Dr. Sung-Tae Jang
Ocean Research Institute, Geosystem Research Corporation
#306 Hanlim Human Tower, 1-40 Geumjeong-Dong, Gunpo-si, 435-824, Korea
Phone: +82-70-7019-0705; Fax: 82-70-7016-0673
E-mail: stjang@geosr.com

Prof. Hun Kang
Department of Environmental Engineering, University of Suwon
San 2-2, Wau-ri, Bongdam-eup, Hwasung-si, Gyeonggi-do, Korea
Phone: +82-1—4220-2146
E-mail: hkang@suwon.ac.kr

Dr. Hyun-Suk Kang
National Institute of Meteorological Research, KMA
61 Yeouidaebangro 16 gil, Dongjak-gu, Seoul 156-720, Korea
Phone: +82-70-7850-6655; Fax: +82-2-834-5922
E-mail: hyunsuk@korea.kr

Dr. Hyoun-Woo Kang
Climate Change and Costal Disaster Research Department
Korea Ocean Research and Development Institute
787 Haeanro Sangrok-ku Ansan 426-744, Korea
Phone: +82-31-400-7801; Fax: +82-31-408-5823
E-mail: hwkang@kordi.re.kr

Dr. Cheol-Ho Kim
Climate Change and Costal Disaster Research Laboratory
Korea Ocean Research and Development Institute
787 Haeanro Sangrok-ku, Ansan 426-744, Korea
Phone: +82-31-400-6128; Fax: +82-31-408-5829
E-mail: chkim@kordi.re.kr

Dr. Dong-Hoon Kim
National Institute of Meteorological Research, KMA
250-3 San, Bangdong-ri Sacheon-myeon, Gangneung-si, Gangwon-do, 210-852, Korea
Phone:+82-10-4725-6843; Fax: +82-33-644-2657
E-mail: mail@dhkim.info

Ms. Hera Kim
Climate Change and Costal Disaster Research Laboratory
Korea Ocean Research and Development Institute
787 Haeanro Sangrok-ku, Ansan 426-744, Korea
Phone: +82-31-400-6317; Fax: +82-31-408-5829
E-mail: herassemu@gmail.com

Mr. Jingwei Liu
LASG, Institute of Atmospheric Physics (IAP)
Hua YanLi No.40, QiJiaHuoZi, Chaoyang District, P.O. Box 9804
Beijing 100029, China
Phone: +8610-82995236
E-mail: liujingwei@mail.iap.ac.cn

Mr. Gyun-Do Pak
School of Earth & Environmental Sciences, Seoul National University
Sillimdong, Gwanak-gu, Seoul 151-747, Korea
Phone: +82-2-872-1679; Fax: +82-2-887-5613
E-mail: gdpak@curl.sun.ac.kr

Dr. Taewook Park
Climate Change and Costal Disaster Research Laboratory
Korea Ocean Research and Development Institute
787 Haeanro Sangrok-ku, Ansan 426-744 ,Korea
Phone: +82-31-400-6123; Fax: +82-31-400-5829
E-mail: twpark.kr@gmail.com

Dr. Myron Peck
Institute for Hydrobiology and Fisheries Science
Olbersweg 24, Hambrug, 22767, Germany
Phone: +49-40-42-838-6602; Fax: +49-40-42-838-6618
E-mail: myron.peck@uni-hamburg.de

Dr. Angelica Pena
Fisheries and Oceans Canada, Institute of Ocean Sciences
P.O. Box 6000, Sidney B.C., V8L 4B2, Canada
Phone: +1-250-363-6306; Fax: +1-250-363-6746
E-mail: Angelica.Pena@dfo-mpo.gc.ca

Dr. Gianmaria Sannino
ENEA (Italian National agency for new Technologies, Energy and sustainable Economic development)
S. Mala Galeria 301, Rome 00123, Italy
Phone: +390630486799; Fax: +390630484264
E-mail: Gianmaria.sannino@enea.it

Mr. Ok Hee Seo
Climate Change and Costal Disaster Research Department
Korea Ocean Research and Development Institute
787 Haeanro Sangrok-ku, Ansan 426-744, Korea
Phone: +82-31-400-7801; Fax: +82-31-408-5823
E-mail: okioki9941@kordi.re.kr

Prof. Corinna Schrum
Geophysical Institute, University of Bergen
Allegaten 70, Bergen 5007, Norway
Phone: + 0047-55582620
E-mail: Corinna.Schrum@gfi.uib.no

Dr. Hyodae Seo
Physical Oceanography Department, Woods Hole Oceanographic Institution
266 Woods Hole Road, MS#21, Woods Hole 02543, USA
Phone: +508-289-2792; Fax: +508-457-2181
E-mail: hseo@whoi.edu

Ms. Jihyeon So
Climate Change and Costal Disaster Research Laboratory
Korea Ocean Research and Development Institute
787 Haeanro Sangrok-ku, Ansan 426-744 ,Korea
Phone: +82-31-400-6317; Fax: +82-31-408-5829
E-mail: sojhwlgus@gmail.com

Ms. Dan Sun
LASG, Institute of Atmospheric Physics (IAP)
Hua YanLi No.40, QiJiaHuoZi, Chaoyang District, P.O. Box 9804
Beijing 100029, China
Phone: +8610-82995328
E-mail: sundan@lasg.iap.ac.cn

Prof. Tianjun Zhou
Institute of Atmospheric Physics, Chinese Academy of Science
Hua YanLi No.40, Beichen West Road, Chaoyang District, P.O. Box 9804
Beijing 100029, China
Phone: +8610-82995279; Fax: +9610-82995172
E-mail: zhoutj@lasg.iap.ac.cn

Mr. Liwei Zou
LASG, Institute of Atmospheric Physics (IAP)
Hua YanLi No.40, QiJiaHuoZi, Chaoyang District, P.O. Box 9804
Beijing 100029, China
Phone: +8610-82995236
E-mail: zouliwei@gmail.com